SIMON FRASER UNIVERSITY
SCIENCE UNDERGRADUATE RESEARCH JOURNAL

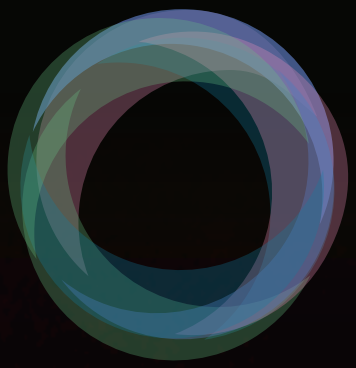

SFU SURJ

2019 - 2020 VOL.5
ISSN:2371-4344

SFU SURJ VOL.5 (2019-2020)

VOL.5

SFU SURJ

SIMON FRASER UNIVERSITY
SCIENCE UNDERGRADUATE RESEARCH JOURNAL

Volume 5, 2019-20

ISSN: 2371-4344

Published by the **Simon Fraser University Science Undergraduate Society**

Printed and bound by the **Simon Fraser Student Society**

Cover photo provided by **Sahil Chandhok**

Cover layout and design by **Melissa Tse**

Cover Image Description

Amyloids are dense, fibrillar, proteinaceous structures that have historically, been associated with a wide variety of systemic and neurological pathologies [1, 2]. These beta-sheet rich aggregates are extremely stable and resistant to degradation [2, 3]. Owing to their prevalence in several pathological conditions, these aggregates have gained a notorious reputation, however, several studies have shown that these structures are also capable of playing a physiological role [1, 4, 5, 6]. The Audas laboratory at SFU, studies a form a of physiological, subnuclear amyloid aggregation. It has been shown that, in response to certain stresses, mammalian cells can undergo a form of physiological amyloid aggregation [7]. These aggregates have been shown to have a cellular protective effect, and are seeded within the nucleoli by long non-coding RNA [7, 8, 9]. These structures share several biophysical properties with classical amyloid aggregates, for example, the proteins that make up these structures are both insolubilized and immobilized [7]. Additionally, these structures also stain positively with classical amyloid binding dyes such as Congo-red and thioflavin S [7]. These structures have been termed as "Amyloid bodies" or "A-bodies" [7]. The picture on the front page shows heat-shocked (43 °C) MCF-7 cells, stained with Congo-red; the bright-red foci are the A-bodies.

The image was taken and processed by using the Zeiss super resolution fluorescence microscope at Simon Fraser University, Burnaby, Canada on April 11, 2019. The Congo-red dye was excited by exposing the cells to green light, with a wavelength of 487 nm and observed using the 62× oil immersion lens.

References

[1] Fabrizio Chiti and Christopher M Dobson. Protein misfolding, functional amyloid, and human disease. *Annu. Rev. Biochem.*, 75:333–366, 2006.

[2] Matthew G Iadanza, Matthew P Jackson, Eric W Hewitt, Neil A Ranson, and Sheena E Radford. A new era for understanding amyloid structures and disease. *Nature Reviews Molecular Cell Biology*, 19(12):755–773, 2018.

[3] Jeffrey F Smith, Tuomas PJ Knowles, Christopher M Dobson, Cait E MacPhee, and Mark E Welland. Characterization of the nanoscale properties of individual amyloid fibrils. *Proceedings of the National Academy of Sciences*, 103(43):15806–15811, 2006.

[4] Christin Bissig, Leila Rochin, and Guillaume Van Niel. Pmel amyloid fibril formation: the bright steps of pigmentation. *International journal of molecular sciences*, 17 (9):1438, 2016.

[5] Samir K Maji, Marilyn H Perrin, Michael R Sawaya, Sebastian Jessberger, Krishna Vadodaria, Robert A Rissman, Praful S Singru, K Peter R Nilsson, Rozalyn Simon, David Schubert, et al. Functional amyloids as natural storage of peptide hormones in pituitary secretory granules. *Science*, 325(5938):328–332, 2009.

[6] Jixi Li, Thomas McQuade, Ansgar B Siemer, Johanna Napetschnig, Kenta Moriwaki, Yu-Shan Hsiao, Ermelinda Damko, David Moquin, Thomas Walz, Ann McDermott, et al. The rip1/rip3 necrosome forms a functional amyloid signaling complex required for programmed necrosis. *Cell*, 150(2):339–350, 2012.

[7] Timothy E Audas, Danielle E Audas, Mathieu D Jacob, JJ David Ho, Mireille Khacho, Miling Wang, J Kishan Perera, Caroline Gardiner, Clay A Bennett, Trajen Head, et al. Adaptation to stressors by systemic protein amyloidogenesis. *Developmental cell*, 39(2):155–168, 2016.

[8] Mathieu D Jacob, Timothy E Audas, James Uniacke, Laura Trinkle-Mulcahy, and Stephen Lee. Environmental cues induce a long noncoding rna–dependent remodeling of the nucleolus. *Molecular biology of the cell*, 24(18):2943–2953, 2013.

[9] Timothy E Audas, Mathieu D Jacob, and Stephen Lee. Immobilization of proteins in the nucleolus by ribosomal intergenic spacer noncoding rna. *Molecular cell*, 45(2): 147–157, 2012.

Acknowledgements

Many hands contributed to production of this journal, and we are extremely grateful. Our thanks to the ongoing support of Kevin Stranack and the folks at the Public Knowledge Project for providing us with the online platform that keeps us organized, and the support to go with it. Thank you to all those at the Simon Fraser Student Society for guiding us through the financial and printing logistics with grace and generosity. Perhaps most importantly, our sincere thanks to the wonderful group of graduate students and professors who provided us with their time and expertise as peer reviewers this year. We are immeasurably grateful. Finally, a big thank you to the generous sponsors who provided us with the means to make this a reality:

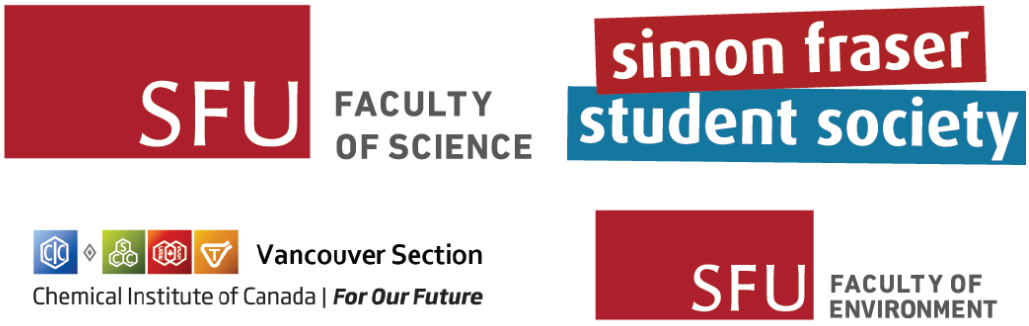

2019-20 Board of Editors

"The important thing is not to stop questioning."
- Albert Einstein

Foreword

Dear Reader,

Established in 2015, the SFU Science Undergraduate Research Journal has cultivated a community of young scientific researchers whose goal is to improve and expand scientific boundaries. Through our annual poster competition and journal publication, SFU SURJ has provided opportunities to encourage students to showcase their work while providing a dynamic environment for students and faculties to engage in scientific discussions. This journal is the product of the endeavours of SFU undergraduate students who care deeply about fostering a scientific community and supporting their fellow students in their research projects. Also, this journal would not be possible if it was not for the hard work of faculty members who took time from their busy schedules to provide constructive feedback to authors.

Due to the COVID–19 pandemic, this year was one of the most difficult years for the SURJ team. The disruption to weekly editorial meetings and the transition to online platforms caused challenges which we had never experienced. Despite this, our team, authors, and reviewers stayed dedicated to the process and overcame many obstacles that came our way. This challenging time revealed the resiliency of our community and that the passion for scientific advancement will be able to weather any storm. We would like to thank everyone involved in the process for their hard work and perseverance for making this publication a reality.

Without further ado, we present to you, the fifth edition of SFU Science Undergraduate Research Journal.

Soheil Saeidiborojeni, Matthew Nguyen, and Elaine Lam

Executive Editors

Table of Contents

Review Articles

SFU SURJ | SIMON FRASER UNIVERSITY SCIENCE UNDERGRADUATE RESEARCH JOURNAL
Vol. 5 (2019-20)

Attract to Kill: Are Male German Cockroaches (*Blattella germanica*) Deterred by the Presence of Permethrin Insecticide; and If So, Does the Surface of Application Matter?

Jessica Willows[1]*, Samantha Li-Jin Lam[1]*, Tasneem Azad[1], Gabriella Prai[1], Anshu Sharma[1], Blake Danis[1], Kevin Lam[1] †

[1]Simon Fraser University, *Department of Biological Sciences*

Abstract

Blattella germanica, the German cockroach, are unsanitary pests that are prolific in human-inhabited areas such as households, hospitals, and commercial kitchens. Pyrethroid insecticides have been used to manage cockroach infestations for decades, and while studies have shown that *B. germanica* populations can evolve resistance to pyrethroid exposure, few studies have determined whether they can also evolve behaviors for avoiding exposure to these insecticides. Therefore, our group aimed to study whether male *B. germanica* were deterred by the permethrin-based insecticide and if so, whether the surface of application of the insecticide mattered through two-choice bioassays. Through the two experiments, our team tested whether the scent of a 0.35% permethrin insecticide affected the attractiveness of rye bread baits to male *B. germanica*. Our team hypothesized that there would be no significant difference between the groups treated with insecticides compared to those with no insecticide and that changing the surface of application to the bread bait would not reduce this deterrence. Traps containing filter paper treated with insecticide and placed adjacent to rye bread baits caught significantly less *B. germanica* than traps containing untreated filter paper. However, there was no significant difference between treated and untreated bread baits. Our findings suggest that when an insecticide is mixed with a bait such as rye bread, *B. germanica* is more likely to be deterred by the insecticide, which can help create new and more efficient ways of managing infestation.

Keywords — German cockroaches, Pests, Pest control, Bait traps

1. Introduction

Blattella germanica are a globally widespread invasive species found on all continents where humans are present, including Alaska [1], and are resilient and unsanitary urban pests. These cockroaches are found close to human settlements, as they have a preference for human and animal waste products [2, 3].

There are numerous urban problems associated with these pests, because *B. germanica* are important carriers of multiple strains of antibiotic resistant bacteria [4]. In

*Equal First Authorship
†Corresponding Author. Contact: klamf@sfu.ca

hospitals, cockroach infestations increase the potential spread of resistant bacterial and fungal infections [5], which is a significant issue for immuno-compromised individuals. *B. germanica* have been suspected of being spreading antibiotic resistant bacterial strains of *Kl. pneumoniae* that causes pneumonia in hospitals [6]. Moreover, *B. germanica* are also capable of carrying virulent strains of bacteria that are associated with food borne diseases such as *Escherichia coli* in their gut, feces, vomit and exoskeleton [6]. German cockroaches also carry allergens that may induce respiratory irritation and asthma attacks [7]. It was observed in the United States that many residents experiencing cockroach infestations were found to have significantly higher levels of allergens in their homes [8]. With the prevalence of asthma increasing in areas with a high frequency of infestations [9], and antibiotic resistant bacteria becoming a global issue [10], there is an increasing need for more effective and efficient methods of baiting, trapping, and killing these harmful pests.

Current strategies to control *B. germanica* populations involve application of pyrethroid-based insecticides. Pyrethroids such as permethrin are highly toxic to *B. germanica* and other species of cockroaches [11], with cockroaches dying upon direct contact with permethrin [12]. As such, permethrin is commonly used as the active ingredient in many insecticides [12, 13]. Of the approximately 907,000 kg of permethrin used in the United States, 41% are applied by homeowners [7].

The most common method of application of permethrin-based insecticide is indoor residual spraying (IRS). IRS refers to spraying a residual insecticide as an aerosol indoors in either a singular spot, spot treatment, or in cracks and crevices in the buildings, such as behind the fridge or under baseboards [13]. A residual aerosol ensures that the insecticide stays on sprayed surfaces until disturbed [12]. Whilst spot treatment is precise, there is a lack of research on its efficacy [13]. Studies have also suggested that crack and crevice application is less effective than baited traps in school environments [13]. This may be due to permethrin's tendency to bind to mobile particles [12] in the crevices. These particles are able to freely distribute themselves within the crevices, thus reducing the concentration and affecting the efficacy of the applied insecticide [13].

Therefore, in an effort to find more efficient methods than spot treatment or crack and crevice application, our team wanted to determine whether we could create effective bait traps by placing permethrin-based insecticides near attractive sources such as rye bread. As *B. germanica* have been observed to develop deterrence for permethrin if not killed upon initial contact [14], our team decided to create bait traps that relied only on *B. germanica*'s sense of smell.

As such, our team had to test whether the permethrin-based insecticide caused an olfactory response and therefore deterrence in *B. germanica*. Our team tested for possible deterrence through a two-choice bioassay which used rye bread placed by itself and rye bread that was in close proximity to filter paper that was treated with the insecticide. Our team then tested if the surface of application affected deterrence through a two-choice bioassay with insecticide applied directly to the rye bread bait and rye bread bait without the insecticide. Through this process, our team aimed to test the preference of the cockroaches and ultimately whether they are deterred, attracted, or indifferent to the insecticide. We also tested to see whether or not the surface of

application for the insecticide matters.

2. Materials and Methods

2.1. Experimental Insects

The cockroaches used in our experiment were obtained from glass enclosures in an insect raising facility [15]. All cockroaches were collected in falcon tubes the day before testing. There were four cockroaches per tube, with a small piece of dampened cotton ball to act as a water source. They were then starved together for 24 hours to make the cockroaches more receptive to the rye bread baits [15].

2.2. Preparing the Bioassay

German cockroaches typically display colonizing behaviours such as following one another or communicating via sonic communication [16]. Therefore, working with one cockroach per bioassay would present fewer confounding variables. However, when *B. germanica* are isolated, they often tend to display unusual behaviour, such as a reduced tendency to explore [16], which could skew experimental data. Our team chose to use eight cockroaches per assay, which was akin to the format of groups used in experiments described by Pol, Gries & Gries [15].

A sixty eight-litre black Husky bin (product number: 1001 036 558, Husky) was used as an arena to hold the cockroaches, electrocuting coffee cans, and all other experimental materials during the 24 hour assay procedure (Fig. 1). Before any testing was done, a lux meter (product number: X000LDS2WZ) was placed inside the bin to measure the amount of light present. *B. germanica* are nocturnal in nature, and as such, they forage for food mainly in the dark [15]. Therefore, by creating a dark environment, our team aimed to create optimal foraging conditions. No light penetrated into the bin, as confirmed by our reading of 0 Lux, so no adjustments were made, as the complete lack of light meant that light would not influence the bioassay.

Before use for the first time, all Husky bins were washed with Nature Clean unscented hypoallergenic soap, dried, and sterilized with ethanol in order to minimize scents and contaminants from previous assays. After each experiment run, the bins and electrocuting coffee cans were only sterilized with ethanol for the same reason. A mixture of 48.8 g petroleum jelly (product number: 03228 JB00) and 110g of mineral oil (product number: 66102-540, Lot: 15F300021) was made in a plastic container and applied around the top rim of the bin with paintbrushes to ensure that the cockroaches would not escape.

The insecticide of choice, targeted for both ants and cockroaches, was Ortho Ant BGon Max (BGon), a residual aerosol (400g) that has 0.35% permethrin listed as the active ingredient. To prepare the filter papers, the insecticide was first sprayed from the aerosol can into a glass petri dish under a fume hood. A micropipette was then used to pipette 0.03 mL of the insecticide into 30 mm diameter Whatman filter paper (CAT No. 1001-329, Lot: 9659074), which was then placed in a fume hood for three minutes to allow evaporation of any fumes. A separate filter paper was left with no insecticide, to be placed into the other coffee can. A petri dish was used as a cookie

cutter on Mestemacher Organic Whole Rye Bread (product number: 2301673) in order to have the bread identical every time. The rye bread was placed in electrocuting coffee cans that would prevent the cockroaches from escaping the cans once they had crawled inside. This allowed for data collection by recording their 'first choices'.

Once all materials were prepared, arena materials were placed in a quiet and undisturbed room (B8241) where the Husky bins were stored. To limit confounding variables, the experiment was run in a setup that was isolated from sound and light so that *B. germanica* would only be influenced by smell. The layout of materials is shown in Fig. 1. Placement of cans and bins was randomized.

2.3. The Bioassay Procedures

2.3.1 Insecticide on Filter Paper ($n = 24$)

After the set up was completed in all six bins, the falcon tubes containing the *B. germanica* were placed in the center of each bin and opened. The bins were then closed and left undisturbed for 24 hours. Once 24 hours had passed, the number of cockroaches in each section of the bin were counted: the can trap containing insecticide covered filter paper, the can trap containing no insecticide on the filter paper or another place. This experiment was conducted four times, over four separate days, with the six bins, giving a total of 24 replicates ($n = 24$).

2.3.2 Insecticide on Bread ($n = 6$)

These experiments were conducted as described above with the exception that the insecticide was applied directly on the bread ($n = 6$). This experiment was conducted once due to time constraints, giving six replicates.

Figure 1 shows a more specific set up that differed between trials where filter papers were used and the trials where no filter paper was used. Together, the two bioassays assessed whether the permethrin based insecticide was a deterrent to *B. germanica* and whether the application surface was a factor.

2.4. Statistics

For all trials, the number of cockroaches in either the can containing insecticide or the can containing no insecticide were converted into percentages by dividing by the total number of cockroaches that were initially released. The mean percent of the number of cockroaches in each respective can was then taken and compared using a paired t-test to determine the amount of difference between the means. Tests were run in JMP®, Version 14.1.0. SAS Institute Inc., Cary, NC, 1989-2019.

3. Results

3.1. Insecticide on Filter Paper

The data collected from the trials where insecticide was applied in close proximity to the rye bread bait, Fig. 2 ($p = 0.0245$) showed that a significant difference was found

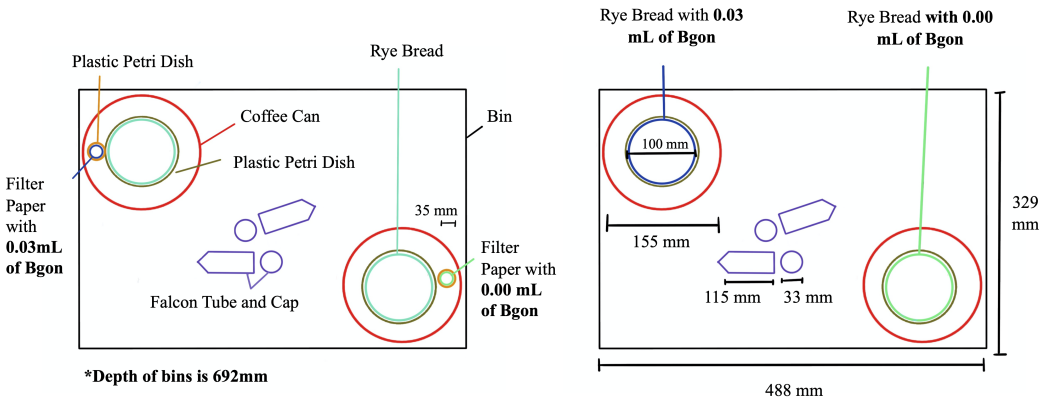

Figure 1: *General Two-Choice Set up for both bioassays. The set up on the left was used in the first bioassay where the insecticide, Ortho Ant BGon Max (Bgon), was applied to the filter paper. The set up on the right was used in the second bioassay where insecticide was applied directly to the rye bread. The copper strip was placed 80 mm from the bottom of the aluminum electrocuting coffee cans. The coffee cans ran an electric current of 7.5 V through the copper. The copper strip prevented cockroaches from crawling out of the cans by shocking them once they had 'made a choice' by crawling inside a can. The eight starved cockroaches were released from the falcon tube in the centre of the arena at the start of the 24 hour bioassay where they could then move into a coffee can containing bread and insecticide or bread and no insecticide, as described above.*

between the rye bread without insecticide in close proximity and the rye bread with insecticide in close proximity. Rye bread without insecticide in close proximity attracted more male *B. germanica*.

3.2. Insecticide on Rye Bread ($n = 6$)

The data collected from the trials where the insecticide was pipetted directly onto the rye bread bait, Fig. 3 ($p = 0.5710$), showed that there was no observed statistical difference between the bread with the insecticide and the bread without insecticide.

4. Discussion

Results from the first bioassay indicated that *B. germanica* were deterred by the insecticide treated filter paper in close proximity to the bread and were attracted to the bread with clean filter paper in close proximity. To explain these results, permethrin, which is the only known ingredient of the insecticide, due to the formulation being protected, was examined as the possible deterrent. Permethrin is non-volatile and thus was shown to not deter *B. germanica* via an olfactory response [17], so it could not have been the

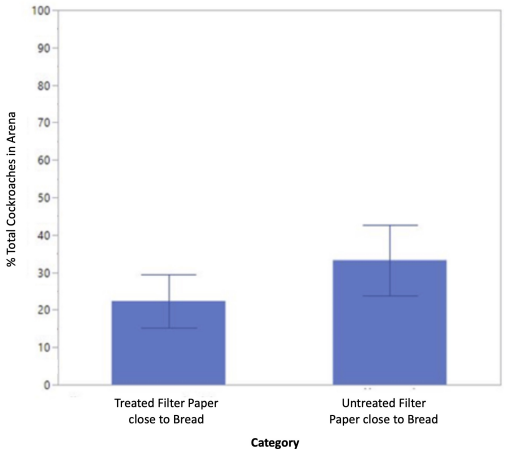

Figure 2: *Trial with insecticide in proximity to a bait (n=24). Percent of cockroaches found in the can trap containing either the filter paper treated with 0.03 mL of Ortho Ant BGon or 0 mL of Ortho Ant BGon. Error bars represent 95% confidence intervals. A significant difference was found, $p = 0.0245$. Percent of total is based on the total number of cockroaches that were present in the arena.*

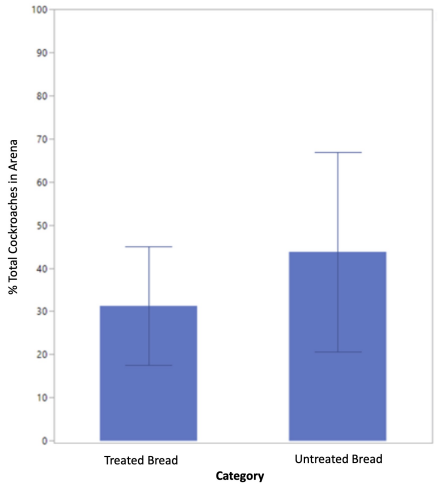

Figure 3: *Trial with insecticide applied directly to a bait ($n = 6$). Percent of cockroaches found in the can trap with either the rye bread treated with 0.03 mL Ortho Ant BGon or the bread treated with 0 mL of Ortho Ant BGon. Error bars represent 95% confidence intervals. No significant difference was found ($p = 0.5710$). Percent of total is based on the total number of cockroaches that were present in the arena.*

deterrent to the cockroaches. Our team proposes that some other volatile compound or a mix of volatile compounds in the formulation may have caused the deterrence.

As a significant difference was not found in the second bioassay, this suggests that *B. germanica* are unable to detect insecticide applied directly onto rye bread. By comparing the two bioassays, our team can safely infer that applying the insecticide directly to the rye bread affected how deterred *B. germanica* were by the insecticide. This could be due to an interaction occurring between the rye bread and the insecticide wherein the volatile compound(s) mentioned possibly had a better binding affinity to the rye bread than to the filter paper. The main ingredients of rye bread used in this study were organic whole kernel rye and organic whole rye flour. Both are mainly composed of soluble fibers which are polar and bioactive compounds which are non-polar [18]. Therefore, there is a basis for polar, non-polar interactions between the insecticide and the rye bread. The lack of a volatile compound in the two choice study arena to induce an olfactory response from *B. germanica* would eliminate the deterrence the insecticide previously had to the cockroaches. More broadly speaking, we can infer from comparing our two bioassays that bait traps where an insecticide is mixed with a bait are more effective compared to those where insecticide and bait are not mixed.

Finding that *B. germanica* cannot detect BGon when it is mixed in with a rye bread bait specifically, could minimize the duration of infestations by making the insecticide harder for cockroaches to avoid. Future experimentation could look into the success rates of these rye-bread bait traps being used in real life settings such as in households or hospitals with *B. germanica* infestations, as this might prove to be more efficient than the current recommended methods of spot treatment or crack and crevice application. Also, the bait in question, rye bread, is relatively inexpensive to consumers, which means there is an ease of accessibility for both households and larger facilities such as hospitals. The minimization of both the size and duration of *B. germanica* infestations would reduce: respiratory distress in those that have asthma [7], and the spread of harmful bacteria [5] and fungi 6. This, in turn, would reduce the risk of infections by antibiotic resistant bacteria strain in hospitals and, as such, reduce the strain on hospital resources.

5. Conclusion

Our team chose a permethrin-based insecticide due to its large availability and accessibility on the market, and lack of available research on its repellency to *B. germanica*. Rye bread is known to be attractive to *B. germanica* and is similarly largely accessible to most households. There was a significant difference between the insecticide group and no insecticide group when the insecticide was in proximity to the rye bread bait ($p = 0.0245$) and no significant difference when the insecticide was applied directly to with the rye bread bait ($p = 0.5710$). Our team has shown that *B. germanica* are deterred by permethrin containing insecticide when it is in proximity to a rye bread bait, but not when the insecticide is applied directly to the rye bread bait. Most interestingly, comparing the two experiments, our team suspect that an interaction occurred between the insecticide and the rye bread resulting in *B. germanica* displaying less deterrence to the insecticide. In future experiments, it would be interesting to see how successful this

method of pest management is when applied in a real world setting. In summary, this experiment has found a more effective method of pest management: using attractant mixed with insecticide as bait traps while also showing how applying insecticide near rye bread versus on it changes deterrence of *B. germanica* to the insecticide.

6. Acknowledgments

Facilities, equipment, and materials were provided by the Department of Biological Sciences at Simon Fraser University (SFU), as part of BISC 212: Biological Research. Initial development of this course was funded by the Dean of Science Office at SFU, through the INSPIRE program. Technical support and expertise were provided by Cheryl Leonard and Danielle Audas. Coffee can setups and guidance for capturing and handling the cockroaches were provided by Regine Gries. Help with analysing statistical tests was provided by Julian Christians.

References

[1] Qian Tang, Thomas Bourguignon, Luc Willenmse, Eliane De Coninck, and Theodore Evans. Global spread of the german cockroach, blattella germanica. *Biological Invasions*, 21(3):693–707, Mar 2019. ISSN 1573-1464. doi:10.1007/s10530-018-1865-2. URL https://doi.org/10.1007/s10530-018-1865-2.

[2] Joshua C Pol, Sebastian Ibarra Jimenez, and Gerhard Gries. New Food Baits for Trapping German Cockroaches, Blattella germanica (L.) (Dictyoptera: Blattellidae). *Journal of Economic Entomology*, 110(6):2518–2526, 09 2017. ISSN 0022-0493. doi:10.1093/jee/tox247. URL https://doi.org/10.1093/jee/tox247.

[3] Donald G. Cochran and Donald E. Mullins. Physiological processes related to nitrogen excretion in cockroaches. *Journal of Experimental Zoology*, 222(3):277–285, 1982. doi:https://doi.org/10.1002/jez.1402220310. URL https://onlinelibrary.wiley.com/doi/abs/10.1002/jez.1402220310.

[4] R. M. Elgderi, K. S. Ghenghesh, and N. Berbash. Carriage by the german cockroach (blattella germanica) of multiple-antibiotic-resistant bacteria that are potentially pathogenic to humans, in hospitals and households in tripoli, libya. *Annals of Tropical Medicine & Parasitology*, 100(1):55–62, 2006. doi:10.1179/136485906X78463. URL https://doi.org/10.1179/136485906X78463. PMID: 16417714.

[5] H. Nasirian. Contamination of cockroaches (insecta: Blattaria) to medically fungi: A systematic review and meta-analysis. *Journal de Mycologie Médicale*, 27(4):427 – 448, 2017. ISSN 1156-5233. doi:https://doi.org/10.1016/j.mycmed.2017.04.012. URL http://www.sciencedirect.com/science/article/pii/S1156523317300227.

[6] D. Leshan Wannigama, Rishabh Dwivedi, and Alireza Zahraei-Ramazani. Prevalence and antibiotic resistance of gram-negative pathogenic bacteria species isolated from periplaneta americana and blattella germanica in varanasi, india.

Journal of arthropod-borne diseases, 8(1):10–20, Dec 2013. ISSN 2322-1984. URL https://pubmed.ncbi.nlm.nih.gov/25629061. 25629061[pmid].

[7] D. C. Do, Y. Zhao, and P. Gao. Cockroach allergen exposure and risk of asthma. *Allergy*, 71(4):463–474, 2016. doi:https://doi.org/10.1111/all.12827. URL https://onlinelibrary.wiley.com/doi/abs/10.1111/all.12827.

[8] M.L. Feo, E. Eljarrat, D. Barceló, and D. Barceló. Determination of pyrethroid insecticides in environmental samples. *TrAC Trends in Analytical Chemistry*, 29(7):692 – 705, 2010. ISSN 0165-9936. doi:https://doi.org/10.1016/j.trac.2010.03.011. URL http://www.sciencedirect.com/science/article/pii/S0165993610001159. Green analytical chemistry.

[9] Xiaoxu Sun, JW Zhao, QY Wang, Guang Shi, JJ Yang, and Liang Ming. Prevalence of allergen sensitization among 15,534 patients with suspected allergic diseases in henan province, china. *Asian Pac J Allergy Immunol*, 37(2):57–64, 2019.

[10] C. Lee Ventola. The antibiotic resistance crisis: part 1: causes and threats. *P & T : a peer-reviewed journal for formulary management*, 40(4):277–283, Apr 2015. ISSN 1052-1372. URL https://pubmed.ncbi.nlm.nih.gov/25859123. 25859123[pmid].

[11] Wangxin Tang, Di Wang, Jiaqi Wang, Zhengwen Wu, Lingyu Li, Mingli Huang, Shaohui Xu, and Dongyun Yan. Pyrethroid pesticide residues in the global environment: An overview. *Chemosphere*, 191:990 – 1007, 2018. ISSN 0045-6535. doi:https://doi.org/10.1016/j.chemosphere.2017.10.115. URL http://www.sciencedirect.com/science/article/pii/S0045653517317009.

[12] G Daniel Todd, David Wohlers, and Mario J Citra. *Toxicological profile for pyrethrins and pyrethroids*. Agency for toxic substances and disease registry, 2003.

[13] Robert Krieger. *Hayes' handbook of pesticide toxicology*, volume 1. Academic press, 2010.

[14] Steven R. Sims, Arthur G. Appel, and Marla J. Eva. Comparative Toxicity and Repellency of Microencapsulated and Other Liquid Insecticide Formulations to the German Cockroach (Dictyoptera: Blattellidae). *Journal of Economic Entomology*, 103(6):2118–2125, 12 2010. ISSN 0022-0493. doi:10.1603/EC09415. URL https://doi.org/10.1603/EC09415.

[15] Joshua Pol, Regine Gries, and Gerhard Gries. Rye bread and synthetic bread odorants – effective trap bait and lure for german cockroaches. *Entomologia Experimentalis et Applicata*, 166(2):81–93, 2018. doi:https://doi.org/10.1111/eea.12620. URL https://onlinelibrary.wiley.com/doi/abs/10.1111/eea.12620.

[16] Craig Mistal, Stephen Takács, and Gerhard Gries. Evidence for sonic communication in the german cockroach (dictyoptera: Blattellidae). *The Canadian Entomologist*, 132(6):867–876, 2000. doi:10.4039/Ent132867-6.

[17] Emiliano Boné, Paola A. González-Audino, and Valeria Sfara. Spatial repellency caused by volatile pyrethroids is olfactory-mediated in the german cockroach

blattella germanica (dictyoptera: Blattellidae). *Neotropical Entomology*, 49(2):275–283, Apr 2020. ISSN 1678-8052. doi:10.1007/s13744-019-00739-9. URL https://doi.org/10.1007/s13744-019-00739-9.

[18] Roger Andersson, Gunnel Fransson, Markus Tietjen, and Per Åman. Content and molecular-weight distribution of dietary fiber components in whole-grain rye flour and bread. *Journal of Agricultural and Food Chemistry*, 57(5):2004–2008, Mar 2009. ISSN 0021-8561. doi:10.1021/jf801280f. URL https://doi.org/10.1021/jf801280f.

SFU SURJ | SIMON FRASER UNIVERSITY SCIENCE UNDERGRADUATE RESEARCH JOURNAL
Vol. 5 (2019-20)

Determining the Greatest Antibacterial Effect on Antibiotic resistant Bacteria along with the Preservative Effect of Naturally Derived Extracts

Maneet Kang[1*], Tiffany Lam[1*], Fatima Osman[1*], Julia Wang[1*]
Blake Danis[1], Kevin Lam[1 †]

[1]Simon Fraser University, *Department of Biological Sciences*

Abstract

Without antibiotics, individuals would be more susceptible to potentially fatal diseases. Due to the overuse of prescription and commercial drugs, mainstream antibiotics may become ineffective due to developed tolerance by bacteria. Several commonly disregarded or discarded resources from the environment contain many potential antimicrobial properties, such as *Carica papaya* seeds (papaya seeds), *Solenopsis invicta* venom (fire ant venom), *Calliphora coloradensis* larvae (blowfly larvae), and *Alnus rubra* bark (red alder bark). Our objective was to test whether papaya seeds, red alder bark, blowfly larvae, and red ant venom are an effective antibiotic on ampicillin resistant *Escherichia coli* (*E. Coli* S17-1) and nalidixic acid resistant *E. coli* (*E. Coli* JMP109). The best performing antibiotic, which ultimately was the *Carica papaya* seeds, was then tested to assess its preservative properties. A paste composed of these *Carica papaya* seeds was used as a food preservative on fish and strawberries. The fish controls began to develop dark brown spots during the testing period, while the treatment groups experienced no new growths in comparison to the control. The strawberry controls changed in color but did not have any growth until the fourth day, while the treatment groups began developing a white fuzzy growth on the third day. Based on these findings we do see some preservative properties in the *Carica papaya* seeds. However, further research should be conducted to determine whether *Carica papaya* seeds could be utilized against other potentially harmful microbes.

Keywords — Papaya seeds, fire ant venom, red alder bark, blowfly larvae, antibiotic, preservative, sustainability

1. Introduction

Due to the misuse or overuse of antibiotics, drugs have the potential to be deemed ineffective due to an increase of antibiotic resistant bacteria [1]. This could eventually lead to a deflation of available resources that were once considered adequate in treating disease and infection before one developed immunity. Therefore, it is important to cultivate new unconventional forms of antibiotics to fight against these resistant bacteria [1] and ensure resources won't be exhausted. Another prominent issue in our world today is waste. As waste products increase, it is accompanied by

*Equal First Authorship
†Corresponding Author. Contact: klamf@sfu.ca

an exponential increase of economic stressors [2]. Several commonly disregarded or discarded resources from the environment, such as papaya seeds, red alder, and various pests, contain many benefits that could simultaneously reduce the amount of environmental impurities and act as a possible solution to the accumulation of antimicrobial resistance. The *Carica papaya*, also known as the papaya fruit, is a great example of a waste product that contains antibacterial properties as an "inhibitor of conjugative R plasmid transfer from *Salmonella typhimurium* to *Escherichia coli*" [3]. Similarly, *Alnus rubra*, known as red alder, is another example of a commonly overlooked substance that also contains attributes that are able to combat the growth of harmful microbes [4]. Certain molecular components found in pests such as ants and blowflies have also been shown to possess the ability to combat harmful microbes, due to the gut bacteria that fights infections, which is found in in these insects [5].

To explore the power of unconventional materials and their impact as antibacterial agents, papaya seeds, red alder, fire ant venom, and blowfly larvae extracts were tested against antibiotic resistant *Escherichia coli*. We then decided to test the preservative properties of the strongest antibiotic, since antibiotics have been experimentally used on fish and red meat products [6]. Preservatives that are found in a variety of foods today are composed of synthetic compounds such as sodium acetate and sodium benzoate, which have been proven to quicken the development of many diseases including cancer, diabetes, and cardiac disease [7]. Thus, the discovery of a new environmentally friendly antibacterial agent that can serve as a potential food preservative, can be very beneficial.

2. Materials and Methods

2.1. Papaya Seed Extraction

One Chula Vista Papaya was cut in half using a serrated knife. We scooped out the papaya seeds manually, and placed them into a mortar and pestle where they were ground into a fine paste. We then transferred 10.52 g - 11.91 g of the papaya seeds into two 20 ml scintillation vials using a scoopula to be later centrifuged and plated with 10 discs for each bacteria to be tested.

2.2. Red Alder Extraction

Using a serrated knife, we cut out a 2.5 by 3 cm piece of bark from a red alder tree which contains antimicrobial properties. The bark was cut using dissecting scissors and further broken down using a mortar and pestle. About 2.8 g of red alder pieces was placed into two 20 ml scintillation vials.

2.3. Blowfly Larvae Extraction

2.8 g of blowfly larvae that pupated for 4 days were picked out of a cow's liver using sterile metal forceps and transferred into a Gentistar tube. The larvae were cleansed by adding 3 ml of distilled water into the Gentistar tube, the lid was then closed and the tube was shaken for one minute. We poured it onto a 4 by 5 cm paper towel to drain the water. The larvae were transferred to a mortar and pestle using metal

forceps, where they were manually homogenized. The paste was transferred to a 20 ml scintillation vial. Once the papaya seeds, red alder, and blowfly larvae were transferred into scintillation vials, we used a serological pipet to add 6 ml of ethyl acetate into the papaya seeds and red alder, and 1 ml was added to the blowfly larvae. Ethyl acetate is a polar aprotic solvent that acts to extract our antibiotic source and concentrate it via evaporation. With the lids on, each sample was mixed using the vortex for 5 minutes. After mixing, we extracted the liquid using a Pasteur pipette and transferred it into centrifuge tubes and centrifuged it at 10×1000 rpm for 10 minutes. We removed the top liquid transparent using a disposable pipet and used it for our experiment.

2.4. Fire Ant Venom Extraction

25 ml of water and 50 ml of hexane was added to a 150 ml beaker. Hexane is a less volatile and a strong nonpolar solvent which allows the water-hexane mixture to separate into two phases [8]. The beaker was then placed inside a 250 ml beaker lined with a plastic bag to stop any fire ants from escaping once they were added (Fig. 1). We had 200 fire ants in a small vial with the opening covered with a cotton ball to entrap the ants inside. We then repeatedly tapped the vial while holding it right side up, to ensure the ant have fallen to the bottom of the vial. Once the ants were sufficiently on the bottom and none were crawling up, we swiftly removed the cotton ball and poured the fire ants inside a beaker containing the hexane-water solution. Once the ants have been submerged in the organic hexane solvent, they would then discharge their venom proteins, possibly due to their aggressive nature [8]. The venom proteins would be suspended in the hexane layer, which floats above the water layer [8] of the hexane-water solution (Fig. 2). After 10 minutes we pipetted out the top hexane layer, with the venom proteins, using a disposable pipet and put it into a centrifuge vial (Fig. 3).

2.5. Disc Diffusion Set

We applied 30 ul of each of the four extracts onto 20 7 mm filter paper discs for a total of 80 discs. Since ethyl acetate was used in the red alder extract along with the blowfly larvae extract, and hexane was used in the fire ant extract, we decided to use ethyl acetate and hexane as our controls. We had two controls which were ethyl acetate and hexane. These discs were then left to evaporate for 10 minutes. One colony of each strain of bacteria was placed into corresponding pre-purchased Muller Hinsten broths in their respective vials, which was then covered with a 9cm by 5 cm piece of aluminum and left in a shaker at 37 degrees Celsius for 27 hours. Following proper aseptic technique, 50 uL of the corresponding strain of bacteria was spread onto each agar plate. Four discs were allocated to each antimicrobial plate and were stored overnight in a 37-degree incubator. Zones of inhibition were then measured using a millimetre caliper after 24 hours.

Figure 1: *Beaker Set Up for Transferring Fire Ants into Hexane Solution. A plastic bag was placed inside of a 250mL beaker. A 150mL beaker, containing hexane and water, was placed within this setup.*

2.6. Preservative Assessment

The papaya extract was created using the same methods from the first experiment, but the organic solvent ethyl acetate was not added so that it could be safe to place onto food. 1000 ul of the pure papaya seed extract was directly pipetted onto strawberries and pacific wild sole fillets in petri-dishes (Fig. 4). The petri-dishes were sealed using parafilm and placed into drawers at room temperature. Both the strawberries and fish each had 10 treatments with 1 mL of papaya seed extract pipetted onto its surface and 10 controls with no extract added. The experiment for the fish and strawberry occurred all at once on the same day. Pictures were taken daily along with corresponding visual observations.

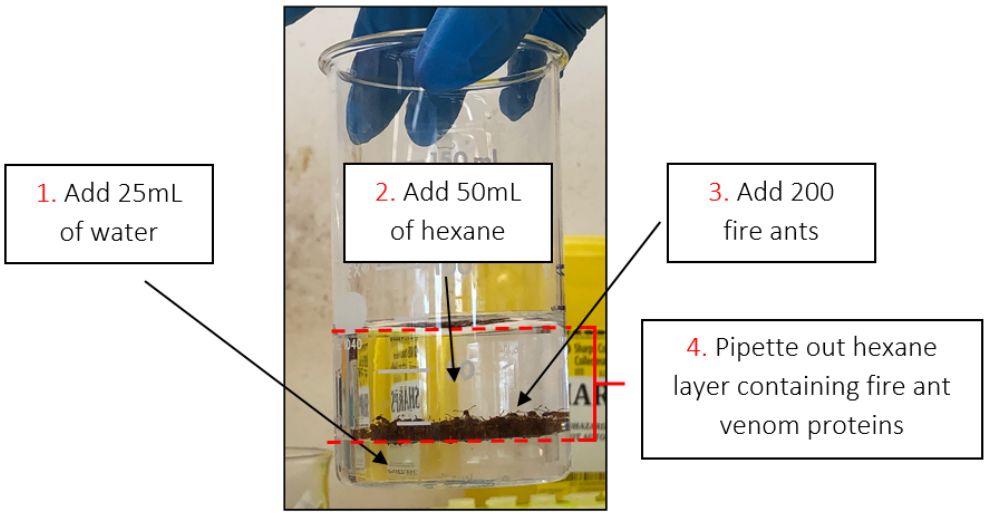

Figure 2: *Extraction Process of Fire Ant Venom using Water and Hexane.*

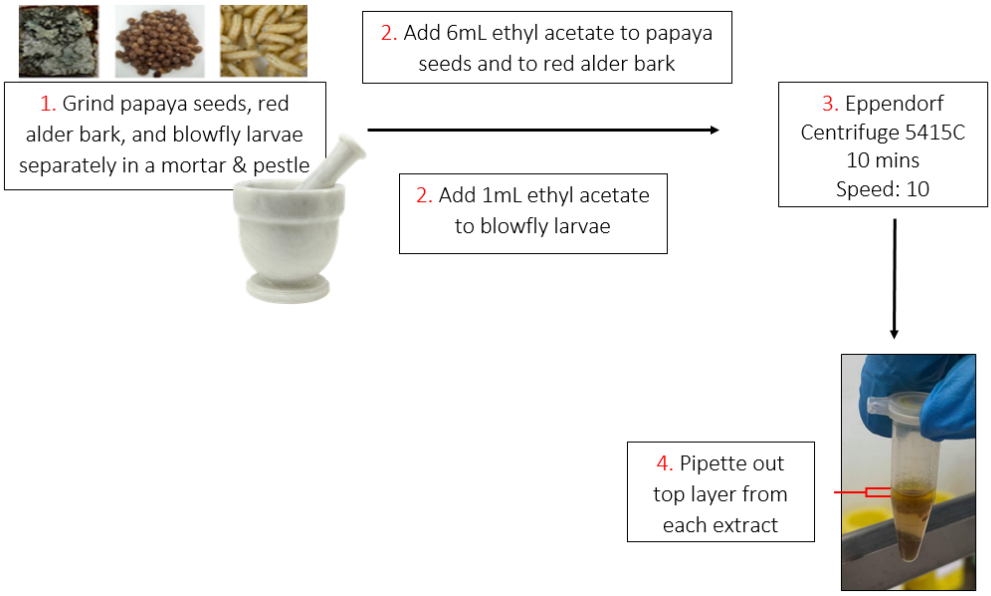

Figure 3: *Extraction Process of Papaya Seeds, Red Alder Bark, and Blowfly Larvae.*

2.7. Data Analysis

2.7.1 Antibacterial Power Assessment

Using an average diametre (mm) of the zones of inhibition, an ANOVA (Analysis of Variance) test at level $\alpha = 0.05$ was conducted first to see if there were differences among the zone of inhibition means of our four extracts and the controls. Our ANOVA

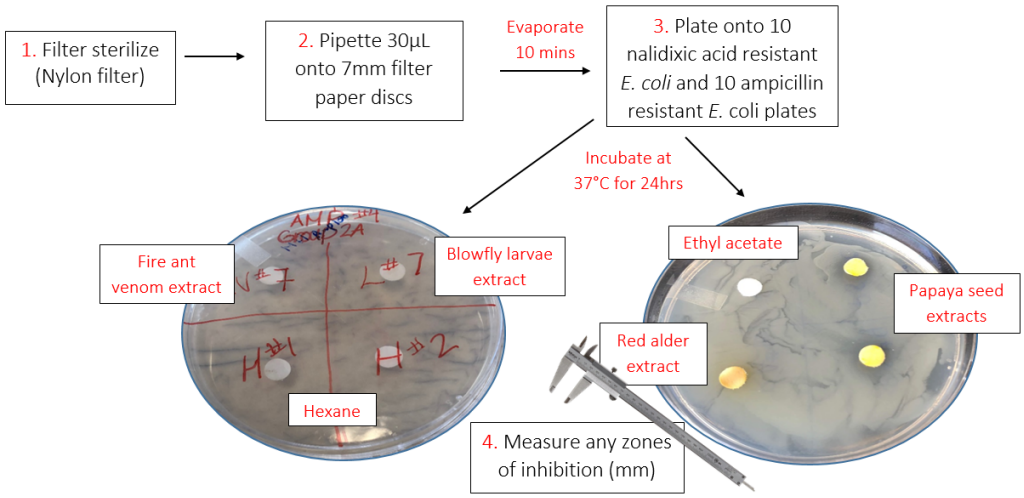

Figure 4: *Extraction Process of Papaya Seeds, Red Alder Bark, and Blowfly Larvae.*

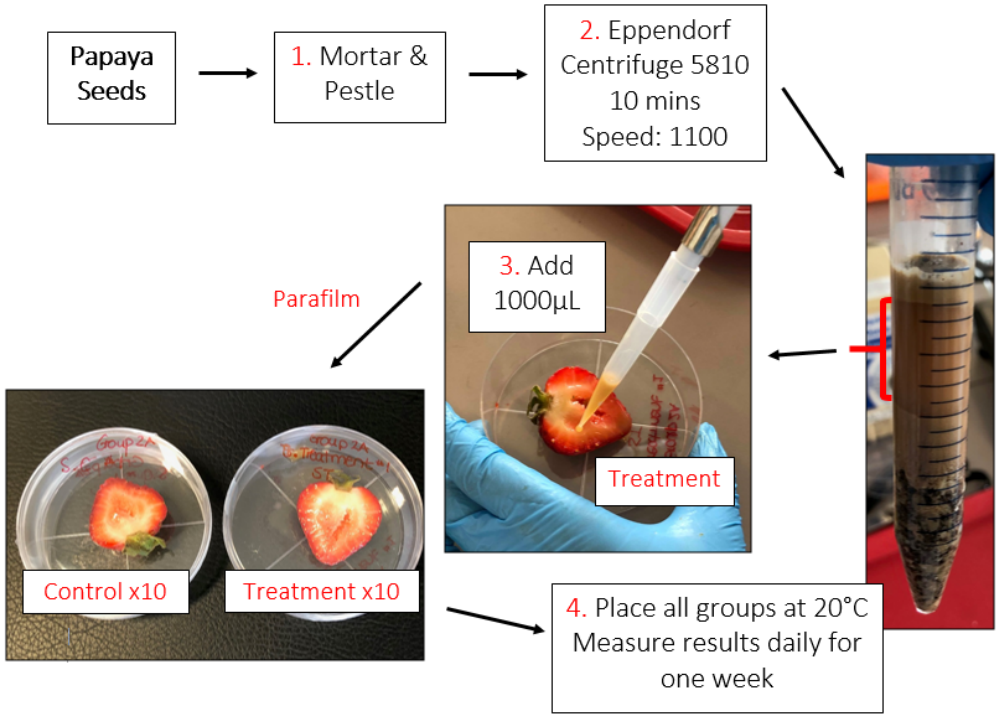

Figure 5: *Preparation of Papaya Seed Extract Treatment Groups. Extract was not added in control groups.*

yielded $p = 0.05$, which allowed us to run our Multiple Comparison Test (MCT) to determine which extract means are significantly different from each other and which show no differences (Fig. 6).

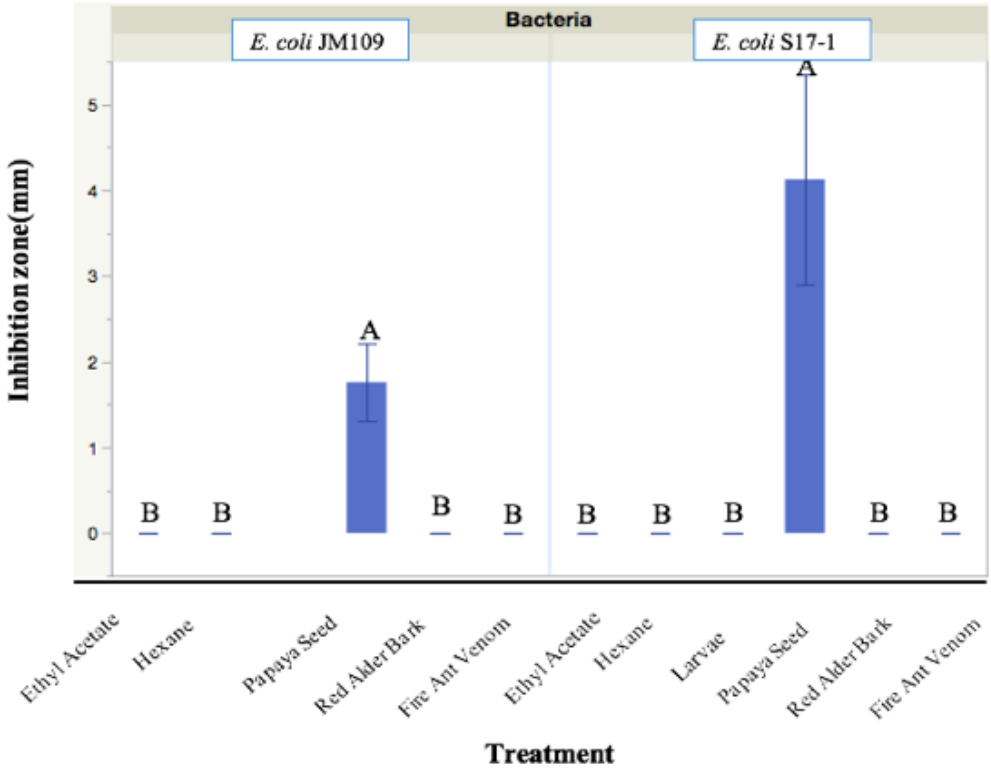

Figure 6: *Mean Zone of Inhibition (mm) by Type of Treatment on E. coli JM109 (nalidixic acid resistant E. coli) and E. coli S17-1 (ampicillin resistant E. coli). Error bars represent 95% confidence intervals. Means sharing the same letter are not significantly different, $\alpha = 0.05$. Ethyl acetate and hexane were used as negative controls. Blowfly larvae was only tested on E. coli S17-1 bacteria.*

2.8. Preservative Assessment

To assess the preservative effects of the papaya seed extract, visual observations were taken each day for a week. Observations on physical appearance such as mold growth on the surface and colour of the strawberries and sole were recorded.

3. Results

3.1. Antibacterial Power Assessment

Our results suggest a significant difference between the papaya seed extract and the other three extracts (Fig. 6; $F(3,72) = 23.9845$, $P = 0.001$). By running a MCT, we see that the papaya seed extract had a far greater impact against the two bacterial strains in comparison to all the other extracts tested (Fig. 6). The papaya seed extract exhibited zones of inhibition on both strains of antibiotic resistant bacteria. The zone of inhibition on the ampicillin resistant *E. coli* had a higher average diameter of 4.43 mm, calculated through all zones found per plate, excluding zones of inhibition of 0

(Fig. 1). In contrast, the papaya seed extracts on the nalidixic resistant bacteria had an average diameter of 1.78 mm. The red alder, fire ant venom, blow fly larvae extracts, and negative controls of ethyl acetate and hexane displayed no zones of inhibitions on both strains of bacteria.

3.2. Preservative Assessment

The strawberry control changed in color but did not have any growth until the fourth day, while the treatment began growing white, fuzzy, fungi characteristics on the third day (Fig. 7). The fish control began to develop dark brown spots during the testing period, while the treatment group experienced no new growths in comparison (Fig. 8).

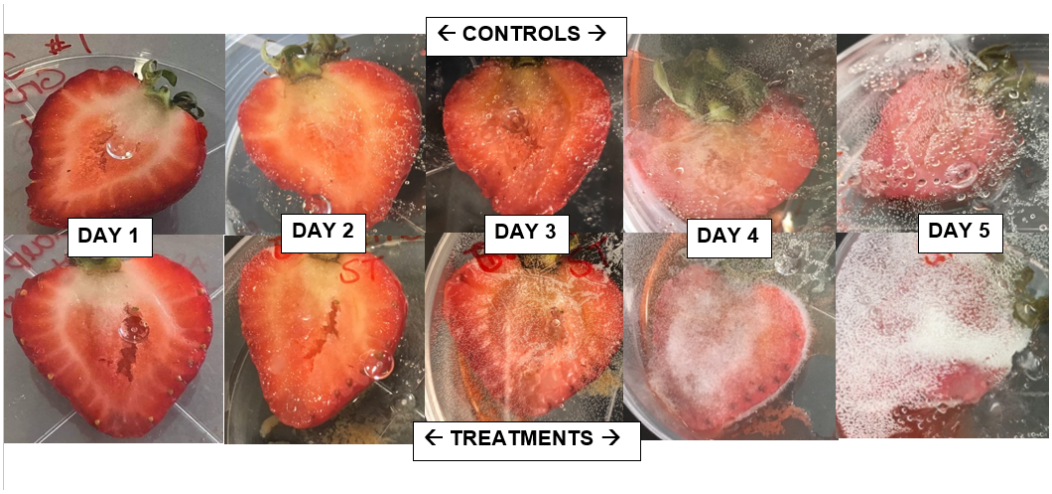

Figure 7: *Treatment and Control of Strawberries for the Duration of Five Days. The treatment (bottom row) strawberry contains 1000 uL of papaya seed extract. The control strawberry (upper row) does not contain papaya seed extract. The treatment strawberry has white fuzz on day four and five. The control strawberry does not have white fuzz on these days.*

4. Discussion

4.1. Antibacterial Power Assessment

Our results suggest that the papaya seed extract has a potential antibacterial effect. The papaya seed extract showed positive results with zones of inhibition on both strains of antibiotic resistant *Escherichia coli*, which suggests that papaya seeds do contain antimicrobial properties that are effective against antibiotic resistant bacteria. The zones of inhibition were lower on the Nalidixic resistant bacteria, which is said to have higher antibiotic resistance. The papaya seed extract being effective may be caused by antimicrobial substrates found in papaya seeds that modify active sites of the target enzymes to inhibit events necessary for bacterial growth [9].

In contrast, the extracts of red alder bark, fire ant venom, and blowfly larvae were not effective at killing bacteria. The negative results may have risen possibly due to the

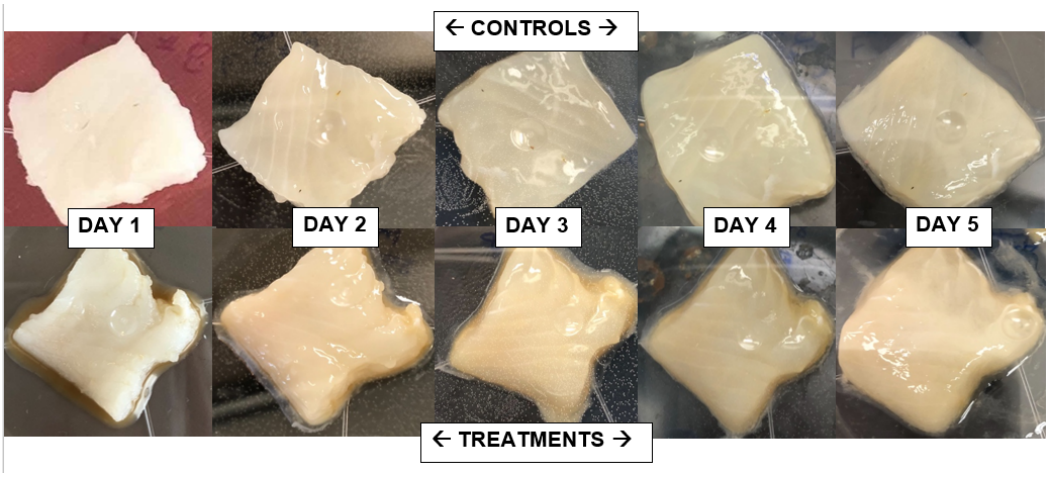

Figure 8: *Treatment Eight and Control Eight of Pacific Sole Fish for the Duration of Five Days. The treatment fish contains 1000 uL of papaya seed extract. The control fish has no papaya seed extract on it. The treatment fish has no spots present. The control fish developed two dark brown dots starting day 2.*

gram-negative bacteria having stable cell walls, which could make it difficult for our extracts to penetrate [9, 10].

Due to resource limitation, we were unable to completely isolate the alkaloid component of the fire ant venom, which is said to be antibacterial [8]. The upper organic phase contains venom alkaloids and cuticular hydrocarbons. Venom alkaloids can be separated from the cuticular hydrocarbons by washing this organic phase with additional hexane through a silica column and then eluting the alkaloids with acetone [8]. This suggests that the fire ant venom may not have any antibacterial properties at all, given the concentration of alkaloids in the amount of venom used. Further experimentation needs to be conducted where the alkaloids in ant venom are isolated and increased in concentration in order to determine the true potential of this substance in terms of a possible antibiotic substitution [11]. Based on the results, the blowfly larvae and red alder extracts were not effective on antibiotic resistant bacteria, as it does not have antibacterial effects on the certain strains of antibiotic resistant bacteria [12]. The secretions of blowfly larvae are expected to contain the antibacterial properties [13]. Due to the resources that were available, the most efficient way to retrieve the antibacterial properties of the blowfly larvae was to homogenize it as a whole. This could have possibly affected the concentration of the antibacterial component of the blowfly larvae leading to the ineffective results. It is also possible that other chemicals that are present in the solution could counteract the effects of the antibacterial chemicals. In red alder bark, the component diarylheptanoids are responsible for antibacterial properties and are the bioactive constituents [14]. The diarylheptanoids contribute antioxidant properties and contribute to inhibitory activity against kappaB activation [14]. Many bacteria activate kappaB pathway and inhibitory property of diarylheptanoids leads to its antibacterial property [14]. It is possible that, due to low concentration of diarylheptanoids in the red alder, it was not effective antibiotic on antibiotic resistant bacteria.

4.2. Preservative Assessment

The treatment sole having fewer or no dark brown dots in comparison to the controls suggests that the papaya seeds extract is antimicrobial as it inhibited the growth of the brown spots. The brown dots could possibly be caused by oxidation, but further experimentation would be necessary to determine this. The papaya seed extracts on the strawberries was not an effective preservative as white growth occurred earlier on the treatment group, possibly because of the added sugar and moisture from the papaya seed extract, which is an essential source for growth and respiration of fungi [15]. Also, the abundance of fungi on our treatment strawberries could be due to papaya seeds having a slightly acidic pH level [16]. This is ideal for fungi growth, but unideal for bacteria due to newly acidic pH level [17]. This suggests that our papaya seed extract may have been effective at inhibiting bacterial growth that is present on food.

Further research could identify the brown dots on the sole and possibly replicate Experiment #2 to account for differences in bacterial concentration. This will guide future experiments done on other foods to replace common chemical preservatives showcasing the power of papaya seed extract and the effects of a single waste product on a major global issue. In addition to the preservative effects the use of natural ingredients with antimicrobial properties such as papaya seeds can be further researched to understand what specific component or molecular contents of the papaya seed contributes to the antimicrobial effect.

5. Acknowledgments

Facilities, equipment, and materials were provided by the Department of Biological Sciences at Simon Fraser University (SFU), as part of BISC 212: Biological Research. Initial development of this course was funded by the Dean of Science Office at SFU, through the INSPIRE program. Technical support and expertise were provided by Cheryl Leonard and Danielle Audas. Fire ants were provided by Jaime Chalissery and blowfly larvae were provided by Regine Gries.

References

[1] Riaz Ullah, Muhammad Yasir, Fehmida Bibi, Turki S. Abujamel, Anwar M. Hashem, Sayed Sartaj Sohrab, Ahmed Al-Ansari, Abdulmohsin A. Al-Sofyani, Ahmed K. Al-Ghamdi, Abdulbasit Al-sieni, and Esam I. Azhar. Taxonomic diversity of antimicrobial-resistant bacteria and genes in the red sea coast. *Science of The Total Environment*, 677:474 – 483, 2019. ISSN 0048-9697. doi:https://doi.org/10.1016/j.scitotenv.2019.04.283. URL http://www.sciencedirect.com/science/article/pii/S0048969719318182.

[2] Milad Kazemi, Faramarz Khodaiyan, and Seyed Saeid Hosseini. Utilization of food processing wastes of eggplant as a high potential pectin source and characterization of extracted pectin. *Food Chemistry*, 294:339 – 346, 2019. ISSN 0308-8146. doi:https://doi.org/10.1016/j.foodchem.2019.05.063. URL http://www.sciencedirect.com/science/article/pii/S0308814619308593.

[3] Ana A. M. Leite, Regina M. D. Nardi, Jacques R. Nicoli, Edmar Chartone-Souza, and Andreacute;a M. A. Nascimento. Carica papaya seed macerate as inhibitor of conjugative r plasmid transfer from salmonella typhimurium to escherichia coli in vitro and in the digestive tract of gnotobiotic mice. *The Journal of General and Applied Microbiology*, 51(1):21–26, 2005. doi:10.2323/jgam.51.21.

[4] Geeta Saxena, Susan Farmer, R. E. W. Hancock, and G. H. N. Towers. Antimicrobial compounds from alnus rubra. *International Journal of Pharmacognosy*, 33 (1):33–36, 1995. doi:10.3109/13880209509088144. URL https://doi.org/10.3109/13880209509088144.

[5] Noor Akbar, Ruqaiyyah Siddiqui, K. A. Sagathevan, and Naveed Ahmed Khan. Gut bacteria of animals/pests living in polluted environments are a potential source of antibacterials. *Applied Microbiology and Biotechnology*, 103(10):3955–3964, May 2019. ISSN 1432-0614. doi:10.1007/s00253-019-09783-2. URL https://doi.org/10.1007/s00253-019-09783-2.

[6] Henry Welch. Antibiotics in food preservation. *Science*, 126(3284):1159–1161, 1957. ISSN 0036-8075. doi:10.1126/science.126.3284.1159. URL https://science.sciencemag.org/content/126/3284/1159.

[7] Hossein Mohammadzadeh-Aghdash, Nader Akbari, Karim Esazadeh, and Jafar Ezzati Nazhad Dolatabadi. Molecular and technical aspects on the interaction of serum albumin with multifunctional food preservatives. *Food Chemistry*, 293:491 – 498, 2019. ISSN 0308-8146. doi:https://doi.org/10.1016/j.foodchem.2019.04.119. URL http://www.sciencedirect.com/science/article/pii/S0308814619307915.

[8] Eduardo Gonçalves Paterson Fox, Daniel Russ Solis, Lucilene Delazari dos Santos, Jose Roberto Aparecido dos Santos Pinto, Anally Ribeiro da Silva Menegasso, Rafael Cardoso Maciel Costa Silva, Mario Sergio Palma, Odair Correa Bueno, and Ednildo de Alcântara Machado. A simple, rapid method for the extraction of whole fire ant venom (insecta: Formicidae: Solenopsis). *Toxicon*, 65:5 – 8, 2013. ISSN 0041-0101. doi:https://doi.org/10.1016/j.toxicon.2012.12.009. URL http://www.sciencedirect.com/science/article/pii/S0041010112008380.

[9] Faisal Rashid Sofi, C. V. Raju, I. P. Lakshmisha, Rajkumar Ratankumar Singh, and All India Coordinated Research Project on Post Harvest Technology. Antioxidant and antimicrobial properties of grape and papaya seed extracts and their application on the preservation of indian mackerel (rastrelliger kanagurta) during ice storage. *Journal of Food Science and Technology*, 53(1):104–117, Jan 2016. ISSN 0975-8402. doi:10.1007/s13197-015-1983-0. URL https://doi.org/10.1007/s13197-015-1983-0.

[10] A T Prasetya, S Mursiti, S Maryan, and N K Jati. Isolation and identification of active compounds from papaya plants and activities as antimicrobial. *IOP Conference Series: Materials Science and Engineering*, 349:012007, apr 2018. doi:10.1088/1757-899x/349/1/012007. URL https://doi.org/10.1088/1757-899x/349/1/012007.

[11] D. P. Jouvenaz, M. S. Blum, and J. G. MacConnell. Antibacterial activity of venom alkaloids from the imported fire ant, solenopsis invicta buren1. *Antimicrobial Agents and Chemotherapy*, 2(4):291–293, 1972. ISSN 0066-4804. doi:10.1128/AAC.2.4.291. URL https://aac.asm.org/content/2/4/291.

[12] Yuan Li, Xiangmei Liu, Lei Tan, Zhenduo Cui, Doudou Jing, Xianjin Yang, Yanqin Liang, Zhaoyang Li, Shengli Zhu, Yufeng Zheng, Kelvin Wai Kwok Yeung, Dong Zheng, Xianbao Wang, and Shuilin Wu. Eradicating multidrug-resistant bacteria rapidly using a multi functional g-c3n4@ bi2s3 nanorod heterojunction with or without antibiotics. *Advanced Functional Materials*, 29(20):1900946, 2019. doi:https://doi.org/10.1002/adfm.201900946. URL https://onlinelibrary.wiley.com/doi/abs/10.1002/adfm.201900946.

[13] A. Kerridge, H. Lappin-Scott, and J. R. Stevens. Antibacterial properties of larval secretions of the blowfly, lucilia sericata. *Medical and Veterinary Entomology*, 19(3): 333–337, 2005. doi:https://doi.org/10.1111/j.1365-2915.2005.00577.x. URL https://onlinelibrary.wiley.com/doi/abs/10.1111/j.1365-2915.2005.00577.x.

[14] Sushil Chandra Sati, Nitin Sati, and O. P. Sati. Bioactive constituents and medicinal importance of genus alnus. *Pharmacognosy reviews*, 5(10):174–183, Jul 2011. ISSN 0976-2787. doi:10.4103/0973-7847.91115. URL https://pubmed.ncbi.nlm.nih.gov/22279375. 22279375[pmid].

[15] JM Brannon. Influence of glucose and fructose on growth of fungi. *Botanical Gazette*, 76(3):257–273, 1923.

[16] Cláudia Mendes dos Santos, Celeste Maria Patto de Abreu, Juliana Mesquita Freire, Estela de Rezende Queiroz, and Marcelle Mendes Mendon Asa. Chemical characterization of the flour of peel and seed from two papaya cultivars. *Food Science and Technology*, 34:353 – 357, 06 2014. ISSN 0101-2061. URL http://www.scielo.br/scielo.php?script=sci_arttext&pid=S0101-20612014000200020&nrm=iso.

[17] M.O. Moss. Fungi, quality and safety issues in fresh fruits and vegetables. *Journal of Applied Microbiology*, 104(5):1239–1243, 2008. doi:https://doi.org/10.1111/j.1365-2672.2007.03705.x. URL https://sfamjournals.onlinelibrary.wiley.com/doi/abs/10.1111/j.1365-2672.2007.03705.x.

SFU SURJ | SIMON FRASER UNIVERSITY SCIENCE UNDERGRADUATE RESEARCH JOURNAL
Vol. 5 (2019-20)

Shocking Results: Investigating the Effects of Direct Current on Copper's Antimicrobial Properties with Applications in Self-Sterilizing Surfaces

Chirag Chopra[1]*, Sharon K. Malhi[1]*, Liam Marshall[1], Eric Chen[1], Blake Daniels[1], Kevin Lam[1] †

[1]Simon Fraser University, *Department of Biological Sciences*

Abstract

Metallic copper has historically been recognized for its antimicrobial properties [1]. Recent research undermines copper's use as a 'self-sterilizing' surface due to bacterial resistance to copper's lysis mechanisms. In response to this burgeoning resistance, we sought to find an innovative method to enhance copper's antimicrobial effects, to reinstate copper as an effective self-sterilizing surface. Research suggests that copper lyses bacteria through a process called cationic lysis, where copper releases cations into its surrounding environment thereby disrupting cellular processes. We hypothesize that by applying a direct current to copper, we can amplify this effect. To test the effects of a direct electrical current through a piece of copper metal on the lysis of *Escherichia coli* ATCC 113303, we ran 9 milliamps of current through 3 by 4 cm copper plates for 15 minutes. We found there were significantly lower colony counts observed on copper plates with the added current compared to copper plates alone. This suggests that the administration of current can be an innovative and effective way to enhance copper's lysis mechanisms. The results indicate that current and copper can be used in conjunction to create a self-sterilizing surface that is significantly more effective than copper alone. This study proposes two novel 'current-copper conjugate' bacterial lysis mechanisms that attempt to explain the observed results.

Keywords — Transmembrane Potential, Escherichia Coli ATCC 11303, Cationic Bacterial Lysis, Self-Sterilizing Surfaces, Antibacterial Resistance

1. Introduction

Frequently used touch surfaces can be highly contaminated with infectious bacteria [1]. Relatively recently, bacterial strains found on these touch surfaces have shown increased resistance to antibiotic compounds in contemporary antibacterial cleaning supplies [2]. A wide array of these cleaning products, commonly used in clinical and non-clinical settings alike, are found to contain broad-spectrum antibiotic additives such as triclosan [2]. In a lab study, the excessive and repetitive use of triclosan in Staphylococcus aureus samples has been linked to supporting the growth of strains that require higher inhibitory concentrations of the additive to be lysed. The

*Equal First Authorship
†Corresponding Author. Contact: klamf@sfu.ca

researchers extrapolated the bacteria's decreased susceptibility to triclosan likely also means a decreased susceptibility to other similar antibiotics and antimicrobial additives [3]. In their review article, Meek, Vyas and Piddock [4] go further in describing that the careless use of antibiotic cleaning supplies creates stressful environments for bacteria in which they are spurred to replicate and transfer plasmids more effectively. The article points out that in naturally occurring bacterial populations, a minority of bacteria are antibiotic-resistant and a lack of environmental stresses which foster plasmid transfer keeps the resistant population in check. As soon as a selective pressure for the resistant strain is applied (e.g. use of antibiotic compounds), resistant bacterial presence increases due to the increased environmental stress conducive for plasmid transfer between bacteria, transferring the resistance horizontally within the same generation which ultimately ensures the vertical transfer of antibiotic-resistant chromosomal mutations [4]. Thus, through these mechanisms, the improper use of antibacterial cleaning supplies is shown to dramatically increase the presence of resistant bacterial species where they pose immediate threats to human well-being [4].

It is due to these issues that the use of self-sterilizing surfaces such as copper have been popularized. Copper proves to be a more effective antimicrobial substance than additives found in cleaning supplies as it employs a different approach to lysing bacteria. At a time where antibiotic resistance is on the rise and the production of new antibiotics is unsustainable, copper's lysis mechanisms provide a new realm of understanding where creating novel methods to support the fight against infectious bacterial strains is possible [5]. Consequently, copper has been widely researched for its lysis mechanisms and evaluated for its use in 'self-sterilizing' surfaces [6]. Research suggests that the core characteristic of copper, which results in its antibiotic properties, is its inherent ability to release copper cations [6]. The cations released from copper metal are strong oxidizing agents [1]. If they hit building blocks of the cell membrane, they can cause localized reductions by 'stealing' electrons and destroying the lipid and protein structures [1]. As well, concentrations of copper compete with other metal ions that play important roles in protein binding sites and displace iron from iron-sulphur clusters [7]. The cell membrane ruptures because of this oxidative stress, leading to loss of membrane potential and cytoplasmic content. Grass et. al. found that copper metal initiates a Fenton-like reaction and forms hydroxyl radicals which in turn damage cellular macromolecules and processes, like the cross-linking of peptidoglycan chains in bacterial cell walls. These radicals also play a part in the degradation of genomic and plasmid DNA, completing the process of bacterial lysis [1]. It is important to note that copper can also prove to be cytotoxic to larger organisms, such as humans, due to the non-specificity of its lysis mechanisms to all plasma membranes. Through similar mechanisms as listed above, copper can cause cellular damage leading to the disruption of biological systems, hence it is important to consider the benefits of its antimicrobial properties versus copper's potential cytotoxicity.

Nevertheless, scientists have also long been recording instances of strains resistant to cationic lysis with some cases even resulting in human infection [8, 9]. Systems of resistance to copper in bacteria occur in a variety of ways, usually stemming from a chromosomal or plasmidal origin [10]. Mechanisms that bacteria use to resist oxidation by copper cations include reduced copper transport, enhanced efflux of cupric ions, or

copper complexation by cell components [11].

Despite the above-mentioned bacterial resistance, copper still proves to be a relatively unexplored frontier of research where innovation in improving its antimicrobial capabilities can be made. Whereas, in the field of traditional antibiotic compounds, the discovery of new antibiotics is slowly coming to a halt and proving to be unsustainable. This study aims to test and propose the basic principles for a new method of increasing copper's self-sterilizing properties making the conjugate more potent than copper metal alone. Our study puts this aim into practice by administering 9 milliamps (mA) of direct electrical current, the highest amount of current a person can safely withstand [12], through a copper surface inoculated with *Escherichia coli*. We hypothesize that the application of the current will amplify the release of cations, thereby resulting in a more efficient and effective decimation of bacterial populations via cationic lysis mechanisms [1].

2. Materials and Methods

These methods are adapted from Douha et al. [13].

2.1. Preparation of the Bacterial Broth

To prepare our bacterial strain, one colony of *Escherichia coli* ATCC 11303 was picked up from a stock plate using a sterile inoculating loop and introduced into 10 mL of tryptic soy broth (TSB) in a test tube. The tube was incubated at 37 °C and 200 rpm for 22 hours (Forma Scientific IN2-MIC E-63 incubator) to grow the colony. This procedure was conducted under a biosafety cabinet to limit the possibility of contamination.

2.2. Preparation of the Copper Plates

hree C110 copper squares (3 cm x 4 cm, the thickness of 0.064 inches, 99.9% pure copper obtained from Metal Supermarket), all one year old with minor oxidation, were initially exposed to an acid wash. To remove some oxidation and expose the pure copper underneath, the copper pieces were submerged in glacial acetic acid for 15 seconds, removed from the acid and then washed with distilled water. The copper pieces were wiped with disposable towels and then allowed to air dry for 30 minutes to ensure the removal of all acid and water. Each copper piece was then placed individually in a glass petri dish and autoclaved. When not in use, petri dishes were para-filmed and placed in a covered drawer to prevent contamination.

2.3. Treatment Conditions

The circuit was set up (Refer to Fig. 1) and the copper squares were hooked up to the circuit using sanitized crocodile leads, which were submerged in 95% ethanol for 15 seconds and flamed to remove excess ethanol. The potentiometer (Bourns Rotary Potentiometer, PDB181 Series) and 1000-ohm resistors were set to work together to draw 9 milliamps of current from a President's Choice 9 V battery. The battery and RoHS (Restriction of Hazardous Substances Directive) compliant wires with crocodile leads

(Batch 50123) were used. The ammeter, resistor and potentiometer were all obtained from SFU's science stores.

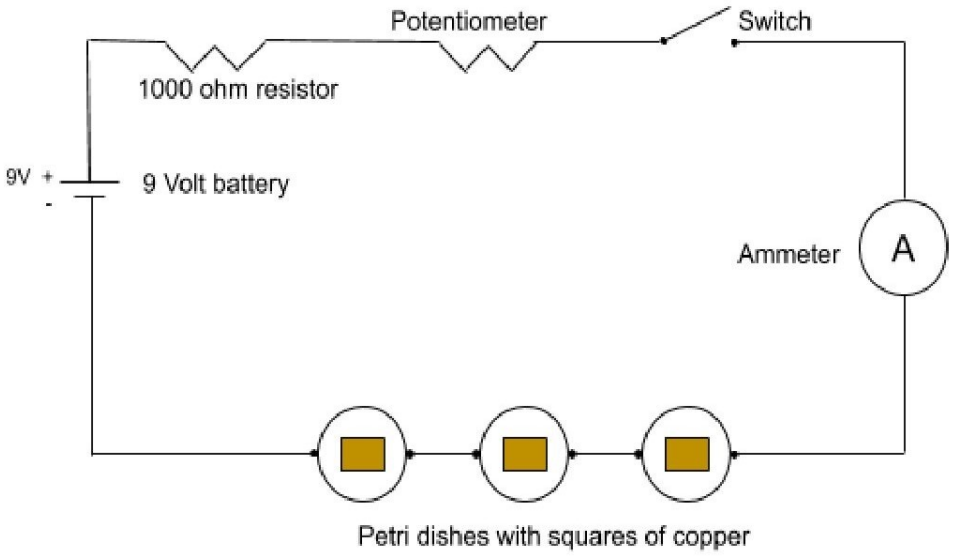

Figure 1: *Setup of the circuit for treatment and control trials. The potentiometer was set to its highest setting and the setting was shifted throughout the replicates to ensure the amperage remained consistent at 9 mA. In the control setup, the switch was turned to the OFF position (as shown) and in the treatment setup, the switch was turned ON.*

Using a P100 pipette, 10 microliters of the *E. coli* broth were pipetted on to each copper square and a plastic inoculation loop was used to spread the broth over the copper, except the corners where the clips were attached [13]. The switch was turned to the 'on' position and a timer was started for 15 minutes. Douha et al 2018 found very little lytic effects of copper at 1 minute and almost a total reduction of bacteria colonies at 30 minutes, hence a median time of 15 minutes was chosen as exposure time for this study. Additionally, preliminary tests determined that a 15-minute exposure to 9 milliamps of current on our copper pieces did not increase temperature or visible change in the structure of metallic properties. It was also ensured by visual observation that the copper remained wet throughout the electrical exposure and at a consistent temperature of 21 °C measured at 2-minute intervals using a laser temperature gun (HDE-B01). When the timer ended, the switch was turned off and using an autoclaved Puritan cotton-tipped applicator, we swabbed the copper square by swiping five times across without turning the swab to determine if any *E. coli* remained on the surface. Immediately, the applicators were put into one millilitre of TSB and swirled for 30 seconds to dislodge the bacteria into the broth. The broth then underwent three 10× serial dilutions and 100 microliters of each diluted broth were plated on tryptic soy agar (TSA) using the spread plate technique to quantify the level of *E. coli* remaining on the copper. After incubation for 24 hours at 37 °C (Forma Scientific IN2-MIC E-63 incubator), colony-forming units were then counted. A total of ten replicates were run.

2.4. Control Conditions

The controls were run similarly to the above description of the treatment trials, but without the application of current. Copper squares in petri dishes were inoculated with 10 microliters of *E. coli* broth and spread. The copper was still hooked to the circuit with sterilized crocodile leads attached, but the switch was placed in the off position for the entirety of the trial. The copper and broth were allowed to interact for 15 minutes and then were swabbed and diluted similar to the treatments. The temperature was kept consistent at 21 degrees Celsius and the copper was visually ensured to remain wet throughout the exposure time. The dilutions were plated on TSA and then counted. A total of six replicates were run.

Results from Douha et al.'s negative control condition establish that copper alone is more efficient than stainless steel at reducing bacterial colony counts over any time period [13]. Due to identical methods between this study and Douha et al., their negative control condition results were extrapolated to also be applicable in our investigation.

2.5. Statistical Analysis

For each of our agar plates, we converted the number of visible colonies into colony-forming units per mL of the original inoculum. We then graphed the log of mean colony forming units (with 95% confidence intervals shown as error bars) of both copper with and without 9 mA of current. Log counts were used to normalize large and small CFUs into a nominal scale.

Statistical tests were performed on original, non-logarithmic data.

3. Results

Colony counts of *E. coli* found on copper plates with the added current were fewer than the counts observed on copper plates without direct current. A statistical F-test was completed to determine the p-value and it was found to be less than 0.05 (Fig. 2; $F(1, 14) = 46.69$, $p < 0.0001$). Due to this statistical confidence, we can say that the colony counts on the copper alone are significantly higher than on the copper with 9 mA of current.

In this study, a titre of the original broth used to inoculate the copper squares could have been completed to determine the density of the original inoculum to enhance replicability and more strongly link the data as a result of bacterial lysis. However, since the exposure time was less than *E. coli*'s average doubling time, we can say that the reduction in colony-forming units in the treatment versus control conditions can be attributed to bacterial lysis since the bacteria likely did not have enough time to proliferate. Regardless, it is recommended that future studies complete an original titre to determine inoculum density and compare initial versus post-exposure inoculum densities to also determine a percentage reduction in the bacterial count and compare with existing literature.

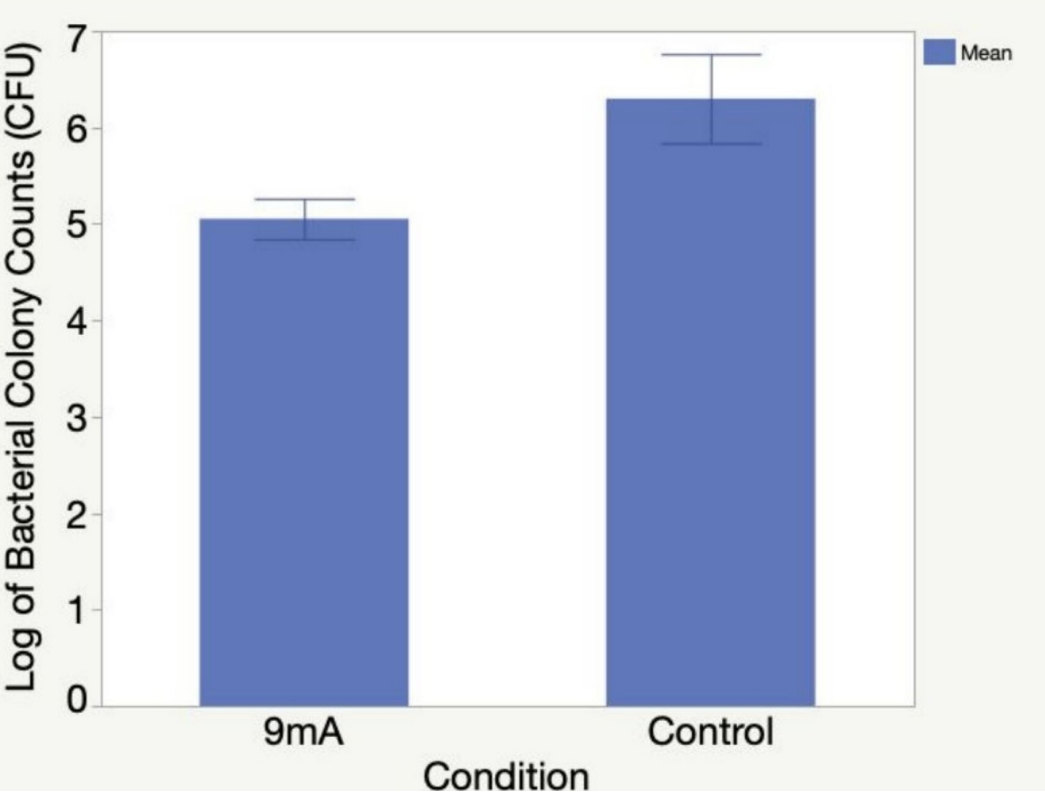

Figure 2: *Mean Escherichia coli strain ATCC 11303 colonies present on copper with and without application of 9 mA of current. The value shown is the logarithm of the mean colony forming units per millilitre. The error bars represent the 95% confidence intervals.*

4. Discussion

Before proceeding to discuss the results of the study and proposing possible mechanisms of lysis, we must briefly discuss the prevalent dry-contact or dissolved cationic basis of microbe destruction debate in the field of heavy metal mediated bacterial lysis. Studies have shown conflicting proposed mechanisms where some claim dry and direct contact between the bacterium and the metal surface is necessary for lysing mechanisms to occur while others claim that an aqueous solution of copper cations is required [14, 15]. The pieces of copper in our treatment were coated with a TSB broth and the bacteria were therefore in an aqueous environment. Although our methodology does not allow us to make specific claims on how or why the aqueous environment is conducive to copper's cationic lysis mechanisms as we did not compare aqueous and dry environments; we can simply state with a reasonable degree of certainty that cationic lysis is possible in aqueous environments and seems to be enhanced by the addition of low currents of electricity. Our results suggest that applying 9 mA of current for fifteen minutes to copper metal results in significantly decreased *E. coli* bacterial counts, compared to the trials on copper without current. Copper metal and an electrical current independently have antibacterial properties [1]. Studies show that copper kills bacteria via a three-pronged attack: oxidative damage of bacterial

membrane, metabolic disruption, and eventual degradation of metabolic processes [1]. Additionally, electric currents generate electric fields that are known to 'charge' the lipid membranes of bacteria disrupting the organism's transmembrane potential [16]. We believe that in the case of our experimental setup where current and copper are working in conjunction, the current plays a supporting role to the lysing mechanisms of copper. Due to the small amount of current applied and the absence of an effective opposing charge in the setup, the likelihood of an electric field is generated that could lyse bacteria on its own is minuscule. We theorize that the multitude of mechanisms already mentioned previously in the paper, conjugated with the two novel mechanisms further proposed in this study, likely played a role in producing the effects we see in our results.

The first novel copper-current conjugate bacterial lysis mechanism that we believe may have occurred, is based on the fact that adding current forces the conducting electrons metallic bonds to move faster unidirectionally [17]. We postulate that when these electrons eventually collide with vibrating cations in the metal, the cations absorb the kinetic energy and are more likely to break their bonds and be released, therefore lysing the cell as the released cations perform the same function as described earlier: oxidative damage of the cellular membrane, metabolic disruption and eventual degradation of metabolic processes [1]. On the other hand, copper cations without the added current are likely to lack the extra kinetic energy provided to the electrons and release cations into an aqueous environment at a lower rate.

Furthermore, our second proposed mechanism is based on an interaction between the current, the copper pieces and their aqueous environment (TSB). In this case, we believe the tryptic soy broth functioned as an electrolyte, as it is inherently composed of a very high ionic concentration. The broth, acting as an electrolyte, conducted some of the current moving through the piece of copper into the aqueous environment and the vicinity of the *E. coli*. Knowledge of how electricity interacts with bacteria is still quite unclear. However, an aspect that has been studied is bacterial conductivity with many strains of bacteria using sensitive electron balances and applying the concept of electroneutrality as a conduit for controlling cellular osmolarity [18]. Intact cells of *Streptococcus faecalis* were found to have electric conductivities of 0.90 mho/m - a number that reflects movements of ions both within the cytoplasm and the cell wall space [19]. We believe that the introduction of electrons near the cell wall and perhaps even within the cell will disrupt the transmembrane potential by disturbing the ionic balance. Without a proper membrane potential and ionic balance, the bacterium fails to uptake and release ions efficiently which hampers vital cell processes.

Evidently, many mechanisms of bacterial lysis attributed to both electrical currents and copper metal, individually and in combination, work in tandem to produce the results we obtained. There is a clearly urgent need for future research to corroborate or provide definite evidence for any of these mechanisms with future research focusing on producing a concrete understanding of the relationship between kill-times, amperages, and types of bacteria. Other types of microorganisms and metals could also be tested. Additionally, a substantial concern for applications of such research in future technologies is copper's cytotoxicity. Before developing enhanced self-sterilizing surface technologies, there is a need to investigate copper's cytotoxic effects in humans.

Innovations in material science must collaborate with these theories to mitigate these concerns whilst preserving copper's antimicrobial effects. Long exposures to low currents, or novel materials that regulate cation release could considerably minimize cytotoxic effects.

A newly identified coronavirus, SARS-CoV-2, has caused a worldwide pandemic of respiratory illness, called COVID-19 [20]. Medical professionals are urgently trying to slow the spread, which can occur by touch if an infected person has used their hands to touch their nose or mouth, making doorknobs and other touch surfaces potential sources of infection [20]. Some studies have shown that copper and current are effective at viral deactivation on MS2 bacteriophages and Influenza A viruses after extended exposure times [7, 21]. Although more research is required specific to the SARS-CoV-2 virus, we can see the potential applicability of copper and current conjunction in preventing similar viral disease outbreaks, which could be a boost to public health efforts as well.

5. Conclusion

Our results suggest that the administration of some current to a copper surface can result in the efficient destruction of gram-negative bacteria, such as *Escherichia coli* (strain ATCC 11303). This concept can be applied in the ground-breaking field of self-sterilizing surfaces. Our study tested the effects of 9 mA of current on bacterial counts after just fifteen minutes. With promising results from low currents, we believe this concept can be applied as a novel solution against bacterial resistance in clinical and non-clinical settings alike.

6. Acknowledgments

We would like to give our sincere thanks to Dr. Andrew Debenidictus for his help and guidance in developing our proposed mechanisms. We also extend our gratitude to Dr. William Ruth for his guidance in the statistics portion of our study. Facilities, equipment, and materials were provided by the Department of Biological Sciences at Simon Fraser University (SFU), as part of BISC 212, a Special Topics Biological Research course. The initial development of this course was funded by the Dean of Science Office at SFU, through the INSPIRE program. Technical support and expertise were provided by Cheryl Leonard. Equipment and guidance for setting up circuitry and using equipment such as the multimeter and potentiometer were provided by Anthony Slater. We are grateful to these individuals and organizations for supporting us throughout this project.

References

[1] Gregor Grass, Christopher Rensing, and Marc Solioz. Metallic copper as an antimicrobial surface. *Applied and Environmental Microbiology*, 77(5):1541–1547,

2011. ISSN 0099-2240. doi:10.1128/AEM.02766-10. URL https://aem.asm.org/content/77/5/1541.

[2] Allison E Aiello, Bonnie Marshall, Stuart B Levy, Phyllis Della-Latta, Susan X Lin, and Elaine Larson. Antibacterial cleaning products and drug resistance. *Emerging infectious diseases*, 11(10):1565, 2005.

[3] M. T. Suller and A. D. Russell. Triclosan and antibiotic resistance in Staphylococcus aureus. *J Antimicrob Chemother*, 46(1):11–18, Jul 2000.

[4] Richard William Meek, Hrushi Vyas, and Laura Jane Violet Piddock. Nonmedical uses of antibiotics: time to restrict their use? *PLoS Biol*, 13(10):e1002266, 2015.

[5] Emily Litvack. Exploring copper's potential as antibiotic, Apr 2019. URL https://news.arizona.edu/story/exploring-coppers-potential-antibiotic.

[6] David J. Weber and William A. Rutala. Self-disinfecting surfaces: Review of current methodologies and future prospects. *American Journal of Infection Control*, 41(5, Supplement):S31 – S35, 2013. ISSN 0196-6553. doi:https://doi.org/10.1016/j.ajic.2012.12.005. URL http://www.sciencedirect.com/science/article/pii/S0196655313000114. Disinfection, Sterilization and Antisepsis: Current Issues, New Research and New Technologies.

[7] Michael Versoza, Wonseok Jung, Mona Loraine Barabad, Sangwon Ko, Minjeong Kim, and Duckshin Park. Reduction of escherichia coli using metal plates with the influenced of applied low current and physical barrier of filter layers. *International Journal of Environmental Research and Public Health*, 16(20), 2019. ISSN 1660-4601. doi:10.3390/ijerph16203887. URL https://www.mdpi.com/1660-4601/16/20/3887.

[8] C Haefeli, C Franklin, and K Hardy. Plasmid-determined silver resistance in pseudomonas stutzeri isolated from a silver mine. *Journal of Bacteriology*, 158(1): 389–392, 1984. ISSN 0021-9193. URL https://jb.asm.org/content/158/1/389.

[9] T J Tetaz and R K Luke. Plasmid-controlled resistance to copper in escherichia coli. *Journal of Bacteriology*, 154(3):1263–1268, 1983. ISSN 0021-9193. URL https://jb.asm.org/content/154/3/1263.

[10] Cathrin Dressler, Ursula Kües, Dietrich H. Nies, and Bärbel Friedrich. Determinants encoding resistance to several heavy metals in newly isolated copper-resistant bacteria. *Applied and Environmental Microbiology*, 57(11):3079–3085, 1991. ISSN 0099-2240. URL https://aem.asm.org/content/57/11/3079.

[11] Carlos Cervantes and Felix Gutierrez-Corona. Copper resistance mechanisms in bacteria and fungi. *FEMS Microbiology Reviews*, 14(2):121–137, 06 1994. ISSN 0168-6445. doi:10.1111/j.1574-6976.1994.tb00083.x. URL https://doi.org/10.1111/j.1574-6976.1994.tb00083.x.

[12] Emily Litvack. Exploring copper's potential as antibiotic, Apr 2019. URL https://news.arizona.edu/story/exploring-coppers-potential-antibiotic.

[13] Samantha Douha, Emma LaCroix, Erin McLelland-Asu, Melissa Vermette, Kirsten A Wilcox, and Kevin Lam. The influence of surface scratches on copper's antibacterial activity. *SFU SURJ*, 3:23–33, 2018. URL https://journals.sfu.ca/sfusurj/index.php/journal/article/view/47/34.

[14] Salima Mathews, Michael Hans, Frank Mücklich, and Marc Solioz. Contact killing of bacteria on copper is suppressed if bacterial-metal contact is prevented and is induced on iron by copper ions. *Applied and Environmental Microbiology*, 79 (8):2605–2611, 2013. ISSN 0099-2240. doi:10.1128/AEM.03608-12. URL https://aem.asm.org/content/79/8/2605.

[15] Marco Zeiger, Marc Solioz, Hervais Edongué, Eduard Arzt, and Andreas S. Schneider. Surface structure influences contact killing of bacteria by copper. *MicrobiologyOpen*, 3(3):327–332, 2014. doi:https://doi.org/10.1002/mbo3.170. URL https://onlinelibrary.wiley.com/doi/abs/10.1002/mbo3.170.

[16] Kevin P Drees, Morteza Abbaszadegan, and Raina M Maier. Comparative electrochemical inactivation of bacteria and bacteriophage. *Water Research*, 37 (10):2291 – 2300, 2003. ISSN 0043-1354. doi:https://doi.org/10.1016/S0043-1354(03)00009-5. URL http://www.sciencedirect.com/science/article/pii/S0043135403000095.

[17] *Chemical Principles, publisher=Cengage Learning Pte Ltd., author=Zumdahl, Steven S. and DeCoste, Donald J., year=2017.*

[18] Janet M. Wood. Osmosensing by bacteria: Signals and membrane-based sensors. *Microbiology and Molecular Biology Reviews*, 63(1):230–262, 1999. ISSN 1092-2172. doi:10.1128/MMBR.63.1.230-262.1999. URL https://mmbr.asm.org/content/63/1/230.

[19] Robert E. Marquis and Edwin L. Carstensen. Electric conductivity and internal osmolality of intact bacterial cells. *Journal of Bacteriology*, 113(3):1198–1206, 1973. ISSN 0021-9193. URL https://jb.asm.org/content/113/3/1198.

[20] Lauren M. Sauer. What is coronavirus? URL https://www.hopkinsmedicine.org/health/conditions-and-diseases/coronavirus.

[21] J. O. Noyce, H. Michels, and C. W. Keevil. Inactivation of influenza a virus on copper versus stainless steel surfaces. *Applied and Environmental Microbiology*, 73 (8):2748–2750, 2007. ISSN 0099-2240. doi:10.1128/AEM.01139-06. URL https://aem.asm.org/content/73/8/2748.

SFU SURJ | SIMON FRASER UNIVERSITY SCIENCE UNDERGRADUATE RESEARCH JOURNAL
Vol. 5 (2019-20)

The Effect of an Ethyl Acetate Extract of Frozen Cranberries Mixed with Amphotericin B as a Growth Inhibitor of *Mucor racemosus*

Jonson Lee[1*], Kyle Newcomb[2*], Jaikaran Sanghera[3*], Caleb Ten[4*], Blake Danis[1], Kevin Lam[1 †]

[1]Simon Fraser University, *Department of Biological Sciences*
[2]Simon Fraser University, *Department of Molecular Biology and Biochemistry*
[3]Simon Fraser University, *Department of Biomedical Physiology and Kinesiology*
[4]Simon Fraser University, *Department of Psychology*

Abstract

Fungal diseases cause billions of dollars in agricultural damage and around one and a half million human deaths each year. To combat this emerging threat, scientists focus on researching ways to improve the effects of current antifungal treatments. Cranberries contain a compound, proanthocyanidin, that is known to kill and reduce the spread of pathogenic fungi infections in human epidermal tissue. However, the use of a general cranberry extract to assist an antifungal agent on fungal fruit infections, such as Mucor rot, has not been heavily studied. By performing three experiments, we studied whether an ethyl acetate extract of frozen cranberries can inhibit the growth of and/or kill *M. racemosus*, as well as whether the extract would degrade at room temperature. A mixture of equal parts extract and amphotericin B were shown to be significantly more effective at inhibiting the growth of the fungi. The extract was shown to degrade significantly when left at room temperature in a sealed container, based on data from the same treatment groups 10 days apart. The data shows that an ethyl acetate extract of frozen cranberries can be used to increase the efficacy of antifungal agents, but storage methods need to be studied to lengthen the half-life.

Keywords — Proanthocyanidin, Vaccinium macrocarpon, Mucormycosis, Mucor Rot, Fungal diseases

1. Introduction

Fungal Fungal diseases are a threat with few current countermeasures in place to arrest their spread [1, 2, 3]. Currently, fungal infections destroy 125 million tonnes of food crops each year and are increasingly being recognized as a worldwide threat to food security [2]. This threat is predicted to expand due to accidental introductions of pathogenic fungi through global agricultural transportation, which is necessary to sustain an ever-growing population around the globe [4, 5]. Studies to combat this emerging threat prioritize inhibiting antifungal resistance properties of fungi to improve the effects of antifungal treatments [6].

*Equal First Authorship
†Corresponding Author. Contact: klamf@sfu.ca

One such fungal disease is *Mucor* rot, which infects fruits such as apples, pears, and tomatoes [7, 8, 9]. The infection originates at the calyx end of the fruit or at wound punctures and matures inside the soft tissue of the fruit [7, 8, 9]. *Mucor* rot is caused by several *Mucor* species including the model organism for our research, *Mucor racemosus*.

Humans are also susceptible to fungal diseases, which account for around one and a half million deaths every year [1, 3, 10]. Mucormycosis is a fungal disease with a high mortality rate that can affect immunocompromised individuals and can be caused by Mucor species, including *M. racemosus* [11]. Mucormycosis can be treated by the intravenous administration of amphotericin B (AB), which has remained effective since its initial synthesis because fungal infections treated with AB do not develop antifungal resistance to this drug due to the phenotypic consequences of doing so [12]. Any AB resistance capable mutations lead to severe growth deficiencies, limiting fitness levels of carriers [12]. Early-stage treatment of mucormycosis is limited by AB's dose-dependent nephrotoxicity [13, 14]. Proanthocyanidin (PAC) is a compound that is found in higher concentrations in cranberries (418.8 ± 75.3 mg/L) relative to its other common dietary sources [15]. PAC has shown to be an effective antifungal agent at inhibiting the growth of *Candida albicans*, which can cause epithelial tissue infections in humans [16, 17, 18, 19]. PAC works by inhibiting *C. albicans*' ability to adhere to human epithelial tissue and preventing the formation of biofilms [**?**]. This stops *C. albicans* from obtaining nutrients from the tissue or spreading to other areas on the host. Severe epidermal *C. albicans* infections in humans, such as candidiasis, can also be treated with AB using the same dosage precautions as treatment of mucormycosis due to the nephrotoxicity risk [13, 14, 19].

Use of PAC-containing grape seed extracts have been shown to have a synergistic effect when used in tandem with AB at reducing *C. albicans* growth [20, 21]. We hypothesize that an ethyl acetate extract of frozen cranberries (CE) mixed with equal parts AB will inhibit the growth of *M. racemosus* more effectively than either CE or AB on their own [21]. If so, we predict that if we run a disk diffusion assay on a grown culture of *M. racemosus*, using the same solute concentrations as in experiment 1, the disk saturated in a mixture of CE and AB should be more effective than the disk saturated in AB. Furthermore, we hypothesize that increasing the ratio of CE to AB to 300:30 uL should be more effective than a 30:30 uL ratio of CE and AB. This experiment will also test the stability of CE over 10 days.

2. Materials and Methods

2.1. Experimental Design

We conducted three experiments to compare the use of an ethyl acetate extract of cranberries (CE) as an antifungal agent against *M. racemosus* grown on potato dextrose agar (PDA). We used amphotericin B (AB; Thermo Fisher, 15290026; 6 mL, 32 mg/mL) as our positive control to compare the zones of inhibition against CE on its own and mixtures of CE and AB. The ratios used were determined by the loading capacity for the filter paper disks that were used. Ethyl acetate was used as the negative control for all experiments. Our initial experiment was designed to determine if a mixture of

30:30 uL of CE and AB was more effective than 30 uL of AB at inhibiting the growth of *M. racemosus*. The second experiment was to determine if a mixture of 30:30 uL of CE and AB could be applied to a filter paper disk to kill *M. racemosus* mycelia. This would be measured by how far the filter paper disks had sunk into the mycelia. The final experiment was to determine if increasing the concentration of CE in the CE and AB mixture to a 300:30 uL ratio would increase the inhibitory effects on growing *M. racemosus* compared to a 30:30 uL mixture and 30 uL of AB.

The first stock plate of *M. racemosus* was provided by SFU's Department of Biology. We inoculated a new stock plate each week to control for the culture's age. Each experiment began with the inoculation of petri dishes using forceps to place a pinch (maximum 2x2 mm^2) of *M. racemosus* mycelia on the agar at the center of each dish (Fig. 1).

Each petri dish used was divided into quadrants which were labelled for their respective solutions. For Experiments 1 and 3, we pipetted our solutions directly onto the agar in 20 mm arcs, 5 mm from the edge of the plate. We used direct application of the solutions to better visualize the zones of inhibition and relative growth rate of the fungus around the treatment zone. Experiment 2 required us to apply the solutions to quadrants via filter paper disks because pipetting directly onto the fungus could outright kill it due to the ethyl acetate.

2.2. Ethyl Acetate Extract of Frozen Cranberries (CE) Preparation

We scooped 44.65 g of President's Choice®frozen cranberries (Loblaws Inc., # 06038399388) into a stone mortar and pestle and ground them into a pulp. The pulp was transferred to a 125 mL glass media bottle (DWK Life Sciences, # 219455) along with 36.1 mL of ethyl acetate (SFU, Department of Biology), with the meniscus just 1-2 mm above the cranberry pulp [21]. The bottle was then sealed with parafilm and vortexed (Maxi Mix II, Thermo Scientific, M37615; 300 rpm) for 10 minutes, then shaken and inverted by hand for 5 minutes. We moved the bottle to an incubator shaker (Barnstead MaxQ 4000, Thermo Scientific, SHKE4000-7; 200 rpm at 27.7°C – 28.4°C) for 19 hours [20].

Using an Eppendorf 5810 centrifuge, we spun four falcon tubes containing CE for 10 minutes at 1100 rpm. We retrieved 15-16 mL of CE supernatant from the tubes. The CE was divided into 3-3.5 mL aliquots among five 15 mL scintillation vials. These vials were left unsealed to allow the ethyl acetate to evaporate and concentrate the extract.

The CE evaporated for 13 hours and 7 minutes at 21°C and the extract was sterilized by pipetting it through a syringe filter (Thermo Scientific, F2513-2) into a new 15 mL scintillation vial and sealed the vial with parafilm. 12 mL of CE remained from the 15-16 mL retrieved.

2.3. Experiment 1: Comparison of a Mixture of 30:30 uL CE + Amphotericin B (AB) to 30 uL of AB on *M. racemosus*

Each petri dish was divided into quadrants and had the solutions pipetted onto the agar in the respective quadrant (Fig. 1). The AB was in an H_2O solution, which has a dielectric constant of 78.54. The CE was in a solution of ethyl acetate, which has a

dielectric constant of 6.02. This difference in dielectric constant means that the solutions were immiscible. To make it so our intended solute mixture occurred, we applied the AB using a micropipette and allowed the water to evaporate for 15 minutes, leaving the solute on the agar before applying the extract in solution. The plates were incubated in a dark cupboard at 21°C for 7 days.

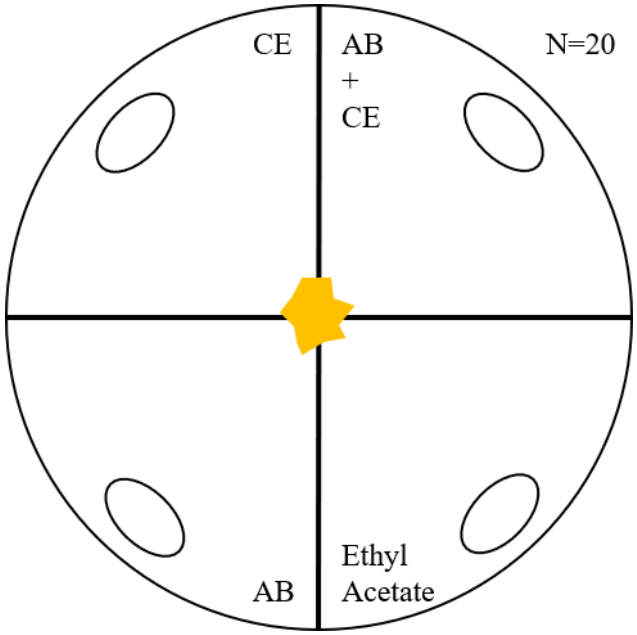

Figure 1: *Application of Mucor racemosus and solutions on PDA plates. 30 uL of each solution (ovals) were pipetted onto the agar, except for the CE+AB quadrant which had 30 uL of AB applied first, then 30 uL of CE applied after 15 minutes. M. racemosus (yellow) was placed on top of the agar. CE = Cranberry Extract. AB = Amphotericin B.*

2.4. Experiment 2: Disk Diffusion Assay Comparing a Mixture of 30:30 uL CE+AB to 30 uL of AB on *M. racemosus*

The fungus was incubated in a dark cupboard at 21°C until each plate was completely blanketed in fungus. Each solution was pipetted onto filter paper disks; volumes applied were the same as in Experiment 1. For the mixture, AB was applied and allowed to dry for 15 minutes before CE was applied. Once the disks were dry, they were placed 10 mm away from the edge of the plate, centered within their quadrant on top of the mycelia (Fig. 2). The plates were incubated in a dark cupboard at 21°C for 2 days.

2.5. Experiment 3: Comparison of Mixtures of 300:30 uL and 30:30 uL CE+AB to 30 uL of AB on *M. racemosus*

CE was stored for 10 days at lab room temperature before Experiment 3 occurred. 8 petri dishes were divided into quadrants; 300:30 uL and 30:30 uL mixtures of CE+AB, 300 uL of ethyl acetate and 30 uL of AB. We applied the 300 uL of CE and ethyl acetate

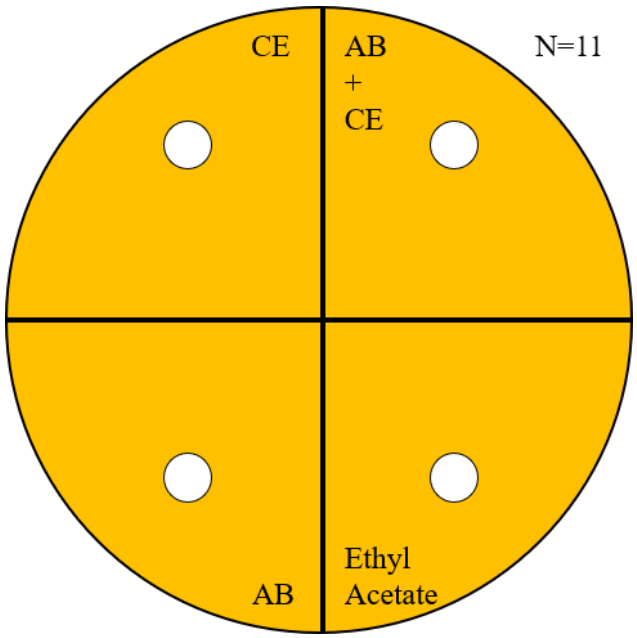

Figure 2: *Placement of filter paper disks onto plates with Mucor racemosus. 30 uL of each solution were applied to filter paper disks; dried for 15 minutes, then placed onto the mycelia. For the CE+AB treatment, 30 uL of CE were applied, dried before applying 30 uL of AB, dried again before transferring onto mycelia. CE = Cranberry Extract. AB = Amphotericin B.*

over ten 30 uL increments, waiting 3 minutes between each increment to control for the area of application by reducing the amount of liquid spread. 30 uL of AB was applied to the corresponding quadrant 10 minutes after the ethyl acetate solutions were applied. Plates were incubated as in Experiment 1.

2.6. Statistical Analysis

We measured the area of any zones of inhibition by tracing over the area clear of *M. racemosus* growth on the petri dishes using 1x1 mm^2 graphing paper and recording the area corresponding to zones of inhibition from the dishes(Fig. 3). For each experiment, we graphed the mean area for zones of inhibition for each treatment, with 95% confidence intervals. A graph that compared the mixture of 30:30 uL CE and AB between Experiment 1 and Experiment 3 was made to determine if the extract was subject to significant degradation over the 10 days between the experiments within either the AB or the CE. We ran F-tests from the collected data using an alpha of 0.05 (JMP®, Version 14. SAS Institute Inc., 1989- 2019).

3. Results

We defined the zone of inhibition as the are which fungal hyphae did not approach, creating a clear area (Fig. 3). In Experiment 1, we found that a mixture of 30 uL of ethyl acetate extract of frozen cranberries (CE) mixed with 30 uL amphotericin B (AB)

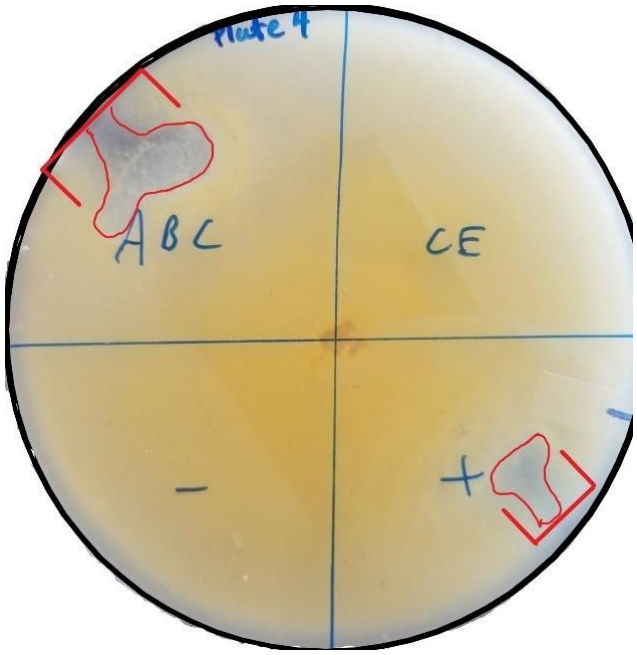

Figure 3: *M. racemosus Growth after 7 Days from Experiment 1. Zones of inhibition (red) were found using 1x1 mm^2 graph paper. ABC = Amphotericin B and Cranberry Extract. "-" = Ethyl Acetate. "+" = Amphotericin B. CE = Cranberry Extract.*

produced a significantly larger mean zone of inhibition than the mean zone of inhibition from AB (Fig. 4; $F(1,38) = 10.2290$, $p = 0.0028$). Both quadrants that contained either 30 uL of CE or ethyl acetate had no zones of inhibition in any of the replicates.

In Experiment 2, we found there to be no observable differences between the plates of *M. racemosus* before the saturated filter paper disks were applied compared to two days after the disks were rested on top of the mycelia. We believe that this could be quantified through a light absorbance test of the fungi, measuring the amount of UV rays that are able to pass through the dish where the disks were resting, but lacked the equipment required. In Experiment 3, we found that there were no significant differences between the mean zones of inhibition of the 300:30 ul mixture of CE to AB compared to the mean zone of inhibition of 30 ul of AB (Fig. 4; $F(2,21) = 0.1816$, $p = 0.8353$). Both quadrants that contained 300 uL of CE or ethyl acetate had no zones of inhibition in any of the replicates. When we compared our results with Experiment 1, we found that the there was a significant decrease in mean zones of inhibition of the CE in Experiment 3 compared to the mean zones of inhibition from CE in experiment 1 (Fig. 6; CE+AB: $F(1,26) = 8.2304$, $p = 0.0081$; AB: $F(1,26) = 0.0160$, $p = 0.9003$). The data sets from both Experiment 1 and 3 were analyzed with a two-way ANOVA to gain further insight (Solution: $F(1,1) = 2.4426$, $p = 0.1241$; Experiment Date: $F(1,1) = 5.6006$, $p = 0.0217$; Solution*Day: $F(1,1) = 3.8025$, $p = 0.0566$).

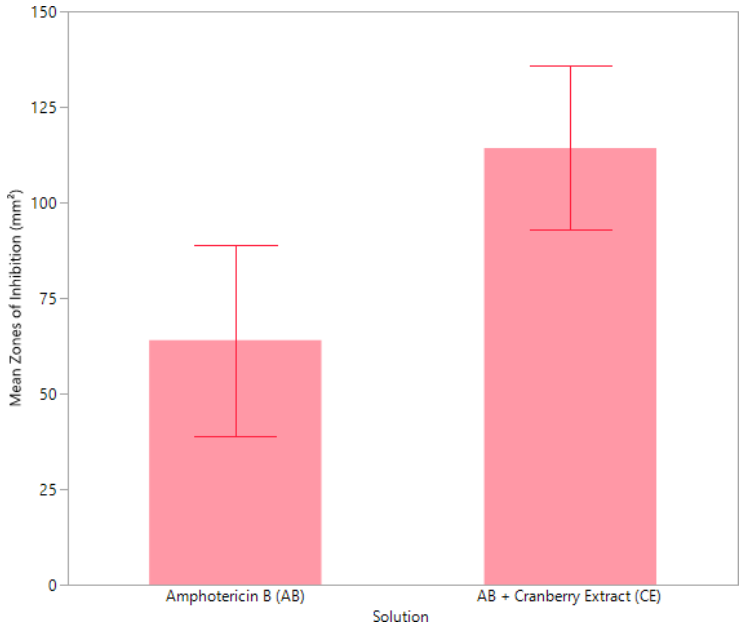

Figure 4: *Comparing mean zones of inhibition measured on M. racemosus between an AB+CE mixture and AB alone. Mixture was made from 30 uL of AB and 30 uL of CE. 30 uL of AB was used in the comparison. Measurements were taken 7 days after solution application. Error bars represent 95% confidence.* $N = 20$.

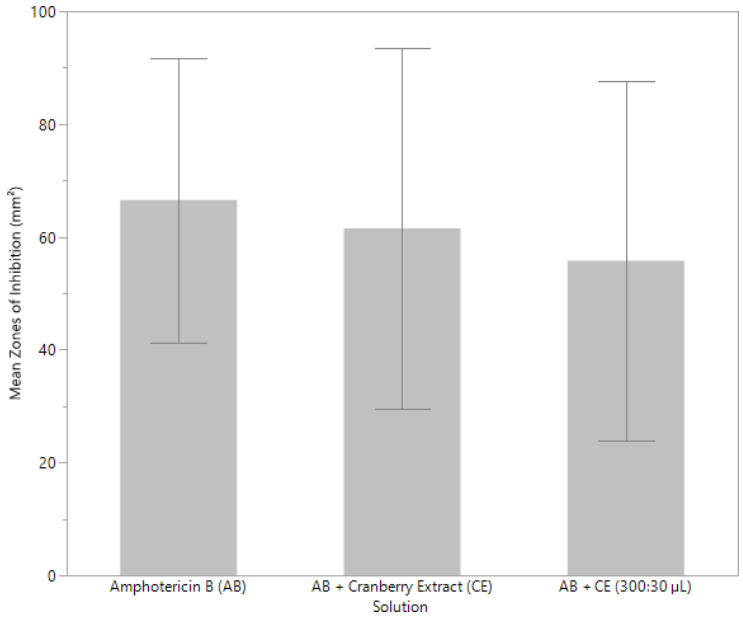

Figure 5: *Comparing mean zones of inhibition on M. racemosus between mixtures of AB+CE with different volumes of CE. 30 uL of AB (Left). Mixture of 30 uL of AB with 30 uL of CE (Middle). Mixture of 30 uL of AB with 300 uL of CE (Right). Measurements taken 7 days after solution application. Error bars represent 95% confidence.* $N = 8$.

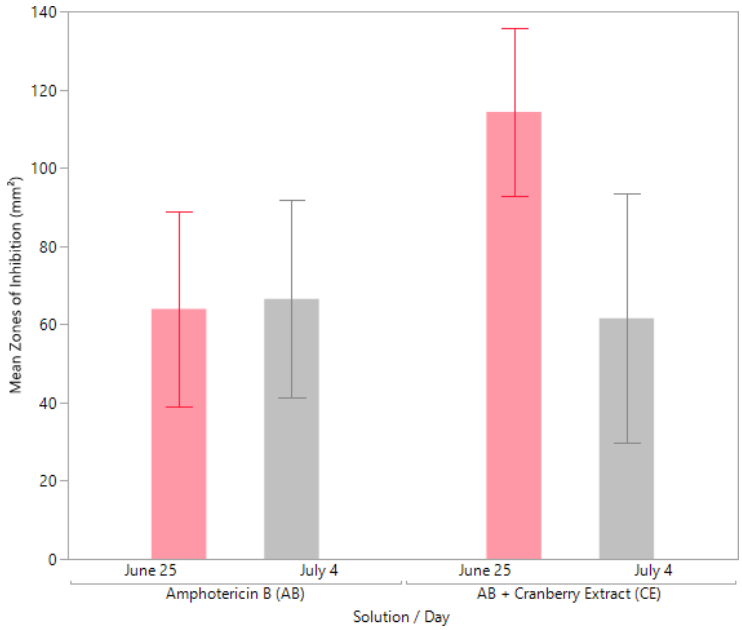

Figure 6: *Mean zones of inhibition on M. racemosus produced by an AB+CE mixture and AB alone, compared between June 25th and July 4th. Mixtures were made of 30 uL of AB with 30 uL of CE. 30 uL of AB was used in the comparisons. Measurements were taken 7 days after solutions were applied. Error bars represent 95% confidence.* $N = 28$.

4. Discussion

The results from our first experiment suggest that the addition of an ethyl acetate extract of frozen cranberries (CE) significantly increased the efficacy of amphotericin B (AB) compared to AB without the extract (Fig. 4). This suggests that there is a compound in CE that could be working with AB to increase the efficacy of AB, yet has no effect when AB is not present (Fig. 3). This supports our primary hypothesis that the CE on its own will not show any antifungal properties, but a mixture of CE and AB will have a larger zone of inhibition than either AB or CE on their own (Fig. 4).

Our second experiment showed no differences among any of the dishes. The *M. racemosus* growth was unaffected by the addition of the saturated disks on top of the mycelia. This could be because the fungus had reached its maximum growth in the dish and stopped absorbing nutrients, so the solutions were unable to enter the fungus and cause any effect.

Previous studies using disk-diffusion assays with AB inhibited the growth of *Mucor* fungi by applying approximately tenfold the amount of AB that we applied to the disks (0.96 mg) [22]. This fails to support our second hypothesis that a mixture of CE and AB can kill *M. racemosus* mycelia more effectively than AB.

Our Experiment 1 and 2 results suggest that a 30:30 uL mixture ratio of CE and AB can prevent the growth of *M. racemosus* but they are inconclusive in determining whether or not this mixture can kill grown fungal cells (Fig. 4). If this mixture were to be used in its current state to fight *Mucor* rot it could be useful to stop further spread

of the pathogen but would have no effect if a fruit was already infected.

In Experiment 3, we found that there was no significant difference in inhibitory zone areas when a 300:30 uL mixture of CE+AB was compared to a 30:30 uL mixture of CE+AB (Fig. 5). This may be due to the difference in age of the CE between Experiment 1 and 3, leading to some degradation of CE. When comparing Experiments 1 and 3, where there was a significant decrease in the mean zones of inhibition area of the 30:30 uL mixture of CE to AB (Fig. 6). A two-way ANOVA analysis of both solutions in Experiments 1 and 3 provided additional evidence that the difference in the mean zone of inhibition was due to the time period between experiments ($F(1,1) = 3.8025$, $p = 0.0566$).

Due to this degradation, we were unable to verify if increasing the relative amount of CE to AB in the mixture would increase the efficacy at preventing fungal growth (Fig. 5). This means that different storage methods would need to be compared to maximize the half-life of the CE. These results suggest that some compound responsible for enhancing the efficacy of AB may have degraded between Experiments 1 and 3. Wissam et al. showed that the lowest yield of proanthocyanidin is obtained using ethyl acetate, compared to water and aqueous ethanol, and the most degradation occurs when the CE is stored at lab room temperature of 20°C [23]. Prior studies show that proanthocyanidin has antifungal properties. Therefore, we hypothesize that the compound in the CE is proanthocyanidin due to the similar decrease in antifungal effectiveness over time suggested by Experiment 3.

Identification of the compound that causes this increase in amphotericin B efficacy would be the ideal focus of future studies. If proanthocyanidin could be confirmed to exist in an ethyl acetate extract of frozen cranberries, such as through high-performance liquid chromatography [24], it could be determined whether it had a large effect on the efficacy of amphotericin B. Once it is identified, further studies should test how the compound interacts with other fungi and antifungal treatments.

Alternatively, a future study could make changes to the extraction and storage methods, as outlined by Wissam et al., to target for high proanthocyanidin yield [23]. This could provide more evidence that proanthocyanidin is possibly the primary compound that improves the efficacy of AB.

5. Conclusion

Our hypothesis that the addition of an ethyl acetate extract of frozen cranberries (CE) would significantly improve the efficacy of amphotericin B (AB) at inhibiting the growth of *Mucor racemosus* when compared to AB alone was supported by the results from Experiment 1 (Fig. 4). Our second hypothesis was not supported by the results of Experiment 2. Experiment 2 failed to work and produced inconclusive results. A comparison of the zones of inhibition from the mixture of CE and AB compared to AB alone between Experiments 1 and 3 suggest that the CE undergoes significant degradation when stored at 21°C (Fig. 6). This degradation prevented us from determining if increasing the CE amount in the mixture would increase the zones of inhibition observed (Fig. 5).

6. Acknowledgments

This study was supported by the Simon Fraser University Dean of Science Office, through INSPIRE program funding for the development for BISC 212: Biological Research. Facilities, equipment, materials, and technical support were provided by the Department of Biological Sciences at SFU. We would also like to thank Cheryl Leonard for providing technical support and expertise. Additional editing and proofreading assistance were provided by Emma Lacroix and Erin McClelland-Asu.

References

[1] Fausto Almeida, Marcio L Rodrigues, and Carolina Coelho. The still underestimated problem of fungal diseases worldwide. *Frontiers in microbiology*, 10:214, 2019.

[2] Matthew C. Fisher, Daniel. A. Henk, Cheryl J. Briggs, John S. Brownstein, Lawrence C. Madoff, Sarah L. McCraw, and Sarah J. Gurr. Emerging fungal threats to animal, plant and ecosystem health. *Nature*, 484(7393):186–194, Apr 2012. ISSN 1476-4687. doi:10.1038/nature10947. URL https://doi.org/10.1038/nature10947.

[3] Gordon D. Brown, David W. Denning, Neil A. R. Gow, Stuart M. Levitz, Mihai G. Netea, and Theodore C. White. Hidden killers: Human fungal infections. *Science Translational Medicine*, 4(165):165rv13–165rv13, 2012. ISSN 1946-6234. doi:10.1126/scitranslmed.3004404. URL https://stm.sciencemag.org/content/4/165/165rv13.

[4] Pedro W. Crous, Johannes Z. Groenewald, Bernard Slippers, and Michael J. Wingfield. Global food and fibre security threatened by current inefficiencies in fungal identification. *Philosophical Transactions of the Royal Society B: Biological Sciences*, 371(1709):20160024, 2016. doi:10.1098/rstb.2016.0024. URL https://royalsocietypublishing.org/doi/abs/10.1098/rstb.2016.0024.

[5] Matthew Pegorie, David W. Denning, and William Welfare. Estimating the burden of invasive and serious fungal disease in the united kingdom. *Journal of Infection*, 74(1):60 – 71, 2017. ISSN 0163-4453. doi:https://doi.org/10.1016/j.jinf.2016.10.005. URL http://www.sciencedirect.com/science/article/pii/S0163445316302730.

[6] Nathan P. Wiederhold. Antifungal resistance: current trends and future strategies to combat. *Infection and drug resistance*, 10:249–259, Aug 2017. ISSN 1178-6973. doi:10.2147/IDR.S124918. URL https://pubmed.ncbi.nlm.nih.gov/28919789. 28919789[pmid].

[7] S. Saito, T. J. Michailides, and C. L. Xiao. Mucor rot—an emerging postharvest disease of mandarin fruit caused by mucor piriformis and other mucor spp. in california. *Plant Disease*, 100(6):1054–1063, 2016. doi:10.1094/PDIS-10-15-1173-RE. URL https://doi.org/10.1094/PDIS-10-15-1173-RE. PMID: 30682278.

[8] Seiya Saito, TJ Michailides, and CL Xiao. Mucor rot—an emerging postharvest disease of mandarin fruit caused by mucor piriformis and other mucor spp. in california. *Plant disease*, 100(6):1054–1063, 2016.

[9] Jin-Hycuk Kwon and Seung-Beom Hong. Soft rot of tomato caused by mucor racemosus in korea. *Mycobiology*, 33(4):240–242, 2005. doi:10.4489/MYCO.2005.33.4.240. URL https://www.tandfonline.com/doi/abs/10.4489/MYCO.2005.33.4.240.

[10] Mucormycosis statistics, May 2020. URL https://www.cdc.gov/fungal/diseases/mucormycosis/statistics.html.

[11] Carlos Rodrigo Camara-Lemarroy, Emmanuel Irineo González-Moreno, René Rodríguez-Gutiérrez, Erick Joel Rendón-Ramírez, Ana Sofía Ayala-Cortés, Martha Lizeth Fraga-Hernández, Laura García-Labastida, and Dionicio Ángel Galarza-Delgado. Clinical features and outcome of mucormycosis. *Interdisciplinary Perspectives on Infectious Diseases*, 2014:562610, Aug 2014. ISSN 1687-708X. doi:10.1155/2014/562610. URL https://doi.org/10.1155/2014/562610.

[12] Benjamin Matteson Vincent, Alex Kelvin Lancaster, Ruth Scherz-Shouval, Luke Whitesell, and Susan Lindquist. Fitness trade-offs restrict the evolution of resistance to amphotericin b. *PLOS Biology*, 11(10):1–17, 10 2013. doi:10.1371/journal.pbio.1001692. URL https://doi.org/10.1371/journal.pbio.1001692.

[13] Diego R. Falci, Franciane B. da Rosa, and Alessandro C. Pasqualotto. Comparison of nephrotoxicity associated to different lipid formulations of amphotericin b: a real-life study. *Mycoses*, 58(2):104–112, 2015. doi:https://doi.org/10.1111/myc.12283. URL https://onlinelibrary.wiley.com/doi/abs/10.1111/myc.12283.

[14] V. Fanos and L. Cataldi. Amphotericin b-induced nephrotoxicity: A review. *Journal of Chemotherapy*, 12(6):463–470, 2000. doi:10.1179/joc.2000.12.6.463. URL https://doi.org/10.1179/joc.2000.12.6.463. PMID: 11154026.

[15] Liwei Gu, Mark A. Kelm, John F. Hammerstone, Gary Beecher, Joanne Holden, David Haytowitz, Susan Gebhardt, and Ronald L. Prior. Concentrations of Proanthocyanidins in Common Foods and Estimations of Normal Consumption. *The Journal of Nutrition*, 134(3):613–617, 03 2004. ISSN 0022-3166. doi:10.1093/jn/134.3.613. URL https://doi.org/10.1093/jn/134.3.613.

[16] Hallie S. Rane, Stella M. Bernardo, Amy B. Howell, and Samuel A. Lee. Cranberry-derived proanthocyanidins prevent formation of Candida albicans biofilms in artificial urine through biofilm- and adherence-specific mechanisms. *Journal of Antimicrobial Chemotherapy*, 69(2):428–436, 10 2013. ISSN 0305-7453. doi:10.1093/jac/dkt398. URL https://doi.org/10.1093/jac/dkt398.

[17] Mark Feldman, Shinichi Tanabe, Amy Howell, and Daniel Grenier. Cranberry proanthocyanidins inhibit the adherence properties of candida albicans and cytokine secretion by oral epithelial cells. *BMC Complementary and Alternative*

Medicine, 12(1):6, Jan 2012. ISSN 1472-6882. doi:10.1186/1472-6882-12-6. URL https://doi.org/10.1186/1472-6882-12-6.

[18] Raul Leal Faria Luiz, Taissa Vieira Machado Vila, João Carlos Palazzo de Mello, Celso Vataru Nakamura, Sonia Rozental, and Kelly Ishida. Proanthocyanidins polymeric tannin from stryphnodendron adstringens are active against candida albicans biofilms. *BMC Complementary and Alternative Medicine*, 15(1):68, Mar 2015. ISSN 1472-6882. doi:10.1186/s12906-015-0597-4. URL https://doi.org/10.1186/s12906-015-0597-4.

[19] James I. Ito and Roya Hooshmand-Rad. Treatment of Candida Infections with Amphotericin B Lipid Complex. *Clinical Infectious Diseases*, 40(Supplement 6): S384–S391, 05 2005. ISSN 1058-4838. doi:10.1086/429330. URL https://doi.org/10.1086/429330.

[20] Yongmoon Han. Synergic effect of grape seed extract with amphotericin b against disseminated candidiasis due to candida albicans. *Phytomedicine*, 14(11):733 – 738, 2007. ISSN 0944-7113. doi:https://doi.org/10.1016/j.phymed.2007.08.004. URL http://www.sciencedirect.com/science/article/pii/S0944711307001985.

[21] Sean X Liu and Elizabeth White. Extraction and characterization of proanthocyanidins from grape seeds. *The Open Food Science Journal*, 6(1), 2012.

[22] A. Espinel-Ingroff and E. Canton. Comparison of neo-sensitabs tablet diffusion assay with clsi broth microdilution m38-a and disk diffusion methods for testing susceptibility of filamentous fungi with amphotericin b, caspofungin, itraconazole, posaconazole, and voriconazole. *Journal of Clinical Microbiology*, 46(5):1793–1803, 2008. ISSN 0095-1137. doi:10.1128/JCM.01883-07. URL https://jcm.asm.org/content/46/5/1793.

[23] Zam Wissam, Bashour Ghada, Abdelwahed Wassim, and Khayata Warid. Effective extraction of polyphenols and proanthocyanidins from pomegranate's peel. *Int J Pharm Pharm Sci*, 4(Suppl 3):675–682, 2012.

[24] J Rigaud, J Perez-Ilzarbe, J.M.Ricardo Da Silva, and V Cheynier. Micro method for the identification of proanthocyanidin using thiolysis monitored by high-performance liquid chromatography. *Journal of Chromatography A*, 540:401 – 405, 1991. ISSN 0021-9673. doi:https://doi.org/10.1016/S0021-9673(01)88830-0. URL http://www.sciencedirect.com/science/article/pii/S0021967301888300.

SFU SURJ | SIMON FRASER UNIVERSITY SCIENCE UNDERGRADUATE RESEARCH JOURNAL
Vol. 5 (2019-20)

Cloning in an AviTag to Minor Pilins for Optimal Display during Antibody Library Screening

Asa Lau[1]

[1]Simon Fraser University, *Department of Molecular Biology and Biochemistry*

Abstract

Bacteria possess intricate systems of rapidly assembling and disassembling filaments called Type IV Pili (T4P), which are responsible for diverse functions including bacterial aggregation, twitching motility, and phage and DNA uptake. Each pilus is a polymer of thousands of copies of the major pilin and small numbers of minor pilins that have roles in assembly, retraction and pilus functions. In simple T4P systems minor pilins form a homotrimer that initiates pilus assembly and localizes to the pilus tip. In the *Vibrio cholerae* toxin coregulated pilus, this minor pilin homotrimer binds to the CTXϕ phage, which is taken into the bacterium by pilus retraction. In complex T4P systems, like those of *Neisseria gonorrhoeae* and *Pseudomonas aeruginosa*, five different minor pilins form a homopentamer that primes pilus assembly and is involved in DNA binding and uptake. The adhesive and retractile features of T4P make them ideal targets for antibody carriers that can deliver antibiotics into the bacterial periplasm. The long term goal of this research is to exploit the T4P machinery as an antibiotic delivery system by selecting from diverse phage display library antibodies that bind to minor pilins at the tip of the pilus that can be used as antibiotic carriers. To this end, this paper demonstrates the successful cloning of an AviTag onto the N-terminus of recombinant minor pilin TcpB of *V. cholerae* but was unable to clone in CofB of enterotoxigenic *Escherichia coli* (ETEC). However, the AviTag of TcpB can then be biotinylated using the biotin ligase BirA, allowing the minor pilin to be immobilized on streptavidin-coated plates in an orientation that mimics the pilus tip for antibody library screening.

Keywords — Antibiotic Resistance, Type IV Pili, Cloning, AviTag, Recombinant Proteins

1. Introduction

Worldwide overuse of antibiotics has resulted in widespread antibiotic resistance, making it increasingly difficult to treat many infectious diseases. Along with developing new drugs, alternative methods for antibiotic delivery should be considered. Gram-negative bacteria tend to be more resistant than Gram-positive bacteria due to the presence of an outer membrane that prevents passage of large antibiotics such as vancomycin [1]. Many bacteria have Type IV Pili (T4P), adhesive protein polymers that rapidly assemble and disassemble, facilitating DNA uptake, microcolony formation, secretion and twitching motility among other processes. We hypothesize that retractile T4P can act as delivery systems for antibiotics. We wish to exploit the binding and retraction mechanism of T4P to introduce antibiotics into the bacterial periplasm. To this end, I plan to produce recombinant Avi-Tagged minor

pilins that can be biotinylated and displayed on microtiter plates for antibody library screens to identify high affinity molecules that will serve as antibiotic carriers.

T4P filaments are made of thousands of copies of a major pilin protein and one or more minor pilins. Pilus assembly occurs at the inner membrane, where pilin subunits dock via electrostatic attractions at the base of the growing pilus, which is incrementally extruded outward with each subunit addition, powered by an assembly ATPase [**?**]. The pilus grows across the periplasm and through an outer membrane secretin channel for display on the bacterial surface. Pilus assembly is initiated by the minor pilins, which are thought to form a "priming complex" in the inner membrane via interactions among their C-terminal periplasmic domains [2, 3]. This priming complex then recruits the major pilins to grow the pilus. The *V. cholerae* and *E. coli* (ETEC) T4P are considered "simple" T4P systems, having a single minor pilin that forms a homotrimer [4, 5, 6], whereas more complex T4P systems, like those of *N. gonorrhoeae* and *N. meningitidis*, have a heteropentameric minor pilin priming complex [2, 3]. The Craig lab previously cloned the minor pilin genes encoding tcpB residues 43-423 and ETEC cofB 25-516 into vector pET15b, and expressed soluble minor pilins in *E. coli*. From there, they were able to solve the crystal structures of Vibrio cholerae minor pilin TcpB and the enterotoxigenic ETEC minor pilin CofB, both of which form homotrimers in the crystal and in solution [5, 6]. Using immunogold labeling they showed that TcpB forms a trimer at the pilus tip and binds to the tip protein of the filamentous bacteriophage CTXϕ to facilitate phage uptake [5]. Similarly, Ellison et al. showed that a second *V. cholerae* T4P, the competence pilus, which is a complex T4P, binds to DNA via its tip, and that minor pilin mutants were defective in DNA uptake [7]. These data support a model in which T4P bind to large substrates, like phage and DNA, via their tip-associated minor pilins, and draw them into the periplasm via pilus retraction. We aim to exploit this system to introduce antibiotics into the bacterium (Fig. 1). By bypassing the outer membrane barrier, this strategy would sensitise Gram-negative bacteria to large antibiotics like vancomycin.

To this end, we plan to screen vast antibody libraries to identify antibodies that bind with high affinity to tip-associated minor pilins as a vehicle to introduce antibiotics into bacteria via pilus retraction. Our goal is to prepare recombinant minor pilins for ETEC, CofB, and *V. cholerae*, TcpB, that can be used to "fish" such carriers out of libraries of millions of antibodies. This goal is divided into three aims: 1) Engineer an AviTag gene segment onto the 5′ end of the minor pilin genes tcpB and cofB in pET15b; 2) Express and purify the engineered minor pilins via the N-terminal His tag; 3) Biotinylate the minor pilins for display on streptavidin-coated plates for library screening. This paper demonstrates the molecular cloning done to achieve the first of the three goals.

2. Results

2.1. Cloning in the 5′ Avitag using Two Successive PCR Reactions

The minor pilin genes *cofB* and *tcpB* were previously cloned into pET15b at the NdeI and BamH1 sites, replacing the α1N α-helix of these pilins with a hexa-histidine tag (His-tag). Primers were designed to clone out the minor pilin gene, insert the AviTag

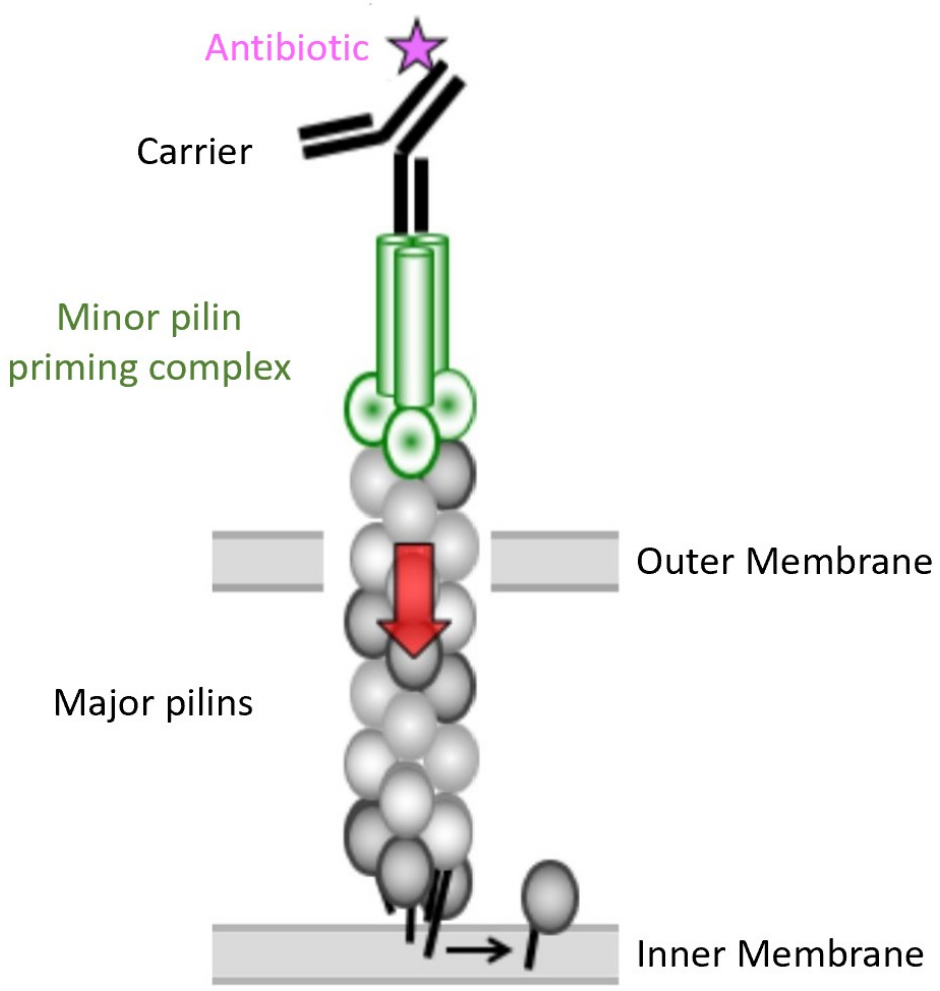

Figure 1: *Structure of the pilus assembly machinery on the bacterial membrane. Antibiotic carriers can bind to minor pilins located at the tip of pilus to enable delivery of antimicrobial agents into the bacteria via retraction.*

gene sequence at the 5′ end of this gene in two PCR steps, then digest the final product with NdeI and BamHI and insert it into these sites in pET15b. This strategy places the His-tag N-terminal to the AviTag, maintaining a thrombin cleavage site that allows the His-tag to be removed, producing an N-terminal AviTag.

To insert the AviTag sequence between the His-tag and the minor pilin, the 3′ half of the AviTag gene was first added via the forward primer during PCR I, while amplifying the minor pilin gene and BamH1 restriction site. The presence of bands in the PCR I gel showed that the 3′ end of the Avitag was successfully cloned into the tcpB and cofB genes at all PCR temperatures, with the exception of tcpB23-423 at 56 oC (Fig. 2). Next, the 5′ half of the AviTag gene was inserted by PCR-amplifying PCR I products using a forward primer containing this segment and the reverse primer used for PCR I. In

addition to the expected product at 1500 base pairs (bps) for PCR II, a second diffuse band was present at 250 bps for all reactions (Fig. 2).

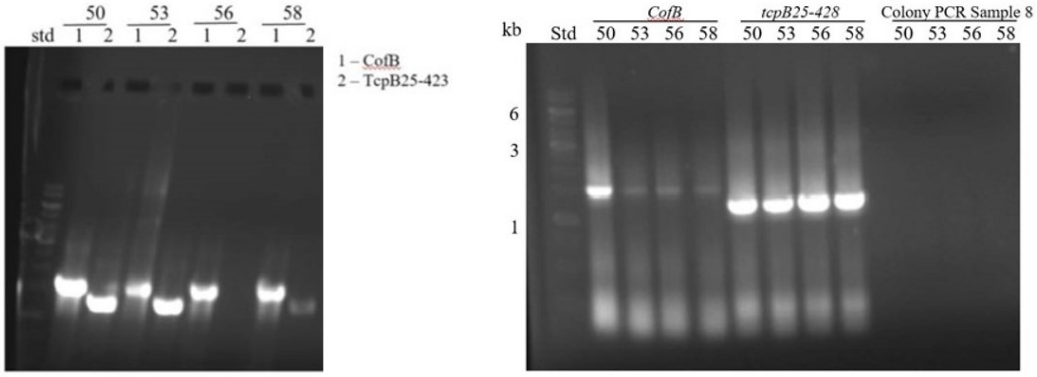

Figure 2: *PCR I and II Results. Bands are seen in all lanes except for tcpB25-423 at 56 oC on a 1% agarose gel in PCR I (left). CofB and tcpB samples show prominent bands at 1500 bp and 1200 bp respectively, with by-products appearing around 250 b on a 1% agarose gel for PCR II (right).*

2.2. Digestion, Ligation, Transformation and Sanger Sequencing

The PCR II products and pET15b were double-digested with NdeI and BamH1 for 6 hr at 37 °C. Single digests were also performed for pET15b, and the reactions were analysed by agarose gel electrophoresis to ensure that both enzymes were active (Fig. 3). The observed mobility shift for each single digest confirmed enzyme activity. The digested PCR II products were purified using the Thermo Scientific GeneJET PCR Purification Kit, where samples were ran on silica-membrane spin columns to remove excess primers, dNTPs, polymerase and buffer. The inserts were then ligated into digested pET15b at various insert:plasmid ratios, and the ligation products were transformed by heat shock into *E. coli* DH5α cells. Cells were grown on LB agar plates with 100 ug/mL ampicillin.

Colony PCRs were performed using the insert-specific primers, revealing bands for all products at 250 bp (Fig. 4) instead of the desired 1500 bp products. External sequencing performed by Genewiz using the Avitag 5'-fpcr primer revealed that only the 3' end of the insert gene is present followed by the BamHI site. There is some alignment with internal regions but no obvious site that would produce a product at 250 bp. Looking back at Fig. 2B, the 250 bp bands may be due to the contamination of a by-product from PCR II that was not removed during the PCR clean-up. Thus, the restriction digestion was repeated on PCR II products and the digested inserts were cut out of the gel to eliminate contaminants. These were ligated into gel extracted, alkaline phosphatase treated pET15b at various insert:plasmid ratios.

The ligation reactions were electroporated into electrocompetent *E. coli* DH5α and cells were grown overnight on LB-Amp plates. The resultant colonies were analysed by colony PCR using the T7 promoter and T7 terminator (Fig. 5). The results showed that both *cofB* plasmids were empty, while the tcpB clone produced a band at approximately

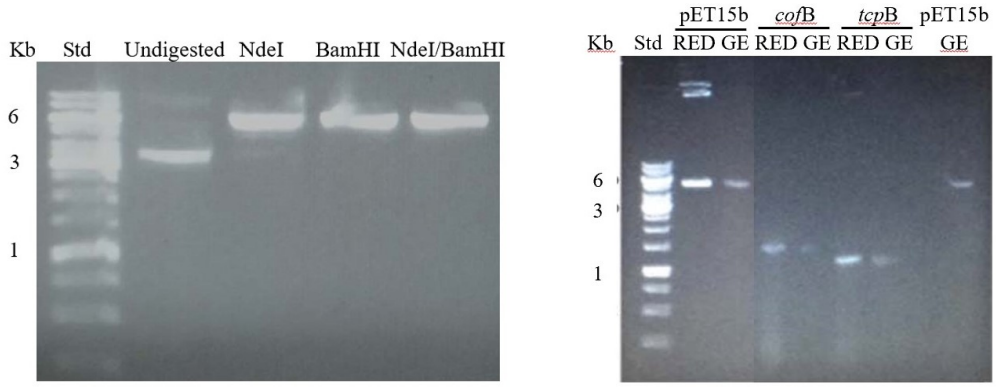

Figure 3: *Diagnostic digest to confirm the activity of both restriction enzymes (left) and a diagnostic gel on restriction enzyme digestion products (RED) and gel-extracted products (GE) (right). The mobility shift seen from the undigested to single and double digests of NdeI and BamHI confirm their activity (left). Estimated 200 ng of pET15b in 5 uL for RED (40n ng/uL) and 80 ng in GE (13 ng/uL). 25 ng in 6 uL of cofB and tcpB (4.3 ng/uL) (right).*

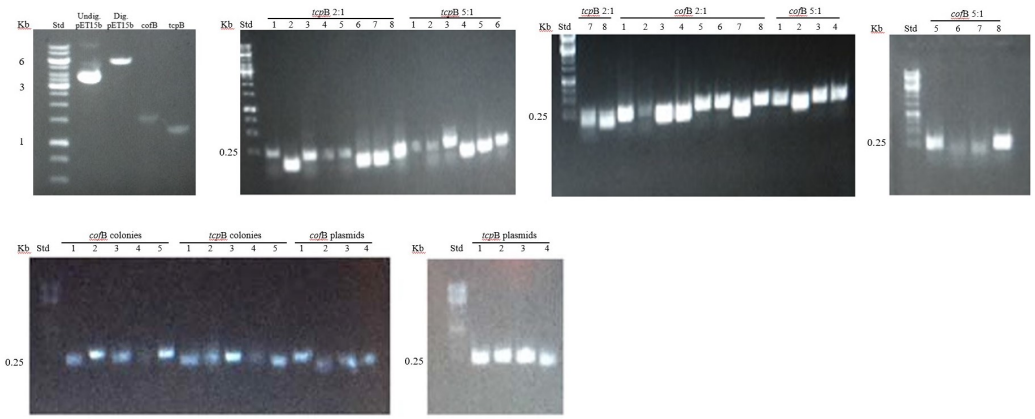

Figure 4: *6-hour digestion gel results (upper left), first colony PCR with a 1-minute extension time (3 gels on upper right), and second colony PCR with a 4 minute extension time (2 gels on bottom). Estimated concentration of 40 ng/uL for pET15b, 8 ng/uL for cofB and 15 ng/uL for tcpB (upper left). All bands appear around 250 bp in the first colony PCR (3 gels on upper right). Both colonies (first transformation) and purified plasmids (second transformation) have products around 250 bp (2 gels on bottom).*

750 bps, consistent with the presence of the correct insert. The sequence of the *tcpB* insert was verified using primers NdeI- Avitag5'-fpcr and Vc-tcpB423-BAM-HI-rpcr.

The 3:1 and 4:1 *cofB* ligations were transformed into pET15b vector via electroporation, yielding colonies in both ratios that were sequenced with the T7 promoter and BamHI reverse primers. However, Genewiz was not able to sequence either plasmids. The results of another colony PCR showed that the bands present in the *cofB* samples ran with the T7 promoter, and terminator primers were empty plasmids, as no band was present using the insert specific primers (Fig. 6).

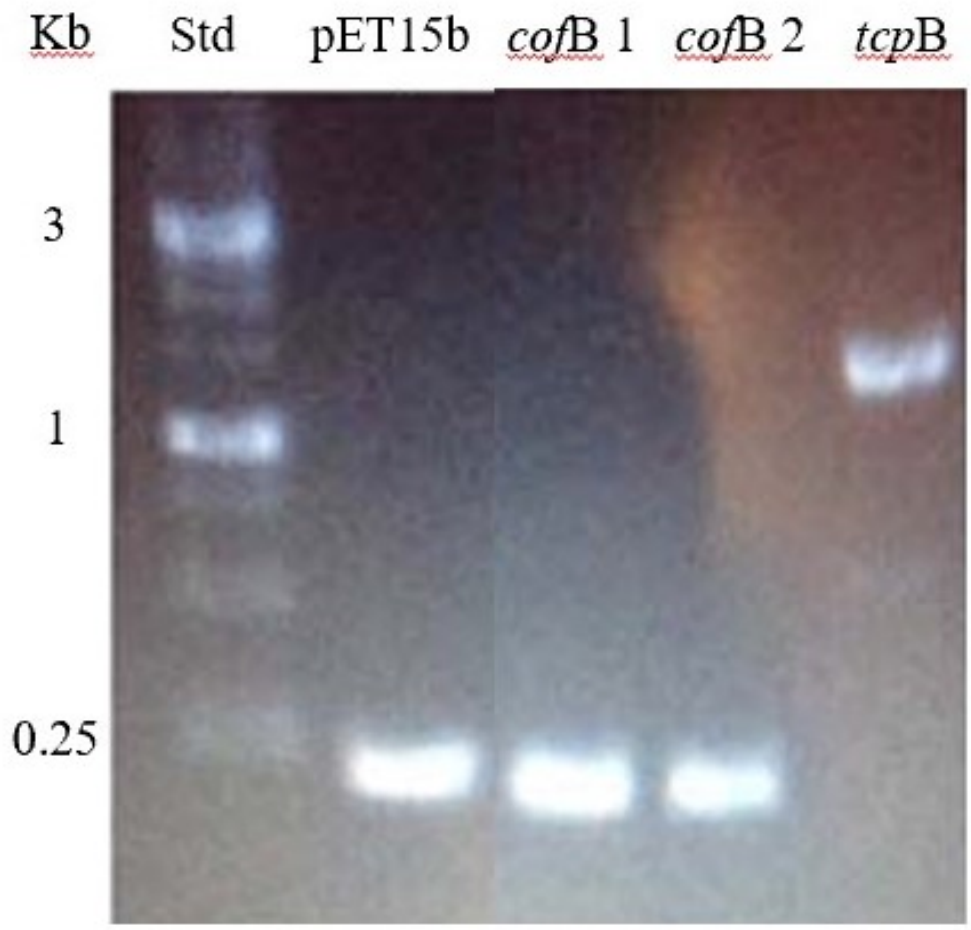

Figure 5: *Colony PCR with gel extracted inserts and alkaline phosphatase treated pET15b. The tcpB colony reveals the expected band at 1200 bp, while both cofB colonies have bands less than 250 bp.*

3. Methods

IDT's OligoAnalyzer tool was used to calculate the primer T_m values and obtain a T_m of 60-65°C. The sequences for the primers are as follows:

- NdeI-AviTag5′-fpcr: 5′ GGAATTCCATATGGGGTCCGGGTTGAATGATATTTTC-GAAGCACAGAAAATTGAATGGCA
- ETEC-cofB-AviTag3′-fpcr: 5′ TATTTTCGAAGCACAGAAAATTGAATGGCAT-GAGGAGAAAGAAGCAGATGAAGCCAGACG
- ETEC-cofB-BamHI-rpcr: 5′ CAGCCGGATCCTTAGGTTTGTGGTTCTGTAC
- Vc-tcpB25-AviTag3′-fpcr: 5′ ATATTTTCGAAGCACAGAAAATTGAATGGCAT-GAGAAGCGGGAAGCTGAACTCATGATTA

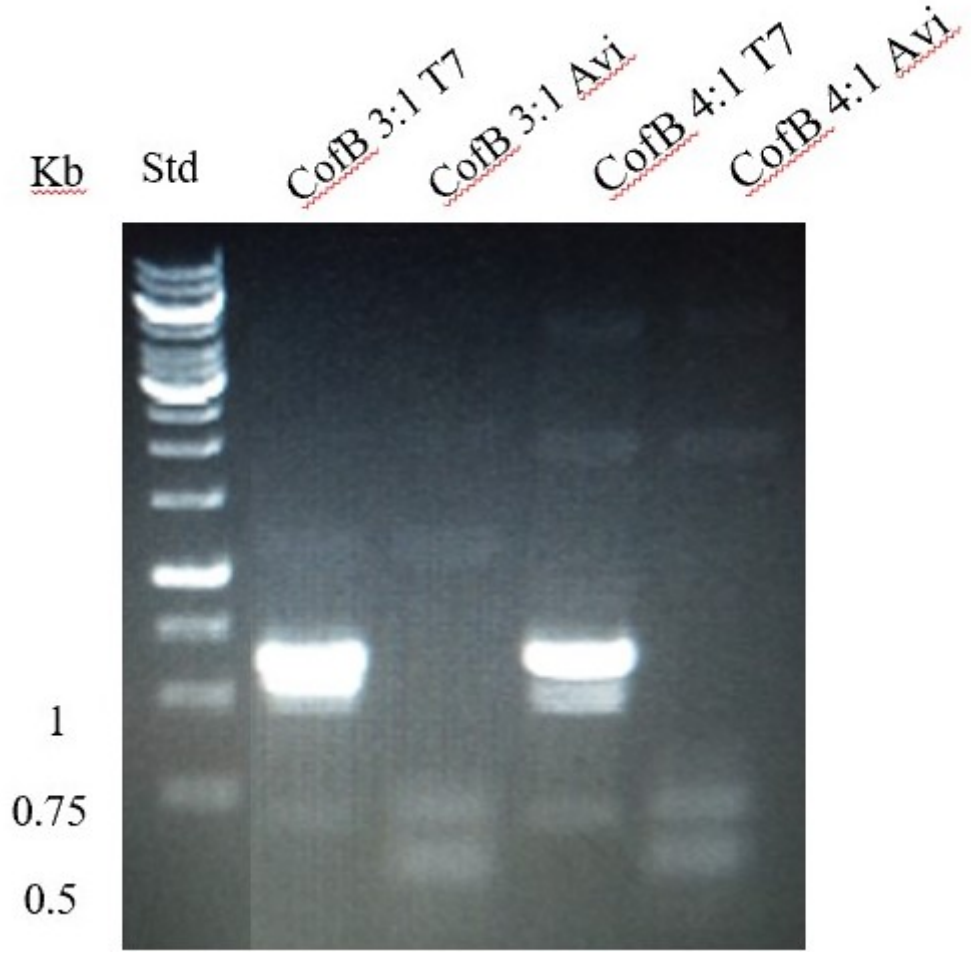

Figure 6: *Colony PCR of the 3:1 and 4:1 cofB colonies using two sets of primers. T7 refers to the T7 Promoter and Terminator primer pairs, while Avi refers to the Avitag5'-fpcr and ETEC-CofB-BamHI-rpcr primer pairs. No bands are seen in the insert specific primer pairs for both cofB samples.*

- Vc-tcpB423-BamHI-rpcr: 5′ CAGCCGGATCCTTAATTTTCACACCATTGAAAC

3.1. Polymerase Chain Reaction (PCR)

Since the AviTag gene segment is 45 nucleotides, it is too long to insert into the 5′ end of the minor pilin genes using a single primer. Therefore, two successive PCR reactions were carried out to first clone *V. cholerae TcpB* (243-423) and ETEC *CofB* (25-516) from pET15b expression plasmids, simultaneously adding the 3′ half of the AviTag gene at the 5′ end and a BamHI site at the 3′ end (Fig. 7). The second PCR reaction added the 5′ half of the AviTag gene to the 5′ end of the first PCR product. Primers were purchased from IDT and resuspended in H2O to give 100 uM, then diluted 1/10 for a 10 uM working stock. The PCR reaction used 5X Q5 buffer at 1X, 1 mM dNTPs, 0.5 uM of forward and reverse primers, 1 ng-1 ug template, 1% DMSO and 20 units/ml of Q5

polymerase. The samples ran at a gradient from 50 °C to 58 °C with a PCR program as follows: 95 °C initial denaturation for 1 minute, 34 cycles of 95 °C denaturation for 1 minute, annealing at a gradient for 0.5 minute, 70 °C extension for 4 minutes (1 minute/400 bases) and a final 72 oC extension for 5 minutes. PCR products were analysed for correct product size on a 1% agarose gel containing 0.1 g/uL ethidium bromide, run at 100 V for 30 minutes. One of the successful reactions was chosen for purification of the PCR product using the ThermoScientific GeneJet PCR I cleanup kit.

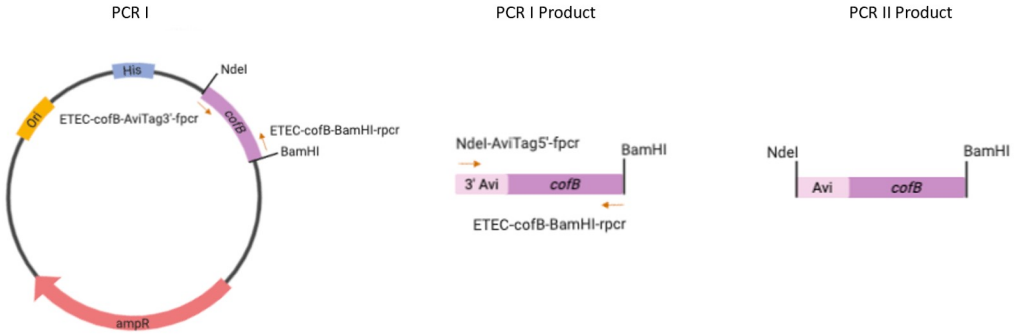

Figure 7: *PCR I was done on previously characterized minor pilins by first adding the 3′ end of the AviTag (left). The PCR I product then had the 5′ end of the AviTag cloned in (middle). The final PCR II product has the entire AviTag cloned in as well the both restriction sites, NdeI and BamHI (right).*

3.2. Restriction Digests and Dephosphorylation of Vector

PCR inserts and the pET15b vector added at 1 ug were digested with 1 uL Thermo FastDigest NdeI and BamHI in 1X FastDigest Green Buffer for 6 hours at 37 °C. To prevent the religation of incompletely digested vector, the sample was treated with 5 units of Antarctic Phosphatase per 1 ug of DNA in the 50 uL reaction, along with 1X AP Reaction Buffer for 30 minutes at 37 °C before heat inactivating at 65 °C for 5 minutes. Another PCR cleanup was performed on the digested products before running an agarose gel to quantify the amount of insert and vector.

3.3. Ligation and Transformation

Ligations were carried out at 4 molar ratios of insert to plasmid: 2:1, 3:1, 4:1 and 5:1. The calculated amount of insert was ligated with 30 ng of NdeI/BamH1-digested pET15b in 1X T4 ligase buffer and 1 uL T4 DNA Ligase. The reaction was incubated at 16 °C for 16 hours before heat inactivating at 65 °C for 20 minutes. Fifty uL aliquots of competent *E. coli* DH5α were used for transforming 5 ng of ligated plasmid. Two methods of transformation were used: heat shock transformation at 42 °C for 45 seconds and electroporation transformation using the Bio-Rad Micropulser. Cells were then grown on LB-Ampicillin plates over the weekend at room temperature.

3.4. Colony PCR, Plasmid Purification and Sanger Sequencing

Colony PCR was used to identity colonies carrying the minor pilin:pET15b plasmids. Half of each test colony was transferred to 20 uL of ddH2O and heated at 94 °C for 5 minutes; 2 ul of the boiled cells was added to a standard PCR reaction with 0.5 uM of each forward and reverse primers (T7 promoter and terminator primers or pilin-specific primers). The PCR program is as follows: 98 °C initial denaturation for 3 minutes, 4 cycles of 98 °C denaturation for 20 seconds, 56 °C annealing for 30 seconds and 72 °C extension for 4 minutes, followed by 32 cycles of 98 °C denaturation for 1 minute, 58 °C annealing for 30 seconds and 72 °C extension for 4 minutes, then an additional 10 minutes of final extension at this temperature. The test colonies were grown overnight in LB at 37 °C shaking, and plasmids were purified from the overnight cultures using the QIAprep Spin Miniprep Kit. The gene inserts were confirmed using the T7 promoter and terminator primers at Genewiz through Sanger sequencing.

4. Discussion

In this paper, we describe the cloning of AviTag gene sequences at the 5′ ends of minor pilin genes *tcpB* from *V. cholerae* and *cofB* from enterotoxigenic *E. coli*. Furthermore, the AviTag-*tcpB* gene was inserted into pET15b, downstream of the gene segment encoding a His-tag and thrombin cleavage site. This plasmid is ready for expression of His-tagged/Avi-Tagged TcpB. Test expressions will be performed at a broader range of temperatures and more cell cultures will be analyzed by SDS-PAGE.

While the *cofB* gene was successfully cloned from its expression plasmid and the AviTag gene was added, I was unable to ligate this construct into pET15b, despite implementing various insert:vector ratios and transformation strategies. Perhaps testing insert to vector molar ratios as high as 10:1 would be effective [8]. Electroporation rather than heat-shock should be used to transform the plasmid into *E. coli* cells as this is seen to have higher transformation efficiency. Once the ligation and transformation are completed, test expressions for both Avi-Tagged minor pilins will be performed at a broader range of temperatures and more cell cultures will be analyzed by SDS-PAGE. These proteins as well as BirA will be expressed in large scale (1-3) and purified using the nickel-NTA column. Biotin will be covalently attached to the AviTag of the minor pilins using purified BirA. The biotinylated proteins will be oriented on a streptavidin-coated plate for screening of antibody libraries. The end goal of the project is to find an antibody that can bind with high affinity to the tips of these minor pilins in hopes to utilize it as an antibiotic delivery system for therapeutic uses.

5. Conclusion

With increasing antibiotic overuse and poor regulation within the health care system, antibiotic resistant strains are becoming more prevalent as this environment is fostering their survival. While the spread of antibiotic resistance worldwide is partially due to misuse, the pause in discovery of new agents to target bacterial infections is also contributing to this issue. As a result, the drugs that are currently available are

becoming less and less effective. The traditional methods of antibiotic uptake through pores and active transport is limited by size, making it difficult for larger agents, like vancomycin, to pass the cell membrane. For this reason, considering alternate methods for uptake, such as through the Type IV pili, can be promising in delivering antibiotics into a cell. The T4P system would rely on binding an antibody intermediate that acts as a carrier of the antimicrobial agent. This study demonstrated the workflow of cloning an AviTag into minor pilins to allow for it to be placed in an orientation that mimics the bacterial surface for testing. More research will need to be done in expressing the Avi-Tagged plasmids generated in this study into proteins, followed by screening antibody libraries to find potential candidates to act as carriers for drug delivery.

6. Acknowledgments

I would like to thank Dr. Lisa Craig from the Department of Molecular Biology and Biochemistry for giving me the opportunity to conduct an Independent Study Semester with her and for all the mentoring she provided me.

References

[1] Anne H. Delcour. Outer membrane permeability and antibiotic resistance. *Biochimica et Biophysica Acta (BBA) - Proteins and Proteomics*, 1794(5):808–816, 2009. ISSN 1570-9639. doi:https://doi.org/10.1016/j.bbapap.2008.11.005. URL https://www.sciencedirect.com/science/article/pii/S1570963908003592. Mechanisms of Drug Efflux and Strategies to Combat Them.

[2] Ylan Nguyen, Seiji Sugiman-Marangos, Hanjeong Harvey, Stephanie D. Bell, Carmen L. Charlton, Murray S. Junop, and Lori L. Burrows. Pseudomonas aeruginosa minor pilins prime type iva pilus assembly and promote surface display of the pily1 adhesin*. *Journal of Biological Chemistry*, 290(1):601–611, 2015. ISSN 0021-9258. doi:https://doi.org/10.1074/jbc.M114.616904. URL https://www.sciencedirect.com/science/article/pii/S0021925820579556.

[3] Mangayarkarasi Nivaskumar, Javier Santos-Moreno, Christian Malosse, Nathalie Nadeau, Julia Chamot-Rooke, Guy Tran Van Nhieu, and Olivera Francetic. Pseudopilin residue e5 is essential for recruitment by the type 2 secretion system assembly platform. *Molecular Microbiology*, 101(6):924–941, 2016. doi:https://doi.org/10.1111/mmi.13432. URL https://onlinelibrary.wiley.com/doi/abs/10.1111/mmi.13432.

[4] Dixon Ng, Tony Harn, Tuba Altindal, Subramania Kolappan, Jarrad M. Marles, Rajan Lala, Ingrid Spielman, Yang Gao, Caitlyn A. Hauke, Gabriela Kovacikova, Zia Verjee, Ronald K. Taylor, Nicolas Biais, and Lisa Craig. The vibrio cholerae minor pilin tcpb initiates assembly and retraction of the toxin-coregulated pilus. *PLOS Pathogens*, 12(12):1–31, 12 2016. doi:10.1371/journal.ppat.1006109. URL https://doi.org/10.1371/journal.ppat.1006109.

[5] Miguel Gutierrez-Rodarte, Subramania Kolappan, Bailey A. Burrell, and Lisa Craig. The vibrio cholerae minor pilin tcpb mediates uptake of the cholera toxin phage ctxϕ. *Journal of Biological Chemistry*, 294(43):15698–15710, 2019. ISSN 0021-9258. doi:https://doi.org/10.1074/jbc.RA119.009980. URL https://www.sciencedirect.com/science/article/pii/S002192582030332X.

[6] Subramania Kolappan, Dixon Ng, Guixiang Yang, Tony Harn, and Lisa Craig. Crystal structure of the minor pilin cofb, the initiator of cfa/iii pilus assembly in enterotoxigenic escherichia coli*. *Journal of Biological Chemistry*, 290(43):25805–25818, 2015. ISSN 0021-9258. doi:https://doi.org/10.1074/jbc.M115.676106. URL https://www.sciencedirect.com/science/article/pii/S0021925820495614.

[7] Courtney K. Ellison, Triana N. Dalia, Alfredo Vidal Ceballos, Joseph Che-Yen Wang, Nicolas Biais, Yves V. Brun, and Ankur B. Dalia. Retraction of dna-bound type iv competence pili initiates dna uptake during natural transformation in vibrio cholerae. *Nature Microbiology*, 3(7):773–780, Jul 2018. ISSN 2058-5276. doi:10.1038/s41564-018-0174-y. URL https://doi.org/10.1038/s41564-018-0174-y.

[8] New England Biolabs. Tips for maximizing ligation efficiencies. URL https://international.neb.com/tools-and-resources/usage-guidelines/tips-for-maximizing-ligation-efficiencies.

[9] Lisa Craig, Katrina T. Forest, and Berenike Maier. Type iv pili: dynamics, biophysics and functional consequences. *Nature Reviews Microbiology*, 17(7):429–440, Jul 2019. ISSN 1740-1534. doi:10.1038/s41579-019-0195-4. URL https://doi.org/10.1038/s41579-019-0195-4.

SFU SURJ | SIMON FRASER UNIVERSITY SCIENCE UNDERGRADUATE RESEARCH JOURNAL
Vol. 5 (2019-20)

Insulin Concentration Impacts the Density of α-Smooth Muscle Actin in Cultured A7r5 Cells

Anni Lu[1*], Irene Choi[1*], Megan Barker[1 †]

[1]Simon Fraser University, *Department of Biomedical Physiology and Kinesiology*

Abstract

Abnormal insulin concentrations in diabetes mellitus have been shown to affect vascular smooth muscle cell (VSMC) phenotype. To investigate if these effects are related to changes in α-smooth muscle actin (α-SMA) in VSMC, we examined the density of α-SMA in A7r5 cells that were incubated in different concentrations of insulin-containing growth media. Glucose concentrations in the media were collected intermittently to monitor insulin function. After incubation, the cells were fixed and immunostained, followed by image capture using fluorescence microscopy. The density of α-SMA was quantified by pixel intensity. Visual comparison and statistical analysis revealed that α-SMA density was significantly higher in the medium insulin condition.

Keywords — Insulin, alpha-smooth muscle actin, A7r5 cells, immunocytochemistry, hyperinsulinemia

1. Introduction

Vascular smooth muscle cells (VSMC) play two critical roles in maintaining optimal arterial wall health and integrity: fully differentiated, contractile VSMC modulate blood vessel contractility and regulate blood pressure, whereas proliferative and non-contractile VSMC repair arterial wall injuries [1]. Consequently, any dysfunctions associated with VSMC may pose prominent risks for vascular pathologies [2]. Abnormal insulin concentrations present in diabetes mellitus have been shown to alter VSMC morphology and phenotype [3]. Other studies have also found that compensatory hyperinsulinemia that is present at varying severities in Type 2 diabetes patients may be correlated with a higher risk for arterial plaques [1]. The underlying cellular mechanism has not been fully understood, however, one study has found that insulin contributes to VSMC differentiation by increasing the level of α-SMA expression [3].

Building on these findings, this study used non-contractile, A7r5 cells in culture to examine the effects of the presence of insulin. We asked whether various concentrations of insulin converted the cultured cells into a contractile phenotype by inducing α-SMA expression or arrangement. We hypothesized that incubation in higher concentrations of insulin would cause increased density of α-SMA in cultured A7r5 cells. We used HUMALOG®insulin lispro, which is a rapid-acting human insulin analog used to lower

*Equal First Authorship
†Corresponding Author. Contact: barker@sfu.ca

blood glucose in patients with Type 1 diabetes [4]. It has the same molecular weight as human insulin but has a slightly different molecular structure [4].

In this experiment, our initial purpose was to obtain insulin concentrations that are physiologically relevant to those present in normal and diabetic individuals through dilution. A healthy individual would have a circulating fasting concentration of 0.018-0.09 nmol/L of insulin, whereas an individual with hyperinsulinemia would have a circulating fasting concentration of approximately 0.109 nmol/L of insulin [5]. Due to insufficient growth media (GM) quantity, we were not able to dilute the insulin to match these concentrations. Therefore, for our low, medium, and high insulin conditions, we chose to dilute 1 uL, 10 uL, and 50 uL of insulin, respectively, in GM, which resulted in insulin concentrations of 375 nmol/L, 3750 nmol/L, and 18800 nmol/L respectively. These values provided adequate differences in insulin concentration, which we hoped would contribute to distinctive results between our four experimental conditions. Moreover, our chosen insulin concentrations, although not equivalent to physiological concentrations in humans, still provided similar intervals to compare insulin concentrations between normal and diabetic individuals [5]. We assessed the effects of insulin concentration on α-SMA density by adding insulin at varying concentrations to A7r5 cells. We chose to use GM because it contains a high concentration of fetal calf serum, which promotes proliferation, but also de-differentiation of smooth muscle cells. This would eliminate the media as a potential, confounding variable, thus, any changes in α-SMA density would likely have been caused by the varying insulin concentrations. The cells were fixed, immunostained for α-SMA, then fluorescent and brightfield images were captured. α-SMA density was quantified by averaging the red pixel intensity of fluorescent microscopy images, which was used in a prior study as a method of quantifying protein expression [6].

Visual comparison of the images, as well as statistical analysis of red pixel intensity demonstrated that A7r5 cells treated with medium concentration insulin exhibited significantly higher α-SMA density compared to the control group. On the other hand, the A7r5 cells treated with low and high insulin concentrations did not show any statistically significant increase in α-SMA density compared to the control condition.

The findings from this experiment are relevant to the current knowledge regarding Type 1 and Type 2 diabetes, which both present as abnormal insulin levels in those who are affected [3]. Considering that abnormal concentrations of insulin may affect VSMC phenotype and morphology, the present experiment may contribute to the understanding of vascular conditions and pathology amongst diabetes patients.

2. Materials and Methods

2.1. Materials

All experimental protocols were adapted from weeks 5, 6, and 7 of the BPK408W Cell Physiology Laboratory Manual [7]. The growth media consisted of Dulbecco's Modified Eagle's Media (with Glutamax, pyruvate, and 25 mM glucose) obtained from Life Technologies, 10% fetal calf serum, and Antibiotic-Antimycotic (100 units/mL penicillin, 100 units/mL streptomycin, 0.25 ug/mL amphotericin B) [7]. The mouse

IgG2a, anti-α-SMA primary antibody was obtained from Santa Cruz Biotech (sc-32251), and the Goat anti-Mouse IgG2a secondary antibody conjugated to Alexa Fluor 555 was obtained from Thermo Fisher Scientific (A-21137) [7]. The insulin used was HUMALOG®insulin lispro which is a human insulin analog.

2.2. Experimental Procedure

A7r5 cells were exposed to four concentrations of insulin: no insulin (control group), low insulin, medium insulin, and high insulin. Each condition was replicated three times. For the four conditions being tested on the A7r5 cells, varying volumes of insulin were diluted in GM to obtain specific concentrations of insulin (Tab. 1). The prepared mixtures were used to replace the original GM in the twelve wells that contained approximately 7×10^4 A7r5 cells at confluence. The control cells were incubated in pure GM, while the experimental cells were exposed to their corresponding concentrations of insulin-containing GM. Each well was filled with 500 uL of media then incubated overnight. After 20 hours, the media in all four experimental groups was replaced with either fresh GM (control group) or insulin-containing GM (insulin groups), and the wells were imaged using a Bio-Rad ZOE microscope to obtain initial brightfield images. After an additional 95-hour incubation period, the cells were imaged using brightfield microscopy to observe any possible changes, then fixed using 1% paraformaldehyde. Hoescht-33342 at 1 ug/mL was used to stain double-stranded DNA in cellular nuclei, then a primary antibody (Mouse IgG2a) at a concentration of 0.67 ug/mL, and a secondary antibody (Goat anti-Mouse IgG2a Secondary Antibody with Alexa Fluor®555) with a dilution factor of 500, were used to immunostain the α-SMA. All of the cells were stained simultaneously under identical experimental conditions.

Images were captured under brightfield, red, and blue channels, and settings such as contrast and exposure were kept constant within each channel. The red channel visualized the Alexa Fluor 555 fluorophore which stained α-SMA, the blue channel visualized Hoescht-33342 dye which stained the nuclei of all cells. The blue channel had an excitation wavelength of 355/40 nm and an emission wavelength of 433/36 nm, while the red channel had an excitation wavelength of 556/20 nm and an emission wavelength of 615/61 nm [7]. Composite images combining the red and the blue channel images were created for comparison to ensure that the red channel images captured α-SMA of all cells.

Before and after the addition of insulin, glucose concentration in the media was measured using a calibrated glucometer (Contour®Next One Smart Meter) and test strips (Contour®Next Test Strips). As insulin is known to promote cellular glucose uptake, the glucose readings provided supplementary results in addition to the microscopy images obtained. It is important to note that we had limited access to the laboratory as well as shared laboratory equipment such as the Bio-Rad ZOE microscope; this put a time constraint on our image collection process. Although it would have provided the most accurate data, we were not able to obtain brightfield and fluorescent images from every single well because some wells had cells that were not stained properly, resulting in blurry images. Hence, only the wells containing A7r5 cells that demonstrated the greatest glucose uptake, and most clarity, were selected and imaged.

Condition	Mixture of Reagents added to each well (µL)	Concentration of Insulin (nmol /L)
Control (no insulin)	No insulin + 500µL GM	0
Low insulin	1µL insulin + 499µL of GM	375
Medium insulin	10µL insulin + 490µL GM	3750
High insulin	50µL insulin + 450µL GM	18800

Table 1: Recipe table for insulin dilution in growth media and the resulting concentrations.

3. Results

3.1. Glucose Concentration Readings

Prior to media replacement in the wells, glucose concentration in the original media was measured to be 25.5 mmol/L. Considering that in GM, 25 mmol of glucose was diluted in serum, the original glucose reading and control data had higher readings than expected. This may have been because the stock media had more concentrated glucose or that the glucometer had a systemic error and consistently measured higher than the actual value. Glucose concentration in media was recorded intermittently throughout the incubation process for all twelve wells. These data were used to monitor whether insulin was exhibiting an effect on the A7r5 cells. Readings were taken immediately after the initial addition of insulin, after 20 hours of incubation, immediately after media was changed at 20 hours of incubation, and after 95 hours of incubation in the changed media. The glucose readings for each condition were averaged over the three replicates (Tab. 2).

The difference in glucose concentration was graphed (Fig. 1) and single-factor ANOVA was computed using Microsoft Excel. It appears that incubation of A7r5 cells in various insulin concentrations did not cause statistically significant differences between glucose concentration for the four conditions ($p = 0.3998$), with $p < 0.05$ considered to be significant. This indicates that the various insulin concentrations exerted insignificant effects on glucose uptake.

3.2. Image Analysis

Following incubation, a visual comparison of these images revealed an increase in the proportion of spindle-like, contractile A7r5 cells in the 95-hour images (Fig. 2 second column). The red channel images displayed minimal α-SMA in the control group, and a slight increase in α-SMA in A7r5 cells of the low insulin condition. Prominent parallel α-SMA was observed in the medium insulin condition, and some increase in α-SMA was observed in A7r5 cells of the high insulin condition, although not as prominent as the medium insulin condition (Fig. 3 right column). It is also important to note that an increase in the number of dead A7r5 cells was noted in the high insulin condition after

			Initial (0 hours)	20 hours incubation	Initial (after media change)	95 hours incubation (after media change)
Concentration of Insulin in Media	Control	1	28.1	27.3	28.6	27.3
		2	29.4	26.6	29.6	18.6
		3	29.4	27.1	28.4	16.9
		Average	29.0	27.0	28.9	20.9
	Low (375 nmol/L)	1	27.9	27.8	28.8	17.5
		2	29.0	23.3	25.3	18.5
		3	26.4	26.5	26.8	23.9
		Average	27.8	25.9	27.0	20.0
	Medium (3750 nmol/L)	1	28.3	22.5	28.8	EX20*
		2	28.3	24.1	28.2	EX20*
		3	28.3	21.8	28.5	16.5
		Average	28.3	22.8	28.5	16.5
	High (18800 nmol/L)	1	27.0	24.5	26.4	18.5
		2	26.6	22.3	26.4	27.5
		3	26.5	24.9	27.8	27.1
		Average	26.7	23.9	26.9	24.4

*Testing error occurred during glucose reading and data was not obtained

Table 2: Glucose concentration reading (mmol/L) from three replications and their averages within each condition, organized by incubation time.

95-hour incubation, which was evident from the numerous round, dark cells that were visible in the brightfield images (Fig. 2D second column). Cell death was observed in the red channel where auto-fluorescence was remarkable, indicating non-specific binding to antibodies by dead cells (Fig. 2D third column) [8]. Additionally, in the control and low insulin conditions, red staining was predominantly localized to the nuclei, whereas there was little red staining in nuclei in the medium and high insulin conditions. This finding was unexpected as α-SMA in VSMC usually traverses the nuclei. We speculate that this could have been a result of a change in cellular phenotype, and the increased peri-nuclei α-SMA may be an indication of a contractile phenotype, however, the underlying signalling pathway is yet to be elucidated.

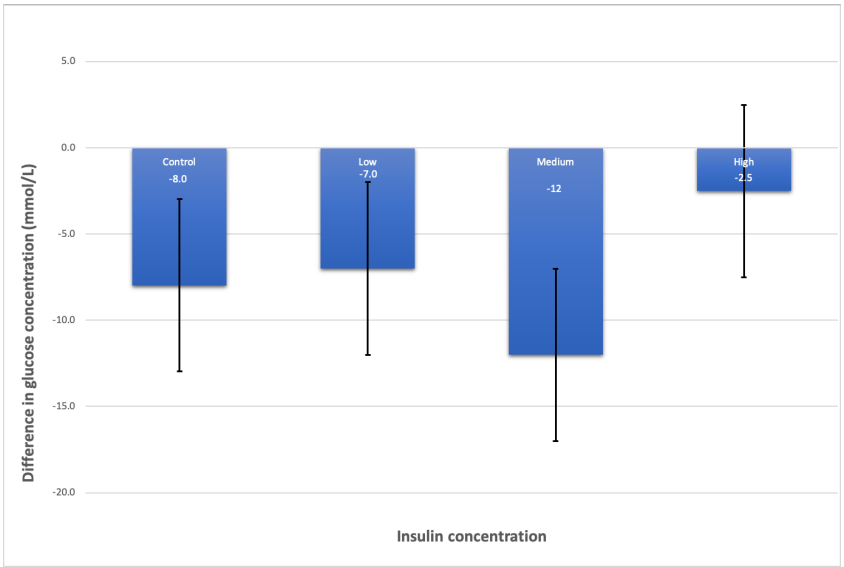

Figure 1: *Differences in glucose concentration after 95 hours of incubation in insulin-containing media. Bar graph displays glucose uptake from all four experimental conditions. Error bars depict within-condition standard deviation, data labels are shown. Single-factor ANOVA: p = 0.3998 with p <0.05 set to be significant.*

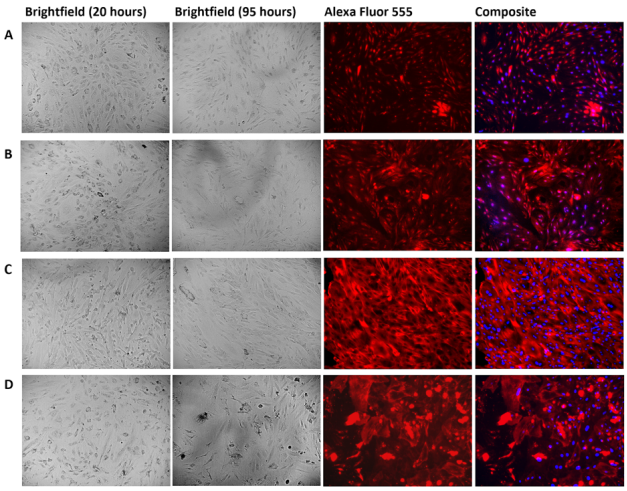

Figure 2: *Representative multi-panel image of A7r5 cells in GM imaged under four conditions. From left to right: unstained cells after 20 hours of insulin exposure, unstained cells after 95 hours of insulin exposure, red channel of immunostained cells, and composite images of immunostained cells. From top to bottom: A) Control B) Low C) Medium, and D) High insulin concentrations.*

From initial visual inspection, it appears that the medium insulin concentration most prominently promoted α-SMA synthesis, because the red channel image displayed the most staining compared to all other conditions (Fig.2C third column). To further quantify this comparison, red channel pixel intensity was averaged using the "Histogram" function in ImageJ software with a minimum threshold of 21, and a maximum

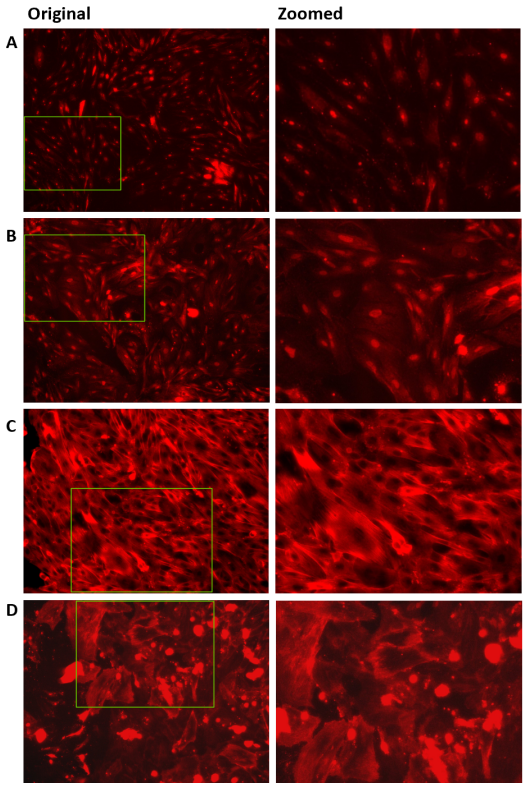

Figure 3: *Representative multi-panel image of Alexa Fluor 555 immunostained A7r5 cells in GM after 95 hours of insulin exposure. Left column shows the original image and the right column shows a zoomed subregion of the same image. From top to bottom: A) Control B) Low C) Medium, and D) High insulin concentrations.*

threshold of 255. The histogram function coupled with a threshold provided an average pixel intensity from every single pixel in an image, while eliminating background intensity from parts of the image in which there were no cells. This allowed for meaningful and unbiased comparison between conditions. The red pixel intensity was then averaged across the two fields-of-view captured from one well of each condition that provided the image with the most clear staining. Figure 4 shows that the average red pixel intensity was considerably higher for images of the medium insulin condition. Single-factor ANOVA yielded a p-value of 0.0017, indicating between-group difference is significant, with $p < 0.05$ considered significant. A two-tailed unpaired t-test was then conducted to confirm which insulin condition produced statistically significant differences compared to the control group. The t-tests yielded $p = 0.855$ for control vs. low insulin, $p = 0.00357$ for control vs. medium insulin, and $p = 0.250$ for control vs. high insulin. A posthoc Bonferroni test was computed to account for the inflation of type I error with multiple t-tests; the Bonferroni-adjusted p-value was 0.0167 ($0.05/3 = 0.0167$). Comparison of the p-values from the t-test to the Bonferroni-adjusted p-value determined that only the images taken from the medium insulin well had red pixel intensity that was significantly higher than that of the control. Hence, this demonstrated that only A7r5 cells in the medium insulin condition had significantly increased α-SMA

density.

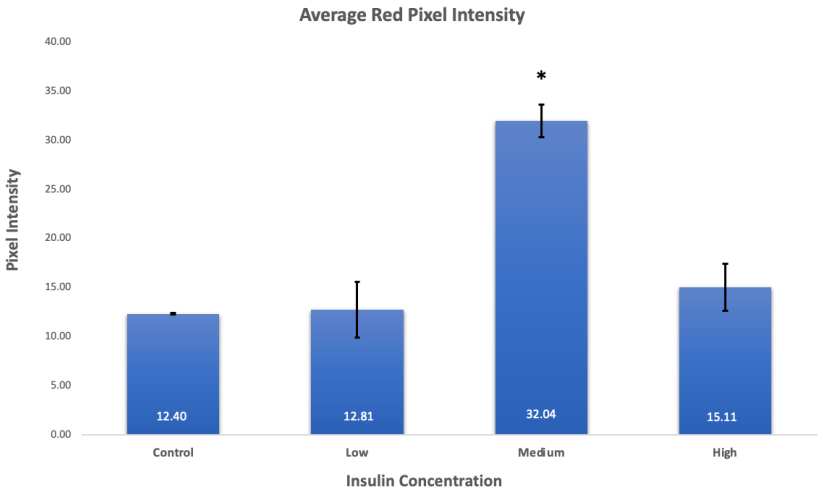

Figure 4: *Bar graph comparing average pixel intensity in red channel measured using ImageJ software between control (no insulin), low insulin concentration, medium insulin concentration, and high insulin concentration in GM. Error bars depict standard deviation within each condition; data labels are displayed. Statistical analysis results shown: * = significant difference at* $p < 0.05$ *(with posthoc Bonferroni test).*

4. Discussion

In the present experiment, the cells treated with the medium concentration insulin (3750 nmol/L) exhibited a significantly higher increase in α-SMA density. This was shown through comparison of red pixel intensities and confirmed using statistical analysis (Fig. 4). Although the mechanism underlying this insulin-dependent increase in α-SMA density is not yet fully understood, one possibility may be that the increased glucose uptake by A7r5 cells allowed for greater ATP production, which provided the cells with more energy to perform cellular functions such as α-SMA synthesis. Conversely, the A7r5 cells treated with the low (375 nmol/L) and high (18800 nmol/L) concentrations of insulin displayed no statistically significant changes in α-SMA compared to the control group. We speculate that the low concentration of insulin may not have been sufficient to induce a significant increase in α-SMA expression, however, the medium concentration of insulin was adequate in inducing a significant increase in α-SMA expression. Contrary to our initial hypothesis that α-SMA expression will increase with increasing concentrations of insulin, the high insulin condition exhibited lower increase of α-SMA density compared to the medium insulin condition. Both visual comparison of the images and quantitative comparison of red pixel intensities confirmed this finding. Additionally, our supplementary data of glucose readings revealed that all three high insulin condition replicates had the least glucose uptake after 95 hours of incubation. This was also inconsistent with our initial prediction that the high concentration of insulin would stimulate the most glucose uptake by A7r5 cells, causing the greatest

reduction of glucose concentration in the media.

Combining the results of image analysis and glucose readings, we speculate that the high insulin concentration of 18800 nmol/L may have contributed to an initial period of excessive intracellular glucose and led to glucose toxicity, which has been studied as a potential cause of pancreatic β-cell apoptosis in patients with Type 2 diabetes [9]. This excessive intracellular glucose may have increased the intracellular osmolarity, which would have caused an influx of water that would have caused cell lysis in early stages of incubation. We speculate that the rationale behind the least glucose uptake in high insulin groups was that the intracellular glucose was released back into the media after cell lysis, and there were less live cells actively taking up glucose. This initial cell lysis and the decrease in total viable cell count early in the incubation process meant that not as many cells survived long enough to synthesize α-SMA, which resulted in lesser α-SMA density observed in the high insulin condition wells. This was also evident in the brightfield image taken 95 hours after incubation, cell death was evident within the high insulin group as many cells appeared round and shrunken with dark borders (Fig. 2D, second column). To further support this speculation, visual analysis of the red channel images from the high insulin condition show that the cells that remained alive until fixation appeared to exhibit increased α-SMA density similar to that observed in the medium insulin condition. However, not as many cells survived long enough until fixation for this to occur, hence, the overall red pixel intensity of images collected from the high insulin concentration wells was lower than that of wells treated with medium insulin concentration.

There were no prior studies that tested this combination of HUMALOG®insulin lispro on A7r5 rat cells, so it was uncertain if the insulin would exert any effect on the cells. We thought wells with little or no change in glucose uptake may have indicated that this pairing was not compatible. Therefore, in conjunction with the time constraint, we selected wells that demonstrated glucose uptake to be analyzed, as this reflected that insulin was indeed affecting the cells in some way. Additionally, this limits the sample size and decreases statistical power, which reduces the possibility of the experiment reflecting the true effect. In other words, if all wells had been included in the analysis, there may be a possibility that insulin's effect on α-SMA density would not be significant in any of the experimental conditions.

Previous studies have found that, under normal physiological conditions, insulin would increase VSMC differentiation and α-SMA density via the phosphoinositide 3-kinase (PI3K) pathway and would minimally stimulate VSMC proliferation via the mitogen-activated protein kinase (MAPK) pathway [3]. With insulin resistance and hyperinsulinemia, the PI3K pathway is disrupted but the MAPK pathway is enhanced, therefore VSMC differentiation would decrease, and proliferation would increase [3]. This is contrary to our results, as our medium insulin condition significantly increased α-SMA density, which is reflective of the differentiated phenotype. This discrepancy could be due to the fact that our study utilized rat VSMC, whereas the referenced study utilized bovine VSMC; it is possible that much higher insulin concentrations are required to mimic the insulin-resistant pathways in A7r5 cells. In addition, it should be emphasized that the HUMALOG®insulin used in our study contained non-medical ingredients, notably glycerol, sodium hydroxide (NaOH), and m-cresol [4]. A

past study found that cell proliferation was significantly decreased in five different cell lines when glycerol concentrations were 2-4% of the media [10]. Porcine VSMCs exposed to NaOH had enhanced proliferation [11]. 4-chloro-m-cresol (4-CMC) is a monochlorinated m-cresol that functions as a ryanodine receptor agonist, and studies have shown that it can stimulate cellular contraction [12, 13]. However, another study found that cultured rat aortic smooth muscle cells do not express ryanodine receptors, hence confounding effects of m-cresol on A7r5 cells in our study may be reduced or eliminated [14]. As the exact concentrations of these ingredients are unknown, it is difficult to state that they affected the A7r5 cells, however, the possibility should be considered.

5. Conclusion

Statistical analysis showed that incubating A7r5 cells in GM with an insulin concentration of 3750nmol/L significantly increased α-SMA density, which is also reflective of a contractile phenotype. However, it is important to emphasize the many limitations of the current study; further improvements and adjustments should be made to the protocol to improve clinical relevance for human models. Due to a lack of available reagents, it was not possible to match physiologically relevant levels of insulin by dilution. Therefore, the concentrations used were unlike what is experienced in physiological conditions. Instead of using tiers of levels, manipulating insulin concentrations to be within the range of healthy and diabetic individuals would aid in excluding variables, such as osmotic stress caused by our high insulin condition. Furthermore, as a result of having limited access to the equipment, we were unable to obtain data at consistent intervals of time. Test points taken at shorter, regular time intervals would help to observe more changes in regard to cell morphology and glucose uptake.

For the present study, we chose to compare α-SMA density between conditions instead of α-SMA arrangement because software that could accurately categorize different cellular morphologies was not available. Without the appropriate software, quantification of α-SMA arrangement would be prone to human error and experimenter bias. We would suggest future studies that wish to use pixel intensity as a method of protein expression quantification, to normalize the intensity to the number of cells. This was challenging for our experiment as our Hoescht-33342 was defective, as a result, we did not obtain accurate total cell counts. In addition, we expected the therapeutic effects of HUMALOG®to be similar to those of human insulin, however, the discrepancy in molecular structure should be considered a potential confounding variable when applying the results of the present study on human models [4]. Hence, future studies could use human arterial smooth muscle cells instead of A7r5 cells, and human insulin could be added to these cells instead of an insulin analog. This would eliminate the molecular structure discrepancy between different types of insulin as a confounding variable. This would also exclude the pairing of the human insulin analog with rat aortic smooth muscle cells as a potential confound since these two molecules were not meant to interact. Lastly, a more accurate and direct alternative to quantify α-SMA density would be to conduct droplet digital polymerase chain reaction (ddPCR) to quantify the level of gene expression of contractile proteins such as α-SMA.

Taking the above experimental limitations into consideration, the present study should be considered a precursor for future studies, and the results may provide additional information into how compensatory hyperinsulinemia that is often present in Type 2 diabetes may increase the risk for vascular pathologies [15]. The increase in α-SMA density may adversely affect blood vessel contractility, which consequently may cause hypertension [15]. Considering that VSMCs also play a critical role in blood vessel injury repair and α-SMA can significantly alter VSMC morphology and phenotype, an abnormally high α-SMA density may exacerbate atherogenesis and increase the risk for atherosclerosis, especially in the presence of repeated injuries [1].

6. Acknowledgments

We would like to express our sincere gratitude to Dr. Megan Barker and Ms. Ba Run Kim for their academic support, and to Mr. Paul MacDonald for providing us with HUMALOG®insulin and glucose test strips, as well as assistance with laboratory equipment.

References

[1] Eugenio Cersosimo, Xiaojing Xu, and Nicolas Musi. Potential role of insulin signaling on vascular smooth muscle cell migration, proliferation, and inflammation pathways. *American Journal of Physiology-Cell Physiology*, 302(4):C652–C657, 2012. doi:10.1152/ajpcell.00022.2011. URL https://doi.org/10.1152/ajpcell.00022.2011. PMID: 22094332.

[2] Marpadga A. Reddy, Sadhan Das, Chen Zhuo, Wen Jin, Mei Wang, Linda Lanting, and Rama Natarajan. Regulation of vascular smooth muscle cell dysfunction under diabetic conditions by mir-504. *Arteriosclerosis, Thrombosis, and Vascular Biology*, 36 (5):864–873, 2016. doi:10.1161/ATVBAHA.115.306770.

[3] Cecilia C. Low Wang, Inga Gurevich, and Boris Draznin. Insulin affects vascular smooth muscle cell phenotype and migration via distinct signaling pathways. *Diabetes*, 52(10):2562–2569, 2003. ISSN 0012-1797. doi:10.2337/diabetes.52.10.2562. URL https://diabetes.diabetesjournals.org/content/52/10/2562.

[4] Humalog (insulin lispro [rdna origin]) for type 1 diabetes: Uses, dosage, side effects, interactions, warnings. URL https://www.rxlist.com/humalog-drug.htm.

[5] Gisela Wilcox. Insulin and insulin resistance. *The Clinical biochemist. Reviews*, 26 (2):19–39, May 2005. ISSN 0159-8090. URL https://pubmed.ncbi.nlm.nih.gov/16278749. 16278749[pmid].

[6] Takumi Higaki, Natsumaro Kutsuna, Toshio Sano, Noriaki Kondo, and Seiichiro Hasezawa. Quantification and cluster analysis of actin cytoskeletal structures in plant cells: role of actin bundling in stomatal movement during diurnal cycles in arabidopsis guard cells. *The Plant Journal*, 61(1):156–

165, 2010. doi:https://doi.org/10.1111/j.1365-313X.2009.04032.x. URL https://onlinelibrary.wiley.com/doi/abs/10.1111/j.1365-313X.2009.04032.x.

[7] M Barker, T Claydon, D Poburko, G Rintoul, and N Wicks. *BPK408W Cell Physiology Laboratory Manual*. Simon Fraser University, 2019.

[8] Jérémy Surre, Claude Saint-Ruf, Valérie Collin, Sylvain Orenga, Mahendrasingh Ramjeet, and Ivan Matic. Strong increase in the autofluorescence of cells signals struggle for survival. *Scientific Reports*, 8(1):12088, Aug 2018. ISSN 2045-2322. doi:10.1038/s41598-018-30623-2. URL https://doi.org/10.1038/s41598-018-30623-2.

[9] Tatsuo Tomita. Apoptosis in pancreatic β-islet cells in type 2 diabetes. *Bosnian journal of basic medical sciences*, 16(3):162–179, Aug 2016. ISSN 1840-4812. URL https://pubmed.ncbi.nlm.nih.gov/27209071. 27209071[pmid].

[10] J.P. Wiebe and C.J. Dinsdale. Inhibition of cell proliferation by glycerol. *Life Sciences*, 48(16):1511–1517, 1991. ISSN 0024-3205. doi:https://doi.org/10.1016/0024-3205(91)90275-G. URL https://www.sciencedirect.com/science/article/pii/002432059190275G.

[11] María Concepción Serrano, María Teresa Portolés, María Vallet-Regí, Isabel Izquierdo, Lorenzo Galletti, Juan Valentín Comas, and Raffaella Pagani. Vascular endothelial and smooth muscle cell culture on naoh-treated poly(ϵ-caprolactone) films: A preliminary study for vascular graft development. *Macromolecular Bioscience*, 5(5):415–423, May 2005. ISSN 1616-5187. doi:10.1002/mabi.200400214. URL https://doi.org/10.1002/mabi.200400214.

[12] Team e. 4-chloro-m-cresol (chebi:34395). URL https://www.ebi.ac.uk/chebi/searchId.do?chebiId=CHEBI:34395.

[13] H. Westerblad, F.H. Andrade, and M.S. Islam. Effects of ryanodine receptor agonist 4-chloro-m-cresol on myoplasmic free ca2+ concentration and force of contraction in mouse skeletal muscle. *Cell Calcium*, 24(2):105–115, 1998. ISSN 0143-4160. doi:https://doi.org/10.1016/S0143-4160(98)90078-1. URL https://www.sciencedirect.com/science/article/pii/S0143416098900781.

[14] Eun Ji Kim, Dong Kwan Kim, Shin Hye Kim, Kyung Moo Lee, Hyung Seo Park, and Se Hoon Kim. Alteration of ryanodine-receptors in cultured rat aortic smooth muscle cells. *The Korean journal of physiology & pharmacology: official journal of the Korean Physiological Society and the Korean Society of Pharmacology*, 15(6):431, 2011.

[15] Valeska Ormazabal, Soumyalekshmi Nair, Omar Elfeky, Claudio Aguayo, Carlos Salomon, and Felipe A. Zuñiga. Association between insulin resistance and the development of cardiovascular disease. *Cardiovascular Diabetology*, 17(1):122, Aug 2018. ISSN 1475-2840. doi:10.1186/s12933-018-0762-4. URL https://doi.org/10.1186/s12933-018-0762-4.

SFU SURJ | SIMON FRASER UNIVERSITY SCIENCE UNDERGRADUATE RESEARCH JOURNAL
Vol. 5 (2019-20)

Inverse Relationship Between Stomatal Density and Nitrogen Level in Salmonberry (*Rubus spectabilis*)

Kara Molgard[1]

[1]Simon Fraser University

Abstract

On the north-western coast of North America, spawning salmon heavily influence riparian communities. An example of this is the positive correlation found between the density of spawning salmon and the stomatal density of Salmonberry (*Rubus spectabilis*) growing nearby. This relationship could exist because when nutrients, including nitrogen, are added to the environment by decomposing salmon, plants are no longer limited by nutrient availability, but instead are limited by CO_2 intake. As a result, plants may increase the stomatal density of new leaves to increase CO_2 intake to support photosynthesis and plant growth. To test this, we grew Salmonberry in low and high nitrogen level solutions. We measured plant growth as stem length, leaf width, and leaf length, and we measured the stomatal density of new leaves. As expected, measurements of growth were significantly higher at high nitrogen levels – average stem length and leaf size were larger – indicating that administration of treatment levels was effective. However, stomatal density was significantly lower at high nitrogen levels, the opposite of what we predicted. The reason for this relationship is unclear, but it may be that larger leaves have larger cell sizes, resulting in fewer stomata per unit area than smaller leaves, even if the leaves have a similar total number of stomata. Overall, the inverse relationship we found between stomatal density and nitrogen level may indicate a different relationship than previous studies indicated, but further studies need to be done that also consider leaf cell size before we can make this conclusion.

Keywords — Stomatal Density, Nutrient Availability, Nitrogen, Salmonberry, Salmon

1. Introduction

On the north-western coast of North America, spawning salmon provide an important source of nutrients to riparian systems, which can shape riparian plant communities [1, 2, 3, 4]. One study found that with an increased density of spawning salmon, there was an increase in the density of pores in the leaves of Salmonberry (*Rubus spectabilis*) that grew on the banks of these streams [5]. The pores in plant leaves are called stomata, and they are the site for the uptake of carbon dioxide (CO_2) and release of water vapour and oxygen (O_2). The positive correlation between the density of spawning salmon and the stomatal density of Salmonberry suggests that stomatal density may increase with nutrient availability. However, this relationship has not been established experimentally.

To understand why there would be a positive relationship between nutrient level and stomatal density, we should first consider Liebig's law of the minimum: at any

point in time, there is only one factor limiting plant growth [6]. Light, water availability, CO_2, and various nutrients are all important for plant growth, but nitrogen is often the limiting factor [7]. This is because, although nitrogen is abundant in the air as nitrogen gas (N_2), nitrogen is only useable to plants in the forms of nitrate (NO_3^-) and ammonium (NH_4^+), which can be lost from the soil by volatilization or being washed away with running water [8]. These forms of nitrogen are supplied to the soil by nitrogen-fixing bacteria, by fertilizer from agricultural fields, and by the decomposition of dead organisms (such as salmon after spawning) [9]. Interestingly, an experimental study found that plant foliar nitrogen was higher around streams where decomposing salmon were added than around control streams [10]. This indicates that nitrogen is subsidized to the riparian plant communities by spawning salmon, and if nitrogen was limiting plant growth, the limitation is lifted to an extent dependent upon the amount of nitrogen subsidized and the plant's need.

If nitrogen's limitation on plant growth is relaxed as a result of subsidization, the next possible limiting factor could be CO_2, which is taken into plants via stomata. However, water-vapour also leaves through the stomata resulting in a trade-off between CO_2 intake and water-loss. Because of this, plants optimize stomatal characteristics – including stomatal aperture and stomatal density – to limit water-loss, while still taking in enough CO_2 for photosynthesis and growth [11]. Stomatal aperture adjusts as environmental conditions fluctuate due to changes in the turgidity of the guard cells that form the stomata [12]. Alternatively, stomatal density is determined during leaf development. When nitrogen levels increase, the capacity for photosynthesis and growth increases as well. Carbon dioxide may then limit photosynthesis, so the plant may change these stomatal characteristics to adjust carbon dioxide intake.

In this study, our goal was to provide experimental evidence of the effects of nutrient subsidies, specifically nitrogen, on stomatal density in plant leaves. Our first hypothesis was that nitrogen would limit plant growth at low levels. However, at high nitrogen levels, CO_2 would replace nitrogen as the limiting factor, so stomatal density in new leaves would increase to facilitate CO_2 uptake. We conducted this experiment by growing Salmonberry stems harvested from a local forest in two different nitrogen concentrations, low and high. Then, we measured growth in terms of stem length, leaf length, and leaf width, and we measured the stomatal density of newly developed leaves. Overall, we predicted that plant growth measurements and stomatal density would all be higher in the high nitrogen level treatment groups.

2. Materials and Methods

2.1. Sampling and Preparation

On May 10th, 2019, we harvested stems of Salmonberry from two different patches just off a path within Naheeno Park, south of Simon Fraser University on Burnaby Mountain, British Columbia. The path is frequented by pedestrians and mountain bikers, and it is at 320 m above sea level. Since Salmonberry clones are < 5 m in diameter, and the patches we sampled from were greater than 5 m apart – roughly 100m apart, we sampled from at least 2 different clones [5]. We prepared one tray of

stems the same day they were harvested and refrigerated the rest in a sealed plastic bag. We prepared the refrigerated stems three days later. We prepared all the stems and trays in the same way: a) we first rinsed the stems under running tap water to dislodge any pests; b) we submerged the stems in water, to prevent air bubbles entering the vascular tissue, and cut the stems into sections containing two leaf nodes each ; c) to lessen water loss, we cut the leaves in half and coated the cut stem tops with "Pruning Sealer" (Green Earth); d) using a razor blade, we longitudinally scarred the last inch of the stem base, dipped them in water, then dipped them in a powdered rooting agent ("Stim-Root No. 3", 0.8% Indole-3-butyric acid); e) we placed the stems in sheets of rockwool cubes with pre-made holes, one stem per cube, and placed the rockwool in a black plastic plant tray. We watered the rockwool with 2 litres of tap water, covered the trays with clear plastic tops to reduce water loss, and placed them side-by-side in a growth chamber. The growth-chamber controlled light levels, temperature, humidity, and air flow – 16 hours of light at 24°C, 8 hours in the dark at 18°C, 90-100% humidity, and a fan speed of 85%. We chose settings conducive to growth and similar to warm summer conditions with humidity high enough to prevent the leaves from drying out. We kept the rock wool damp by adding water as needed, and we removed any stems that died. After two weeks, we found pests on the plants, so we sprayed all the plant surfaces once with "Safer's 3-in-1 Garden Spray" – a fungicide, insecticide, and miticide. If we found the plants were drying too quickly, or they were too damp, we adjusted the position of the plastic coverings accordingly.

Initiating Roots and New Leaves After three weeks, we added a 1 g/L solution of 20:20:20 fertilizer to the base of the stems to promote root growth. To reduce the chance of fungal growth, we increased airflow around the plants by placing the plastic covers slightly ajar from the plant trays. Five weeks into the experiment, root growth had increased, but no new leaves had started growing. To break dormancy, we placed the trays in a cold dark room for 17 days, then treated the nodes with a 500 mL solution of 50 uL of 1 mM benzyl adenine purine in dimethylsulfoxide, 0.200 g gibberellic acid potassium salt 10%, and 0.50 mL "Agral 90" wetting agent before placing them back in the growth chamber with the plastic covers. Three days later, all plants were growing roots, and new leaves were initiated, so we removed the plastic covers.

2.2. Treatment Design

We rinsed all rockwool cubes to remove any left-over fertilizer, then put each cube – each containing one stem – into its own clear plastic container. We filled 5 containers with 7 ppm nitrogen solution and 5 containers with 224 ppm nitrogen solution to a depth of approximately 5 mm. The nitrogen used in the solutions was in the form of potassium nitrate (KNO_3), calcium nitrate ($Ca(NO_3)_2 \cdot 4H_2O$), and ammonium molybdate ($(NH_4)_6Mo_7O_{24} \cdot 4H2O$). The treatment solutions only varied nitrogen concentration but contained the same levels of all other important nutrients for plant growth [13]. We also added "Funginex 6.5" fungicide to each nutrient solution at 1.67 ml/L nutrient solution. We kept the stock solutions refrigerated throughout the experiment. We labelled each box with the treatment solution we used, distributed the containers in a random arrangement within the plant trays, covered them with clear plastic covers, and placed them next to each other in the growth chamber.

2.3. Maintenance

Weekly, we removed the old nutrient solution from each container, put in fresh solution, and rearranged the positions of the containers. During the week, we kept the solution at the same level to prevent the roots from drying by topping-up with water. Algae started growing a few days after the initial addition of the nutrient solutions, so we rinsed the containers and rockwool plugs each time the nutrient solution was changed, and we scrubbed the containers two different times throughout the experiment. Initially, we kept the plastic covers on the trays to prevent drying. However, to allow the plants to transpire, we removed the plastic covers and increased the level of solution to approximately 2.5 cm deep (Fig. 1). If flower buds started growing, we cut them off. We gave the plants nutrient solution as described for 6 weeks, then we topped-up the containers only with tap water. This was because useable leaves had already grown and adding nutrient solution was not required to keep the plants alive for the duration of data collection.

2.4. Data Collection

We collected data from a total of 10 plants – 5 replicates in each of 2 different nitrogen level solutions – and measured stem length for each plant. We also measured the length and width of 3 leaves per plant for a total of 30 leaves measured. For each leaf, we measured the stomatal density of 2 segments for a total of 60 segments measured.

We measured the stem length of the longest stem from the leaf node it arose from to the tip. To do this, we ran string along the stem from the node to the apical meristem. Then, we measured the string to get the stem length measurements.

Counting the apical meristem as the first leaf, unless it was a flower bud, we harvested the middle leaflet of the third and fourth leaves from each stem, as well as the middle leaflet of the second leaf after bud-break. For each leaf, we measured the length as the distance from the tip to where the leaf met the petiole. We measured the width at the widest part of the leaf. We did not determine leaf area from leaf length and leaf width because some leaves were immature, and the leaflets had not separated yet, resulting in varied leaf shapes in our sample.

We dissected 2 segments from each leaf of roughly 10 mm by 5 mm. The segments were taken directly adjacent to the midvein, on the left and right sides, and between the second and third secondary veins. We placed the segments in labelled microcentrifuge tubes filled with a fixative solution of 6-parts 95% ethanol and 1-part glacial acetic acid. We fixed the leaf segments over 24 days. Once all the leaf segments were fixed, we replaced the fixative in the microcentrifuge tube with lactic acid. Then, we heated the samples at 90°C for 2 hours until the samples were transparent. We mounted the segments on slides and took pictures of one area of each segment, adjusting the focus between each picture. We took enough pictures of the area to capture the whole area in focus, resulting in a range of 5 to 11 photos taken per segment. The pictures were taken using a Canon 5D Mark II camera, attached to a Nikon Eclipse 600 microscope, with a Nikon plan fluor 20× objective, and a Nikon 2.5× phototube lens using brightfield illumination. In Adobe Photoshop CC 2018, we viewed all the pictures from each leaf and marked a black dot over each stoma on a blank layer. Then, using the software

ImageJ, we counted the black dots and recorded the stomatal count. To get the stomatal density, we divided the stomatal count by the area captured in the picture, which was 0.1944 mm^2.

2.5. Analysis

For the stomatal density measurements on each side of the leaf midvein, we performed a regression analysis to determine if the two stomatal density measurements from each leaf could be averaged for further use in analyses. Since leaf width, leaf length, and stomatal density were measured on the third, fourth, and bottom leaves, leaf position could have had some influence on those response variables, so we conducted two-way ANOVAs, using Excel version 1902, to see if there were any significant interactions between leaf position and nitrogen level effects on our response variables. If there were no interaction effects between leaf position and treatment level for leaf width, leaf length, and stomatal density, we could average the leaf measurements within each plant and perform one-way ANOVAs to determine the variation in our response variables between treatment groups. We also did a one-way ANOVA for stem length, which only had one measurement per plant.

3. Results

After running a regression analysis, we determined we could average the stomatal density for each leaf (Fig. 2). Moreover, there were no significant interactions between leaf position and nitrogen level effects for leaf length ($F(2,24) = 1.32$, $p = 0.29$), leaf width ($F(2,24) = 0.17$, $p = 0.85$), or stomatal density ($F(2,24) = 0.14$, $p = 0.87$), so we averaged the measurements within each plant.

We found that nitrogen concentration had a significant effect on leaf length ($F(1,8) = 19.5$, $p = 0.0022$; Fig. 3), leaf width ($F(1,8) = 20.4$, $p = 0.0020$; Fig. 4), and stem length ($F(1,8) = 5.94$, $p = 0.041$; Fig. 5). Higher levels of nitrogen increased plant growth in all measurements; in high nitrogen levels average leaf length was 52% greater, average leaf width was 44% greater, and average stem length was 167% greater. Nitrogen concentration also had a significant effect on stomatal density ($F(1,8) = 7.95$, $p = 0.022$; Fig. 6). At high levels of nitrogen, average stomatal density was 61% lower.

4. Discussion

First, consistent with our hypotheses and predictions, all measurements representing plant growth – stem length, leaf length, leaf width – were significantly greater in the high nitrogen concentration treatment group than in the low nitrogen concentration treatment group. These findings are consistent with previous laboratory studies that show that increasing the nitrogen available to plants increases plant growth [14]. Moreover, these results indicate that we successfully administered two different treatment levels of nitrogen, different enough to observe differing effects between the

treatment groups. Therefore, we can be confident that we successfully applied the intended treatments.

Since we observed effects on plant growth consistent with our intended treatment levels, our findings for stomatal density by treatment group were surprising. We hypothesized that stomatal density would be greater in the high nitrogen treatment group due to an increase in demand for CO_2 uptake to support the increase in photosynthesis and growth. Although stomatal density was significantly different between the treatment groups, the effect was in the opposite direction than we predicted; stomatal density decreased with an increase in nitrogen concentration. Because we have reason to believe that the plants received the intended nitrogen levels, our results indicate that nitrogen does affect stomatal density, and that there is an inverse relationship between the two. The reason for this relationship is unclear, but it is possible that in our experiment it was related to leaf size.

We observed that lower nitrogen levels resulted in smaller leaf sizes as measured by leaf length and width. This is important because developing leaves go through two phases, cell proliferation and cell expansion [15]. The initial leaf cells divide, for a time, and once this phase ends, the cells only expand. Therefore, small mature leaves can have the same number of cells as large mature leaves, but because their cells have not expanded as much, they are smaller in size. If the number of stomata is the same between leaves of different sizes, the small leaf would have more stomata per unit area than the large leaf. In this way, the difference in leaf size between the nitrogen level treatment groups could have affected our measured stomatal density. Future studies should control for cell and leaf size by measuring stomatal density on leaves of similar sizes or, better yet, measure the size of the cells and consider cell size when analyzing differences in stomatal density. Another explanation for our results could be that Salmonberry has a non-linear response curve to nitrogen levels, and we did not use enough nitrogen levels to observe that relationship. One study done in southeastern Alaska measured nitrates and ammonium in soil where decomposing salmon were placed and compared it with control soil nearby (3). In control samples, nitrogen levels were under 5µg/g (5ppm) while in plots with decomposing salmon, the highest nitrogen levels were around 150 ug/g (150 ppm) [3]). These levels indicate that our low nitrogen concentration level (7 ppm) was similar to field levels, but our high nitrogen concentration level (224 ppm) may not be. Considering this information, it is possible that the response we saw in stomatal density was due to a non-linear response curve to nitrogen level; at very high levels of nitrogen like in our fertilizer, stomatal density may decrease, but we may see an increase in stomatal density from low to moderate nitrogen levels. Future studies should ensure that the nitrogen levels used are reflective of natural levels, and a larger range of nitrogen levels should be used to rule out non-linear relationships.

Moreover, our study focused on isolating the relationship between nitrogen and stomatal density, but other nutrients may also be responsible for effects on stomatal density in the field. Research into the relationship between specific sources of nutrients on stomatal density such as spawning salmon, or seabird guano, could use different levels of these sources as fertilizer instead to take into account other nutrients and factors present in those sources that may affect stomatal density in the field.

5. Conclusion

By growing Salmonberry in two different nitrogen levels, we found experimental evidence that stomatal density has an inverse relationship with nitrogen level. We also observed significant increases in plant growth at higher levels of nitrogen, indicating that nitrogen limited plant growth at low levels, and that the plants were successfully exposed to the intended nitrogen treatment levels. Although our results indicate an inverse relationship between stomatal density and nitrogen level, it is possible leaf cell size differences between the treatment groups affected the measured stomatal density due to smaller cell sizes in small leaves. Future studies should control for leaf size or measure epidermal cell size as well. It is also important to consider that the stomatal density response curve to nitrogen level may not be linear, so more concentrations need to be used, and at levels reflective of natural environments.

6. Acknowledgments

I would like to thank Dr. Ronald Ydenberg and Dr. Jim Mattsson for providing their guidance and expertise throughout this experiment. Also, thank you to everyone in Dr. Mattsson's lab who kindly provided their advice when I needed it.

References

[1] Robert E. Bilby, Eric W. Beach, Brian R. Fransen, Jason K. Walter, and Peter A. Bisson. Transfer of nutrients from spawning salmon to riparian vegetation in western washington. *Transactions of the American Fisheries Society*, 132(4):733–745, 2003. doi:10.1577/T02-089. URL https://doi.org/10.1577/T02-089.

[2] Scott M. Gende, Amy E. Miller, and Eran Hood. The effects of salmon carcasses on soil nitrogen pools in a riparian forest of southeastern alaska. *Canadian Journal of Forest Research*, 37(7):1194–1202, 2007. doi:10.1139/X06-318. URL https://doi.org/10.1139/X06-318.

[3] Daniel J. Rinella, Mark S. Wipfli, Coowe M. Walker, Craig A. Stricker, and Ron A. Heintz. Seasonal persistence of marine-derived nutrients in south-central alaskan salmon streams. *Ecosphere*, 4(10):art122, 2013. doi:https://doi.org/10.1890/ES13-00112.1. URL https://esajournals.onlinelibrary.wiley.com/doi/abs/10.1890/ES13-00112.1.

[4] C. E. Wilkinson, M. D. Hocking, and T. E Reimchen. Uptake of salmon-derived nitrogen by mosses and liverworts in coastal british columbia. *Oikos*, 108(1): 85–98, 2005. doi:https://doi.org/10.1111/j.0030-1299.2005.13277.x. URL https://onlinelibrary.wiley.com/doi/abs/10.1111/j.0030-1299.2005.13277.x.

[5] Gregory G. van den Top, John D. Reynolds, Herbert H. T. Prins, Jim Mattsson, David J. Green, and Ronald C. Ydenberg. From salmon to salmonberry: The effects of salmon-derived nutrients on the stomatal density of leaves of

the nitriphilic shrub rubus spectabilis. *Functional Ecology*, 32(11):2625–2633, 2018. doi:https://doi.org/10.1111/1365-2435.13202. URL https://besjournals.onlinelibrary.wiley.com/doi/abs/10.1111/1365-2435.13202.

[6] M C Dash and S P Dash. *Fundamentals of Ecology*. Tata McGraw-Hill, 3 edition, 2009.

[7] Peter M. Vitousek and Robert W. Howarth. Nitrogen limitation on land and in the sea: How can it occur? *Biogeochemistry*, 13(2):87–115, Jan 1991. ISSN 1573-515X. doi:10.1007/BF00002772. URL https://doi.org/10.1007/BF00002772.

[8] K.C. Cameron, H.J. Di, and J.L. Moir. Nitrogen losses from the soil/plant system: a review. *Annals of Applied Biology*, 162(2):145–173, 2013. doi:https://doi.org/10.1111/aab.12014. URL https://onlinelibrary.wiley.com/doi/abs/10.1111/aab.12014.

[9] Hannah M. Franklin, Brett H. Robinson, and Nicholas M. Dickinson. Plants for nitrogen management in riparian zones: A proposed trait-based framework to select effective species. *Ecological Management & Restoration*, 20(3):202–213, 2019. doi:https://doi.org/10.1111/emr.12380. URL https://onlinelibrary.wiley.com/doi/abs/10.1111/emr.12380.

[10] Morgan D. Hocking and John D. Reynolds. Nitrogen uptake by plants subsidized by pacific salmon carcasses: a hierarchical experiment. *Canadian Journal of Forest Research*, 42(5):908–917, 2012. doi:10.1139/x2012-045. URL https://doi.org/10.1139/x2012-045.

[11] Peter J. Franks and David J. Beerling. Maximum leaf conductance driven by co2 effects on stomatal size and density over geologic time. *Proceedings of the National Academy of Sciences*, 106(25):10343–10347, 2009. ISSN 0027-8424. doi:10.1073/pnas.0904209106. URL https://www.pnas.org/content/106/25/10343.

[12] Stefano Manzoni, Giulia Vico, Sari Palmroth, Amilcare Porporato, and Gabriel Katul. Optimization of stomatal conductance for maximum carbon gain under dynamic soil moisture. *Advances in Water Resources*, 62:90–105, 2013. ISSN 0309-1708. doi:https://doi.org/10.1016/j.advwatres.2013.09.020. URL https://www.sciencedirect.com/science/article/pii/S0309170813001814.

[13] R HEWITSON, J; PRICE. Plant mineral nutrition in the classroom: the radish, raphanus sativus l is a good plant for such studies. *School science review*, 1994. ISSN 0036-6811.

[14] Itay Cohen, Tal Rapaport, Vered Chalifa-Caspi, and Shimon Rachmilevitch. Synergistic effects of abiotic stresses in plants: a case study of nitrogen limitation and saturating light intensity in arabidopsis thaliana. *Physiologia Plantarum*, 165(4):755–767, 2019. doi:https://doi.org/10.1111/ppl.12765. URL https://onlinelibrary.wiley.com/doi/abs/10.1111/ppl.12765.

[15] Nathalie Gonzalez, Hannes Vanhaeren, and Dirk Inzé. Leaf size control: complex coordination of cell division and expansion. *Trends in Plant Science*, 17(6):332–340, Jun 2012. ISSN 1360-1385. URL https://www.sciencedirect.com/science/article/pii/S1360138512000313.

7. Tables and Figures

Figure 1: *Stems growing in nutrient solution within clear containers placed in black trays within the growth chamber.*

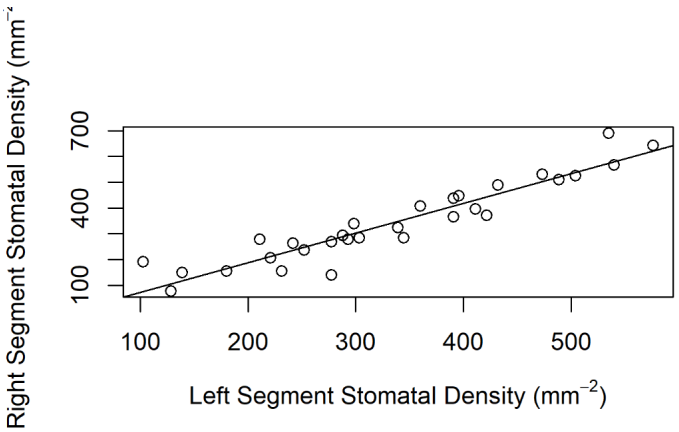

Figure 2: *Stomatal density measured on the right side of the midvein as a function of the stomatal density measured on the left side. The near-linear relationship indicates no major difference between sides in each leaf ($R^2 = 0.8846$).*

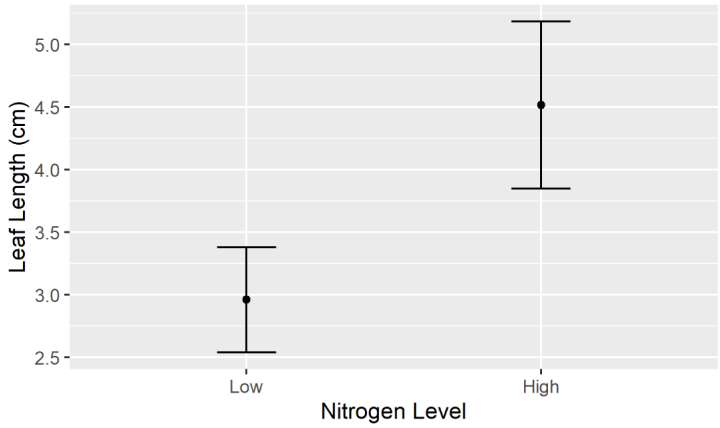

Figure 3: *Mean leaf length ± one standard deviation for plants grown in low and high nitrogen level solutions. Leaf length was significantly higher in the high nitrogen level solution than in the low nitrogen level solution ($F(1,8) = 19.5$, $p = 0.0022$).*

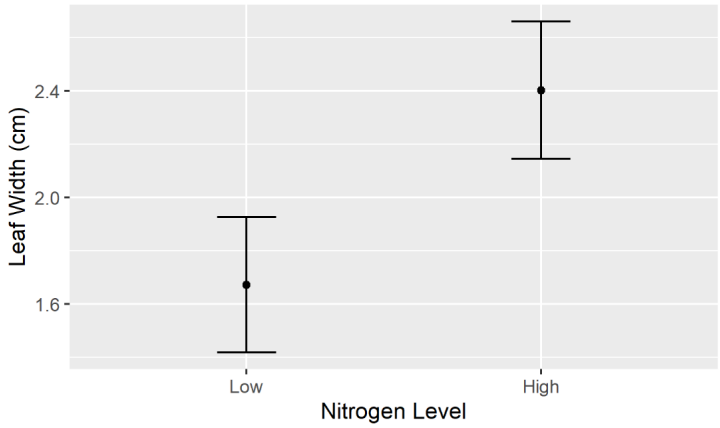

Figure 4: *Mean leaf width ± one standard deviation for plants grown in low and high nitrogen level solutions. Leaf width was significantly higher in the high nitrogen level solution than in the low nitrogen level solution ($F(1,8) = 20.4$, $p = 0.0020$).*

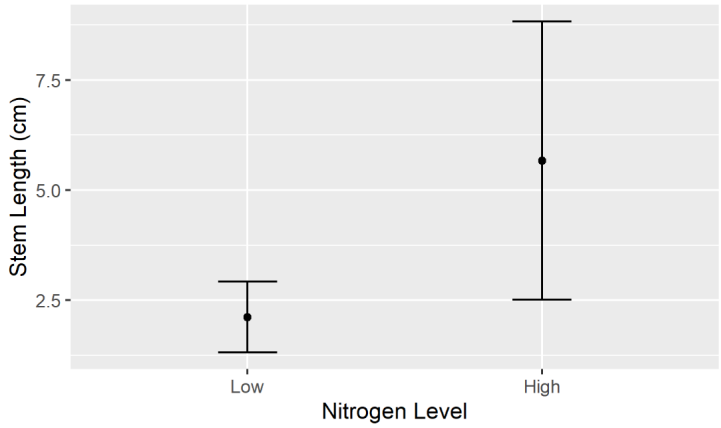

Figure 5: *Mean stem length ± one standard deviation for plants grown in low and high nitrogen level solutions. Stem length was marginally significantly higher in the high nitrogen level solution than in the low nitrogen level solution* ($F(1,8) = 5.94$, $p = 0.041$).

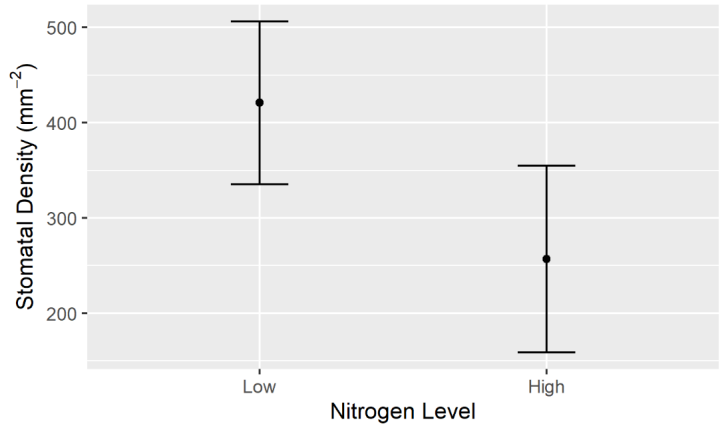

Figure 6: *Mean stomatal density ± one standard deviation for plants grown in low and high nitrogen level solutions. Stomatal density was significantly higher in the low-level nitrogen solution* ($F(1,8) = 7.95$, $p = 0.022$).

SFU SURJ | SIMON FRASER UNIVERSITY SCIENCE UNDERGRADUATE RESEARCH JOURNAL
Vol. 5 (2019-20)

Environmental Justice and Ambient Air Pollutant Exposure in North America

Sumara Stroshein[1], Tim Takaro[1*]

[1]Simon Fraser University

Abstract

Large bodies of international research have demonstrated that there are variations in air pollutant levels (including NO_2 and $PM_{2.5}$) by numerous socioeconomic status (SES) indicators, often with higher levels of air pollution exposure in groups with lower SES. This literature review describes the overall trends that emerge from the literature in North America, discusses methods used to assess the relationship between SES and air pollutant exposure, and discusses differences in trends observed between urban and rural regions. Additionally, challenges related to assessing environmental justice trends in air pollution research are explored. The results of the 21 studies examined in this review suggest that there are significant associations between measures of social and material deprivation (including income, education, unemployment, and individuals living alone) and NO_2 and $PM_{2.5}$ air pollution exposure, typically with lower SES individuals and communities being exposed to higher levels of certain air pollutants. Future research in this area is required to expand our understanding of inequalities in air pollution exposure and health impacts across urban and rural regions of North America to inform public health policy development for the protection of vulnerable populations.

Keywords — Air Pollution, Environment, North America, NO2, PM2.5

1. Introduction

The field of environmental justice aims to assess and address inequalities in the distribution of environmental risk factors [1, 2]. Previous research efforts have generated the triple-jeopardy hypothesis [3]. This hypothesis states that low socioeconomic status (SES) communities not only experience higher exposure to environmental contaminants but are also more susceptible to negative health consequences (due to psycho-social stressors and lack of opportunity to engage in health promoting activities) which ultimately result in environmentally-driven health disparities [3]. While there have been significant research efforts investigating susceptibility to negative health impacts, it is believed that differences in exposure based on SES indicators may be the mechanism that has been least thoroughly researched [4].

Ambient air pollution exposure to air pollutants (including NO_2 and $PM_{2.5}$) has been identified as a major planetary health risk and the fifth highest risk factor for global mortality (5,6). For example, it is estimated that air pollution contributed to approximately 1 in 10 deaths in 2017, for a global total of 5 million deaths [5]. Since the 1950s, there have been significant global efforts to protect public health through the

*Corresponding author. Contact e-mail:ttakaro@sfu.ca

reduction of air pollution levels [6]. However, air pollution exposure continues to have significant impacts on morbidity and mortality rates in both developing and developed countries [7, 8]. At a national level in Canada, air pollution related disease has been estimated to cost between $ 3.6-9.1 billion annually and contribute to a diverse number of health impacts including over 78,000 hospitalizations for cardiovascular disease [8].

Large bodies of international research have demonstrated that there are variations in air pollution exposure by numerous socioeconomic indicators, often with higher levels of air pollution exposure in groups with lower socioeconomic status [6, 9]. A global review paper in 2015 demonstrated that the relationship between air pollution and indicators of SES varies depending on the region of the world where the study takes place [3]. Overall, while there were some variations by pollutant type and in specific cities, there was a consistent trend in North American studies indicating that lower SES individuals and communities bear a disproportionate burden of air pollution exposure for primary pollutants such as NO2 and $PM_{2.5}$ [3]. However, several studies show that the relationship between SES and air pollution may differ over time and space, perhaps resulting from unique differences in regional urban development characteristics [3, 10].

Generally, research has tended to analyze and document disparities in exposure levels rather than investigating the processes that contribute to the inequalities [9]. However, there are several hypotheses and theoretical frameworks that have been proposed to explain the relationship between socioeconomic status and air pollution exposure [9]. Processes such as housing market dynamics and systemic racial discrimination may have contributed to spatial clustering of air pollution sources and "class-based residential segregation" [3, 9, 11]. Within country and regional boundaries, individuals of lower socioeconomic status and more deprived communities tend to be in closer proximity to high traffic density roads and industrial facilities [6, 8]. This may be because these individuals may have limited financial resources that constrain their ability to move away as well as less political power to advocate against undesirable land use such as industrial sites or major roadways within their communities [4, 8, 11]. In many countries, including the United States, research indicates that some minority ethnicity groups are exposed to higher levels of air pollution, even after adjusting for community poverty levels and other individual and community level factors [12]. Lievanos et al. argue that variations in exposure to $PM_{2.5}$ by race in the United States reflect broader social inequities including the ongoing impacts of structural racism on exposure to environmental health threats [12]. The objective of this paper is to review environmental equity research regarding exposure to air pollution (specifically $PM_{2.5}$ and NO_2) in North America. Specifically, the review will include studies that describe unequal exposure levels of pollutants rather than studies that explore the processes contributing to unequal exposures or the health effects resulting from differential exposures. While there has been a significant amount of research regarding differences in air pollution exposure in the United States, there is a dearth of research on this topic in Canada [8]. For example, a review article from 2015 identified that only two ambient air pollutants (total suspended particles and NO_2) have been investigated and in only three locations across the country [8]. The review considers $PM_{2.5}$ and NO_2 exposures because of the relevance of these primary pollutants for adverse health outcomes [13]. Additionally, the review will focus on socioeconomic indicators rather

than racial characteristics of communities because they are more consistently recorded and interpretable across different regions in Canada [3]. The goal of this literature review is to qualitatively describe the overall trends that emerge from the literature and discuss methods used to assess the relationship between deprivation and air pollutant exposure.

2. Methods

A scoping literature review was performed to comprehensively explore the established literature regarding the relationship between community deprivation measures of SES and air pollutant exposure ($PM_{2.5}$ and NO_2) in North America. The requirements for the PRISMA tracking system (Preferred Reporting Items for Systematic Reviews and Meta-Analyses) were followed.

Literature searches were performed in PubMed using the following set of search terms: "socioeconomic inequality", "socioeconomic injustice", "socioeconomic disparity", "air pollution", "air pollution exposure", "air quality", "material deprivation", "social deprivation", "community deprivation", "neighbourhood deprivation", "neighborhood deprivation", "environmental justice", "environmental inequality", "environmental disparity", "environmental injustice", "particulate matter", "$PM_{2.5}$", nitrogen dioxide", and "NO_2." A comprehensive set of 22 searches using each combination of search terms was performed. The database searches yielded 2181 records published between 2000-2019. An additional 21 papers were identified from Google Scholar and the reference lists of the identified papers. There were 1501 records remaining after duplicates were removed. The title and abstract of the 1501 records were screened, resulting in the exclusion of 1420 records mainly due to authors not considering inequalities in exposure (Tab. 1). Following screening, each of the remaining 81 papers was then tagged in the Zotero library to indicate the geographic location of the study. Articles were identified as being from North America (38), South American (1), Africa (1), Europe (20), Asia (9), and Oceania (1). There were also 11 review articles that did not conduct original primary research. The 38 North American studies were assessed for eligibility and ultimately 21 eligible records were identified. The exclusion criteria were modeled after the criteria used by Hajat et al. in their global review conducted in 2015 [3]. Table 1 shows the reasons for exclusion at each stage of the screening process. Figure 1 shows the PRISMA reporting flowchart for this literature review.

3. Results

Table 2 in the Appendix summarizes the methods and results of the 21 North American articles included in this review.

3.1. Canadian Studies

There are only three studies identified that investigated inequalities in air pollution exposure in Canada and met criteria for inclusion in the review. Each of these studies

Assessment Stage	Reason for Exclusion	Number of Articles Excluded	Number of Remaining Eligible Articles
Title and Abstract Screening (1420 articles excluded out of 1501)	The article focused only on indoor air pollution and did not investigate outdoor air pollution exposure.	108	
	The article focused on health outcomes resulting from air pollution exposure and did not explore inequalities in exposures.	1071	
	The article only evaluated socioeconomic status as a modifier between air pollution exposure and health outcomes.	13	
	The article focused on air quality policy or air pollution assessment methodology/monitoring systems (without assessing inequalities in exposure).	218	
	The researchers only evaluated race/ethnicity without analyzing socioeconomic data to evaluate inequality.	2	
	The article focused on climate change projections of air quality rather than current air quality measurements.	8	81
Location Screening (38 North American articles selected from 81 papers)	Research not conducted in North America: i. South America (1) ii. Africa (1) iii. Europe (20) iv. Asia (9) v. Oceania (1)	32	
	Review Article (no primary research conducted)	11	38
Full-Text Eligibility Assessment (21 articles selected from 38 North American articles)	The researchers did not evaluate NO2 and/or PM2.5.	6	
	The researchers combined air pollutants into an index without performing analysis for individual pollutants.	3	
	The researchers only evaluated race/ethnicity without analyzing socioeconomic data to evaluate inequality.	4	
	The researchers assessed health outcomes and/or mortality but did not assess differences in exposure by socioeconomic variables.	4	21

Table 1: Reason for Exclusion and Number of Articles Excluded at each Stage of the Screening Process.

investigated NO_2 distribution by SES indicators. Crouse et al. investigated NO_2 distribution at a census tract level in Montreal and included 14 indicators of SES including measures of material deprivation (education and income) and social deprivation (unemployment, lone parents, and individuals living alone) [4]. Through their analysis, they demonstrated associations between NO_2 levels and neighbourhood level indicators of material and social deprivation [4]. While the majority of the associations were in the expected direction (e.g. neighbourhoods with lower socioeconomic indicators were associated with higher air pollution exposure), there were also important exceptions to this trend that the authors suggest could be attributable to unique community-level

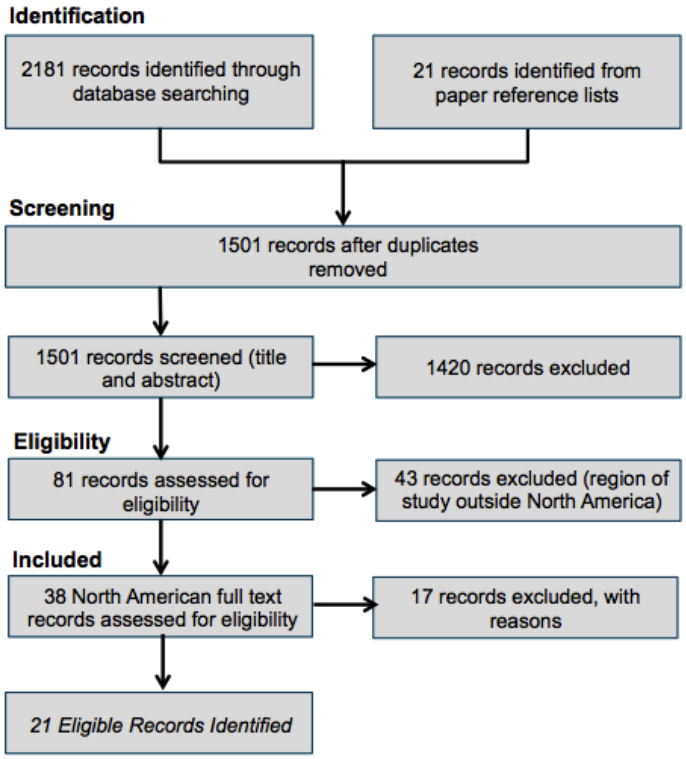

Figure 1: *PRISMA flow diagram: Overview of the PRISMA results from the search process.*

characteristics such as dense student neighbourhoods in downtown Montreal [4].

Pinault et al. performed two studies of inequalities in NO_2 exposure by socioeconomic status in Vancouver, Toronto, and Montreal in 2016 [14, 15]. In the first study, the researchers investigated the differences in NO_2 exposure between children of different socioeconomic status using ordinary least square regression and spatial autoregressive modeling approaches [15]. Their analysis suggests that there is a mean exposure level difference of 1.71 ppb between the lowest (mean NO_2 20.56 ppb) and highest (mean NO_2 22.27 ppb) income quintile, indicating that children from lower income families tend to be exposed to higher NO_2 levels [15]. In the second study, the researchers investigated the associations between socioeconomic status and NO_2 pollution exposure at the dissemination area unit of analysis [14]. In this study, the researchers considered multiple indicators of social and material deprivation and used a simultaneous autoregressive (SAR) model to identify associations between deprivation indicators and air pollution exposure [14]. Their analysis suggests that positive associations exist between measures of social deprivation (e.g. proportion of people living alone) in each of the three major Canadian cities. However, they did not identify any associations between more traditional measures of material deprivation (e.g. unemployment) and NO_2 exposures [14].

Ultimately, the results of the three Canadian studies suggest a trend for a positive association between lower SES and higher levels of NO_2 exposure in urban settings

using multiple ecological study analytic approaches and units of analysis [4, 14, 15]. A review paper published in 2015 reported that only 6 analytical environmental inequality exposure studies had been performed in a Canadian setting in only three different locations (the majority of which investigated total suspended particles as a measure of air pollution rather than direct measures of NO_2 or $PM_{2.5}$) [8]. When compared to the review completed by Miao et al., this review indicates that there has not been a significant expansion of air pollution exposure inequality research in Canada since 2015 and future research efforts should be expanded to consider a wider variety of SES indicators and pollutants in a more comprehensive set of locations across Canada. Additionally, none of the studies identified investigated rural regions, suggesting that the results generated may only be relevant to major urban settings.

3.2. U.S. Studies

In the United States, there has been significantly more research regarding inequalities in air pollution exposure by SES. 18 studies were identified that analyzed air pollution exposure by individual and neighbourhood level socioeconomic status indicators including education, employment, and proportion of renters, among others. Additionally, some of the studies employed index measures such as social deprivation, material deprivation, and neighbourhood quality [16, 17]. In contrast to the Canadian studies, the American studies investigated a much wider range of locations within the United States including urban and rural region-specific analyses as well as studies that investigated the entire country.

The general trend that is observed from these studies is that there is a significant positive association between low SES and high levels of primary air pollutants including NO_2 and $PM_{2.5}$. There were numerous innovative approaches applied in the studies conducted in the United States including analysis of individual pollutant components, use of an individual level unit of analysis, monitoring shifts in inequality trends over time, and applying geographic weighted regression models to allow for the detection of spatial variability in the relationship between indicators of SES and pollutant exposure [11, 18, 19, 20]. For example, Hajat et al. aimed to address a gap in the research regarding the spatial association of individual (rather than neighbourhood) SES characteristics with $PM_{2.5}$ and nitrogen oxide (NO) pollutants across multiple regions [11]. The researchers reported that average $PM_{2.5}$ and NO levels tended to decrease as SES increased [11]. Interestingly, neighbourhood SES measures were more strongly associated with air pollutant levels than individual SES measures [11]. This demonstrates the critical importance of selecting boundaries that appropriately define neighbourhoods and communities in order to generate results that are relevant at an individual level [11].

The majority of regression analyses performed in the North American studies rely on ordinary least squares regression or spatial autoregressive models. While spatial autoregressive models are advantageous over ordinary least squares regression models due to their ability to account for spatial autocorrelation in air pollution data, neither model allows for the assessment of spatial variability in the relationship between air pollution and indicators of SES [3]. Previous analyses using these methods have relied on the assumption that the association between SES and air pollution levels is

stable across space, an assumption which multiple studies have called into question [20]. Through the application of a geographic weighted regression model, Grineski et al. demonstrated spatial variability in the association between income and PM2.5 exposure [20]. The results of their analysis provide support for the association between income and $PM_{2.5}$ exposure but demonstrate that this relationship is not necessarily consistent across space [20]. The researchers argue that GWR can be implemented as a powerful approach for generating a more comprehensive understanding of the complex intersections between environmental exposures such as air pollution, SES indicators such as income, and health inequalities such as asthma outcomes [20].

As demonstrated by the examples discussed above and the summary of results presented in Tab. 1 in the appendix, the general trend that is observed from the studies in the United States is that there is a positive association between low SES and high levels of primary air pollutants, including $PM_{2.5}$ and NO_2. However, there were also inconsistencies identified in the analyses for different regions, pollutants, SES indicators, and units of analysis. For example, Li et al. identified inconsistent results in their analysis of $PM_{2.5}$, PM_{10}, and SO_2 emissions in Texas and found that higher median household income was associated with higher air pollution levels [21]. The researchers suggest that the conflicting results for different SES indicators may occur because industrial facilities that emit pollutants may contribute to the economic activities of neighbourhoods, demonstrating the complex nature of the relationship between pollution exposure levels and SES [21]. Additionally, differences in the social geography of different cities can influence the consistency of the results within and between regions [22]. For example, in major cities including New York, Los Angeles, Rome, and Montreal, studies have demonstrated that there is a concentration of wealthy individuals living in the dense urban core of the city that are exposed to relatively high levels of air pollution [16, 22]. Therefore, the context-specific historical development characteristics and current social geography of a region must be considered when interpreting the results of environmental justice air quality research.

3.3. Analytic Approaches

A wide variety of analytical methods were employed in the 21 studies included in this review. Each of the Canadian studies included in the review performed ecological studies with a census tract or dissemination area unit of analysis [4, 14, 15]. However, each study applied a unique analytical approach. Crouse et al. calculated Pearsons correlation coefficients and 95% confidence intervals while both studies by Pinault et al. applied regression approaches (ordinary least squares regression and/or spatial autoregressive models). For the studies conducted in the United States, the most common unit of analysis was the census track. However, a variety of units of analysis were applied including (by increasing geographic unit size): individual households, $1km^2$ blocks, $12km^2$ blocks, census blocks, and counties. The majority of studies conducted were ecological studies. However, there were four studies that also performed individual level analysis [11, 17, 20, 23]. Analytic methods applied include descriptive statistics and ANOVA, adjusted and unadjusted linear regression models, spatial regression approaches such as the spatial autoregressive model, the Gini Coefficient and Atkinson Index, factor analysis, and geographically weighted regression models.

3.4. Urban-Rural Differences in Trends

Due to the complex relationship between SES and environmental pollution exposures, it is critical to assess results in a context-specific manner [20, 21]. For example, research in European countries including Spain, England, and Italy has demonstrated variability in the association between indicators of SES and air pollution exposure in rural and urban regions [10, 24, 25].

In a North American setting, the majority of air pollution exposure inequality assessments are performed in urban regions. For example, all three Canadian studies identified in this review focused on major urban centres and did not make any comparisons to rural regions, which likely exhibit different pollution distribution and inequality characteristics [18]. This lack of coverage of rural regions may exist due to a lack of air-monitor coverage in Canada that prevents adequate investigation of exposure inequality in rural populations [18]. However, several studies in the United States have briefly reported on variability in the relationship between SES and air pollutants by rural-urban status [26]. An analysis performed by Clark et al. in 2014 investigated the entire contiguous US population, including both rural and urban populations. Their Atkinson Index (AI) results demonstrated that the inequality measures differ between urban and rural regions [26]. Overall, NO_2 inequality as measured by the Atkinson Index tended to be slightly higher in urban regions. However, not all studies have demonstrated differences in the association between SES and air pollution levels by urban-rural status. For example, Brochu et al. investigated the relationship between education levels and $PM_{2.5}$ levels in census tracts across rural and urban regions of Northeastern US and identified consistent results in both urban and rural classified census tracts, demonstrating that low levels of education are associated with increases in $PM_{2.5}$ in both urban and rural regions [27].

4. Discussion

4.1. Methodological Challenges

Despite the progress that has been made in the field of air pollution exposure and inequality assessment, there are still many challenges inherent to these types of analyses that must be considered ([3]. Some of the major challenges that must be addressed include the modifiable areal unit problem, spatial autocorrelation of the data, correcting for confounders in the relationship between the variables such as population density, assessing individual level exposures, and allowing for spatial variability in the association between deprivation and air pollution [3, 4, 11**?**].

The modifiable areal unit problem is a common problem in ecological research that refers to situations where the units of analysis are arbitrarily chosen and do not represent true boundaries [4]. This can result in inconsistent results in environmental inequality studies that are performed using different units of analysis [3]. For example, many of the studies discussed in this review use neighbourhood level measurements for air pollution and SES with a census tract or dissemination area unit of analysis, despite these boundaries not having any true meaning for delineations in air pollution levels [3, 4]. Using the smallest possible units is often encouraged in order to retain

meaningful variation in the data, capture spatial variation at a fine resolution, and improve the reliability of the research [3, 4]. Analyses performed with individual level data are important to thoroughly assess the relationship between deprivation and air pollution exposure and expanding the use of cross-sectional, cohort, and case-control studies to assess environmental inequality would provide valuable and robust individual-level analyses [8, 11].

Another major methodological challenge inherent to environmental inequality air pollution research is the fact that air pollution often exhibits spatial autocorrelation and cannot be accurately analyzed using traditional regression approaches [3]. Regression based approaches are often applied to investigate the magnitude and direction of inequality in air pollution exposure, using air pollution as the dependent variable [3]. Linear regression approaches assume that the observations of the dependent variable are independent [3]. However, air pollution data often exhibits spatial autocorrelation, meaning that linear regression analysis results may not be reliable [3, 6]. Several of the studies reviewed in this paper used linear regression and did not account for or report if they assessed spatial autocorrelation (air pollutant data tends to exhibit positive spatial autocorrelation with nearby observations exhibiting similar values) in air pollution data [21, 28, 29, 30]. It is critical for future research to assess and report spatial autocorrelation in data using a measure such as Morans I that indicates the extent of spatial autocorrelation in a spatial variable [3, 6].

Adjusting models for confounding is critically important in air pollution exposure inequality research [3]. The air pollution and SES association is likely influenced by multiple confounding variables including population density and land use characteristics [3]. While adjusted models are created in some studies, many environmental inequality studies have historically not adequately adjusted for confounding variables [3]. In studies that provide a comparison of unadjusted and adjusted models, the adjusted results appear to be attenuated, demonstrating their relevance in properly assessing the association between air pollution and deprivation [3]. Further exploration of possible confounding variables in the association between air pollution and deprivation is necessary to determine whether the confounders are population specific and to eventually produce less biased measures of the association between deprivation and air pollution [3].

As noted above, the association between air pollution and deprivation can differ over space [3, 20**?**]. Approaches such as linear and spatial regression can fail to capture this variability and therefore present an oversimplified view of the relationship between these variables [**?**]. There are several approaches for accounting for this variation including performing stratified rather than pooled analyses and performing a geographic weighted regression that allow for spatial variability in regression coefficients [3**?**]. Papers that present pooled and stratified data demonstrate that pooled analysis has the potential to mask spatial patterns in the data that may be meaningful [3]. Beyond performing multiple stratified analyses of different locations, another option is to use geographic weighted regression, a modeling approach that does not impose a geographically fixed relationship between the variables [**?**]. Bailey et al. argue that this approach should become more widespread in environmental equity research because it does not assume a universal norm and therefore supports the consideration of a

wider set of theoretical perspectives regarding the complex and variable relationship between air pollution and measures of deprivation [**?**]. It is critical to perform refined environmental justice analyses to assess disparities in exposure because disadvantaged communities are likely to be more susceptible to and suffer disproportionately from the health impacts of air pollution exposures, therefore resulting in a double burden in communities that are both over-exposed and extra-susceptible to air pollution [2, 22].

5. Conclusion

Generally, the North American studies assessed in this review align with previous environmental justice studies that have demonstrated that individuals and communities with lower SES are exposed to higher levels of $PM_{2.5}$ and NO_2 air pollution [3, 8]. The studies discussed above demonstrate that this relationship has been examined using multiple units of analysis, analytic approaches, air pollutants, and measures of deprivation. While there is strong support for the relationship between SES and $PM_{2.5}$ and NO_2 air pollutants, the studies demonstrated variable results in different contexts as found in Montreal and New York City. Therefore, flexible and innovative data analysis approaches are required to support the exploration of a wide set of theoretical perspectives regarding the complex relationship between air pollution and deprivation. Through the application of individual level analysis and analytic approaches that allow for spatial variation in the association between multiple measures of deprivation and air pollution, more comprehensive insight will be generated into the complex relationship between these variables. The results of this review highlight the importance of local analyses that consider context-specific community characteristics in order to provide policy-relevant information for public health intervention delivery. From a social justice perspective, air pollution inequality research provides important information for the protection of public health in more vulnerable populations [4]. Future research in this area is required to expand our understanding of inequalities in air pollution exposure and health impacts across urban and rural regions of North America, particularly in Canada [8].

6. Acknowledgments

I would like to express my appreciation to my supervisor Dr. Tim Takaro for his constructive suggestions and guidance during the planning, writing and revision stages of developing this review paper. His willingness to give his time so generously has been very much appreciated. I would also like to thank Jordan Brubacher from Dr. Takaros Climate Change, Health Impacts, and Early Childhood Asthma Research Group for his willingness to discuss and explain environmental justice theoretical perspectives and analytical approaches.

References

[1] S Morrison, FM Fordyce, and E Marian Scott. An initial assessment of spatial relationships between respiratory cases, soil metal content, air quality and deprivation indicators in glasgow, scotland, uk: relevance to the environmental justice agenda. *Environmental geochemistry and health*, 36(2):319–332, 2014.

[2] Jamie Pearce and Simon Kingham. Environmental inequalities in new zealand: A national study of air pollution and environmental justice. *Geoforum*, 39(2):980–993, 2008. ISSN 0016-7185. doi:https://doi.org/10.1016/j.geoforum.2007.10.007. URL https://www.sciencedirect.com/science/article/pii/S0016718507001613. Conversations Across the Divide The Time and Place for Political Ecology: The Life-Work of Piers Blaikie Biocomplexity in Coupled Human-Natural Systems: The Study of Population-Environment Interactions.

[3] Anjum Hajat, Charlene Hsia, and Marie S. O'Neill. Socioeconomic disparities and air pollution exposure: a global review. *Current Environmental Health Reports*, 2(4):440–450, Dec 2015. ISSN 2196-5412. doi:10.1007/s40572-015-0069-5. URL https://doi.org/10.1007/s40572-015-0069-5.

[4] Dan L. Crouse, Nancy A. Ross, and Mark S. Goldberg. Double burden of deprivation and high concentrations of ambient air pollution at the neighbourhood scale in montreal, canada. *Social Science & Medicine*, 69(6):971–981, 2009. ISSN 0277-9536. doi:https://doi.org/10.1016/j.socscimed.2009.07.010. URL https://www.sciencedirect.com/science/article/pii/S0277953609004444. Part Special Issue: Women, Mothers and HIV Care in Resource Poor Settings.

[5] Health Effects Institute. State of global air 2019: Air pollution a significant risk factor worldwide., 2019.

[6] Bin Zou, Fen Peng, Neng Wan, Keita Mamady, and Gaines J. Wilson. Spatial cluster detection of air pollution exposure inequities across the united states. *PLOS ONE*, 9(3):1–14, 03 2014. doi:10.1371/journal.pone.0091917. URL https://doi.org/10.1371/journal.pone.0091917.

[7] Health Effects Institute. State of global air 2019: What is the impact on your health?, 2019.

[8] Qun Miao, Dongmei Chen, Michael Buzzelli, and Kristan J. Aronson. Environmental equity research: Review with focus on outdoor air pollution research methods and analytic tools. *Archives of Environmental & Occupational Health*, 70(1):47–55, 2015. doi:10.1080/19338244.2014.904266. URL https://doi.org/10.1080/19338244.2014.904266. PMID: 24972259.

[9] Marie S O'Neill, Michael Jerrett, Ichiro Kawachi, Jonathan I Levy, Aaron J Cohen, Nelson Gouveia, Paul Wilkinson, Tony Fletcher, Luis Cifuentes, Joel Schwartz, and null null. Health, wealth, and air pollution: advancing theory and methods. *Environmental Health Perspectives*, 111(16):1861–1870, 2003. doi:10.1289/ehp.6334. URL https://ehp.niehs.nih.gov/doi/abs/10.1289/ehp.6334.

[10] Alice Mannocci, Immacolata Ciarlo, Valeria DEgidio, Angela Del Cimmuto, Maria de Giusti, Paolo Villari, and Giuseppe La Torre. Socioeconomic deprivation status and air pollution by pm10 and no2: An assessment at municipal level of 11 years in italy. *Journal of environmental and public health*, 2019, 2019.

[11] Anjum Hajat, Ana V. Diez-Roux, Sara D. Adar, Amy H. Auchincloss, Gina S. Lovasi, Marie S. ONeill, Lianne Sheppard, and Joel D. Kaufman. Air pollution and individual and neighborhood socioeconomic status: Evidence from the multi-ethnic study of atherosclerosis (mesa). *Environmental Health Perspectives*, 121(11-12): 1325–1333, 2013. doi:10.1289/ehp.1206337. URL https://ehp.niehs.nih.gov/doi/abs/10.1289/ehp.1206337.

[12] Raoul S. Liévanos. Racialized structural vulnerability: Neighborhood racial composition, concentrated disadvantage, and fine particulate matter in california, 2019. ISSN 1660-4601. URL https://doi.org/10.3390/ijerph16173196.

[13] Health Canada. Health effects of air pollution, Jan 2021. URL https://www.canada.ca/en/health-canada/services/air-quality/health-effects-indoor-air-pollution.html.

[14] Lauren Pinault, Daniel Crouse, Michael Jerrett, Michael Brauer, and Michael Tjepkema. Spatial associations between socioeconomic groups and no2 air pollution exposure within three large canadian cities. *Environmental Research*, 147:373–382, 2016. ISSN 0013-9351. doi:https://doi.org/10.1016/j.envres.2016.02.033. URL https://www.sciencedirect.com/science/article/pii/S0013935116300755.

[15] Lauren Pinault, Daniel Crouse, Michael Jerrett, Michael Brauer, and Michael Tjepkema. Socioeconomic differences in nitrogen dioxide ambient air pollution exposure among children in the three largest canadian cities. *Health reports*, 27(7): 3, 2016.

[16] Jessie L.C. Shmool, Jennifer F. Bobb, Kazuhiko Ito, Beth Elston, David A. Savitz, Zev Ross, Thomas D. Matte, Sarah Johnson, Francesca Dominici, and Jane E. Clougherty. Area-level socioeconomic deprivation, nitrogen dioxide exposure, and term birth weight in new york city. *Environmental Research*, 142:624–632, 2015. ISSN 0013-9351. doi:https://doi.org/10.1016/j.envres.2015.08.019. URL https://www.sciencedirect.com/science/article/pii/S0013935115300633.

[17] Michelle Wilhelm, Lei Qian, and Beate Ritz. Outdoor air pollution, family and neighborhood environment, and asthma in la fans children. *Health & place*, 15 (1):25–36, Mar 2009. ISSN 1353-8292. doi:10.1016/j.healthplace.2008.02.002. URL https://pubmed.ncbi.nlm.nih.gov/18373944. 18373944[pmid].

[18] Michelle L. Bell and Keita Ebisu. Environmental inequality in exposures to airborne particulate matter components in the united states. *Environmental health perspectives*, 120(12):1699–1704, Dec 2012. ISSN 1552-9924. doi:10.1289/ehp.1205201. URL https://pubmed.ncbi.nlm.nih.gov/22889745. 22889745[pmid].

[19] Neal Fann, Evan Coffman, Brian Timin, and James T. Kelly. The estimated change in the level and distribution of pm(2.5)-attributable health impacts in the united states: 2005-2014. *Environmental research*, 167:506–514, Nov 2018. ISSN 1096-0953. doi:10.1016/j.envres.2018.08.018. URL https://pubmed.ncbi.nlm.nih.gov/30142626. 30142626[pmid].

[20] Sara E. Grineski, Timothy W. Collins, and Hector A. Olvera. Local variability in the impacts of residential particulate matter and pest exposure on children's wheezing severity: A geographically weighted regression analysis of environmental health justice. *Population and environment*, 37(1):22–43, Sep 2015. ISSN 0199-0039. doi:10.1007/s11111-015-0230-y. URL https://pubmed.ncbi.nlm.nih.gov/26527848. 26527848[pmid].

[21] Zhengyan Li, David M. Konisky, and Nikolaos Zirogiannis. Racial, ethnic, and income disparities in air pollution: A study of excess emissions in texas. *PloS one*, 14(8):e0220696–e0220696, Aug 2019. ISSN 1932-6203. doi:10.1371/journal.pone.0220696. URL https://pubmed.ncbi.nlm.nih.gov/31374099. 31374099[pmid].

[22] Dan L. Crouse, Nancy A. Ross, and Mark S. Goldberg. Double burden of deprivation and high concentrations of ambient air pollution at the neighbourhood scale in montreal, canada. *Social Science & Medicine*, 69(6):971–981, 2009. ISSN 0277-9536. doi:https://doi.org/10.1016/j.socscimed.2009.07.010. URL https://www.sciencedirect.com/science/article/pii/S0277953609004444. Part Special Issue: Women, Mothers and HIV Care in Resource Poor Settings.

[23] Julian D. Marshall. Environmental inequality: Air pollution exposures in california's south coast air basin. *Atmospheric Environment*, 42(21):5499–5503, 2008. ISSN 1352-2310. doi:https://doi.org/10.1016/j.atmosenv.2008.02.005. URL https://www.sciencedirect.com/science/article/pii/S1352231008001350.

[24] Ana Fernández-Somoano and Adonina Tardon. Socioeconomic status and exposure to outdoor no2 and benzene in the asturias inma birth cohort, spain. *Journal of epidemiology and community health*, 68(1):29–36, Jan 2014. ISSN 1470-2738. doi:10.1136/jech-2013-202722. URL https://pubmed.ncbi.nlm.nih.gov/23999377. 23999377[pmid].

[25] Ai Milojevic, Claire L. Niedzwiedz, Jamie Pearce, James Milner, Ian A. MacKenzie, Ruth M. Doherty, and Paul Wilkinson. Socioeconomic and urban-rural differentials in exposure to air pollution and mortality burden in england. *Environmental health : a global access science source*, 16(1):104–104, Oct 2017. ISSN 1476-069X. doi:10.1186/s12940-017-0314-5. URL https://pubmed.ncbi.nlm.nih.gov/28985761. 28985761[pmid].

[26] Lara P. Clark, Dylan B. Millet, and Julian D. Marshall. National patterns in environmental injustice and inequality: outdoor no2 air pollution in the united states. *PloS one*, 9(4):e94431–e94431, Apr 2014. ISSN 1932-6203. doi:10.1371/journal.pone.0094431. URL https://pubmed.ncbi.nlm.nih.gov/24736569. 24736569[pmid].

[27] Paul J. Brochu, Jeff D. Yanosky, Christopher J. Paciorek, Joel Schwartz, Jarvis T. Chen, Robert F. Herrick, and Helen H. Suh. Particulate air pollution and socioeconomic position in rural and urban areas of the northeastern united states. *American journal of public health*, 101 Suppl 1(Suppl 1):S224–S230, Dec 2011. ISSN 1541-0048. doi:10.2105/AJPH.2011.300232. URL https://pubmed.ncbi.nlm.nih.gov/21836114. 21836114[pmid].

[28] Simone C. Gray, Sharon E. Edwards, Bradley D. Schultz, and Marie Lynn Miranda. Assessing the impact of race, social factors and air pollution on birth outcomes: a population-based study. *Environmental health : a global access science source*, 13 (1):4–4, Jan 2014. ISSN 1476-069X. doi:10.1186/1476-069X-13-4. URL https://pubmed.ncbi.nlm.nih.gov/24476365. 24476365[pmid].

[29] Sara Grineski, Bob Bolin, and Christopher Boone. Criteria air pollution and marginalized populations: Environmental inequity in metropolitan phoenix, arizona*. *Social Science Quarterly*, 88(2):535–554, 2007. doi:https://doi.org/10.1111/j.1540-6237.2007.00470.x. URL https://onlinelibrary.wiley.com/doi/abs/10.1111/j.1540-6237.2007.00470.x.

[30] Jia Coco Liu, Ander Wilson, Loretta J. Mickley, Keita Ebisu, Melissa P. Sulprizio, Yun Wang, Roger D. Peng, Xu Yue, Francesca Dominici, and Michelle L. Bell. Who among the elderly is most vulnerable to exposure to and health risks of fine particulate matter from wildfire smoke? *American journal of epidemiology*, 186(6):730–735, Sep 2017. ISSN 1476-6256. doi:10.1093/aje/kwx141. URL https://pubmed.ncbi.nlm.nih.gov/28525551. 28525551[pmid].

[31] K Balakrishnan, S Dey, T Gupta, et al. India state-level disease burden initiative air pollution collaborators. *The impact of air pollution on deaths, disease burden, and life expectancy across the states of India: The Global Burden of Disease Study*, 2017.

[32] Mercedes A. Bravo, Rebecca Anthopolos, Michelle L. Bell, and Marie Lynn Miranda. Racial isolation and exposure to airborne particulate matter and ozone in understudied us populations: Environmental justice applications of downscaled numerical model output. *Environment International*, 92-93:247–255, 2016. ISSN 0160-4120. doi:https://doi.org/10.1016/j.envint.2016.04.008. URL https://www.sciencedirect.com/science/article/pii/S0160412016301386.

[33] Lara P. Clark, Dylan B. Millet, and Julian D. Marshall. Changes in transportation-related air pollution exposures by race-ethnicity and socioeconomic status: Outdoor nitrogen dioxide in the united states in 2000 and 2010. *Environmental health perspectives*, 125(9):097012–097012, Sep 2017. ISSN 1552-9924. doi:10.1289/EHP959. URL https://pubmed.ncbi.nlm.nih.gov/28930515. 28930515[pmid].

[34] Simone C. Gray, Sharon E. Edwards, and Marie Lynn Miranda. Race, socioeconomic status, and air pollution exposure in north carolina. *Environmental Research*, 126:152–158, 2013. ISSN 0013-9351. doi:https://doi.org/10.1016/j.envres.2013.06.005. URL https://www.sciencedirect.com/science/article/pii/S0013935113001138.

[35] Ihab Mikati, Adam F. Benson, Thomas J. Luben, Jason D. Sacks, and Jennifer Richmond-Bryant. Disparities in distribution of particulate matter emission sources by race and poverty status. *American journal of public health*, 108(4):480–485, Apr 2018. ISSN 1541-0048. doi:10.2105/AJPH.2017.304297. URL https://pubmed.ncbi.nlm.nih.gov/29470121. 29470121[pmid].

[36] Anna Rosofsky, Jonathan I. Levy, Antonella Zanobetti, Patricia Janulewicz, and M. Patricia Fabian. Temporal trends in air pollution exposure inequality in massachusetts. *Environmental research*, 161:76–86, Feb 2018. ISSN 1096-0953. doi:10.1016/j.envres.2017.10.028. URL https://pubmed.ncbi.nlm.nih.gov/29101831. 29101831[pmid].

APPENDIX

Summary of North American Studies of Air Pollution Exposure Inequities by SES Measures

Canada

First Author	Year	Location	Unit(s) of Analysis	SES Indicator(s)	Pollutant(s)	Analysis Method	Results
Crouse	2009	Montreal	Census tract	14 SES variables (including material and social deprivation measures)	NO2	Pearson correlation coefficients and 95% confidence intervals (CI)	Positive: demonstrated associations between NO2 and neighbourhood-level indicators of material deprivation (including median household income) and indicators of social deprivation (including proportion of people living alone)
Pinault	2016	Toronto, Vancouver, Montreal	Dissemination Area	Social and material deprivation measures	NO2	Spatial autoregressive model	Positive: demonstrated associations between NO2 concentrations and indicators of social deprivation, but not other measues of deprivation (e.g. income).
Pinault	2016	Toronto, Vancouver, Montreal	Dissemination Area	Children socioeconomic measures (Neighbourhood level SES)	NO2	Regression models (OLS and simultaneous autoregressive models)	Posotive: demonstrated association between NO2 concentrations and low income. Some social deprivation measures associated with NO2 (differed by community).

United States

First Author	Year	Location	Unit(s) of Analysis	SES Indicator(s)	Pollutant(s)	Analysis Method	Results
Bell	2012	215 US Census Tracts	Census Tract	Education, Poverty status, Employment, Earnings	PM2.5	Univariate regression	Positive: demonstrated association between lower SES and higher exposures, with some exceptions.
Bravo	2016	Urban and Rural US Regions	Census Tract	Education, Socioeconomic status, Racial isolation (RI)	PM2.5 and O3	ANOVA	Positive: demonstrated association for low education with higher exposures. No clear patterns in PM2.5 exposure by other measures.
Brochu	2011	Rural and Urban Areas of the Northeastern US	Census Tract	Poverty, Education, Income	PM2.5 and PM10	Generalized additive models.	Positive: demonstrated association between low SES and high PM exposures.
Clark	2017	Contiguous USA	Census Blocks	Race-ethnicity, Socioeconomic status, Lan- guage, Education, Age	NO2	Estimated changes in NO2 concentrations by demographic groups.	Positive: Larger NO2 disparities by race-ethnicity than by income. Decreasing disparity levels between 2000-2010.
Clark	2014	Contiguous US	Census Blocks	Race-ethnicity, Household income, Poverty status, Education status, Age	NO2	Calculate population-weighted mean NO2 concentrations by SES indicators.	Positive: demonstrated significant disparities in NO2 concentrations for specific socioeconomic groups (by race, education, and income). Different patterns in urban vs. rural regions.
Fann	2018	Contiguous USA	12 km by 12 km	Education	PM2.5	Gini Coefficient and Atkinson Index	Positive: demonstrated association between low education and greater exposure and higher mortality (but inequalities are decreasing over time).

United States (page 2)

First Author	Year	Location	Unit(s) of Analysis	SES Indicator(s)	Pollutant(s)	Analysis Method	Results
Gray	2013	North Carolina	Census Tract	SES, Racial composition	PM2.5 and O3	Linear mixed regression models	Positive: Lower SES and higher proportion minority population were associated with higher levels of PM2.5 (opposite for O3).
Grineski	2007	Phoenix, Arizona	Census Block	SES, Proportion of renters	NOx, CO, O3	Multiple regression equation	Positive: demonstrated an association between exposure and low-education or identifying as an ethnic minority.
Grineski	2015	Texas	Residential home	Income	Outdoor PM2.5	Geographically weighted regression	Positive: Lower income children exposed to more PM2.5
Hajat	2013	USA [6,140 participants from the Multi-Ethnic Study of Atherosclerosis (MESA)]	Residential home, Census tract	Individual and neighbourhood SES measures	PM2.5, NO	Spatial regression (spatial intrinsic conditional autoregressive)	Positive: Found statistically significant associations of SES measures with predicted air pollutant concentrations (significant variability between regions).
Li	2019	Texas	Census tract level, Facility level	7 demographic measures (including percent owner-occupied, income, education)	PM, SO2 (among others)	Multinomial logit model, ordinary least squares regression	Inconsistent: Higher median household income associated with excess emissions. Education, median housing value, and percentage of owner-occupied housing unit are negatively associated with excess emission.
Liu	2016	Western USA	Counties	Education, Poverty level	PM2.5 (wildfire smoke)	Log-linear Poisson mixed-effects regression model	Positive: Proportionof residents exposed to intense smoke waves decreased as poverty decreased.
Marshall	2008	California	Individual and community lev	Ethnicity, Income	PM2.5	Linear regression	Positive: demonstrated association between nonwhite, lower-income populations and higher exposure to primary pollutants.
Mikati	2018	USA	Census Block	Ethnicity, poverty status	PM2.5	Proportional exposure burdens based on total emissions in census block.	Postive: For PM2.5, those in poverty had 1.35 times higher burden than did the overall population, and non-Whites had 1.28 times higher burden.
Miranda	2011	USA	County-level	Poverty demographics	O3, PM2.5	Population-weighted univariate t-tests and multivariate logistic regression controlling for county population	Positive: Low income and minority communities tend to experience higher ambient pollution levels.
Rosofsky	2018	Massachusetts	1 km by 1km, Census Block	Income, Education	PM2.5 and NO2	Summary statistics, Population-Weighted Concentrations, Atkinson Index (AI)	Postive: Urban racial/ethnic minorities, low income and education groups have highest exposure levels.
Schmool	2015	New York City	Census Tract	Composite index of area-level deprivation	NO2 and PM2.5	Summary statistics, regression models	Inconsistent: Estimated NO2 exposures were highest among individuals residing in the most-affluent census tracts, and lowest among those in mid-range deprivation tracts.
Wilhelm	2009	Los Angeles	Census Tract, Family-level, Individual-level	SES, Neighborhood quality, Social support	CO, NO2, O3, PM10 and PM2.5	Correlation coefficients and factor analysis	Positive but weak: NO2 levels tended to increase as neighborhood quality decreased (r ~ 0.3 or lower).

A summary of articles included in the review